Proceedings of the I·R·E

JUNE 1939

VOLUME 27 NUMBER 6

Institute of Radio Engineers

National Convention

San Francisco, California, June 27–30, 1939

Fourteenth Annual Convention

New York, N. Y., September 20–23, 1929

Rochester Fall Meeting

November 13, 14, and 15, 1939

New York Meeting—Engineering Societies Building—June 7

33 West 39th Street, New York, N. Y.

SECTION MEETINGS

CINCINNATI June 13	LOS ANGELES June 20	PITTSBURGH June 20
DETROIT June 16	NEW ORLEANS June 16	WASHINGTON June 12

SECTIONS

ATLANTA—Chairman, Ben Akerman; Secretary, J. G. Preston, 230 Ansley St., Decatur, Ga.
BOSTON—Chairman, H. W. Lamson; Secretary, E. B. Dallin, 64 Oakland Ave., Arlington, Mass.
BUFFALO-NIAGARA—Chairman, H. C. Tittle; Secretary, E. C. Waud, 235 Huntington Ave., Buffalo, N. Y.
CHICAGO—Chairman, V. J. Andrew; Secretary, G. I. Martin, RCA Institutes, 1154 Merchandise Mart, Chicago, Ill.
CINCINNATI—Chairman, H. J. Tyzzer; Secretary, J. M. McDonald, Crosley Radio Corp., 1329 Arlington, Cincinnati, Ohio.
CLEVELAND—Chairman, S. E. Leonard; Secretary, H. C. Williams, Rm. 1932, 750 Huron Rd., Cleveland, Ohio.
CONNECTICUT VALLEY—Chairman, E. R. Sanders; Secretary, W. R. G. Baker, General Electric Co., Bridgeport, Conn.
DETROIT—Chairman, L. C. Smeby; Secretary, R. J. Schaefer, 9753 N. Martindale, Detroit, Mich.
EMPORIUM—Chairman, R. K. McClintock; Secretary, D. R. Kiser, Hygrade Sylvania Corp., Emporium, Penna.
INDIANAPOLIS—Chairman, L. M. Slater; Secretary, B. V. K. French, P. R. Mallory & Co., E. Washington, St., Indianapolis, Ind.
LOS ANGELES—Chairman, F. G. Albin; Secretary, M. T. Smith, General Radio Co., 1000 N. Seward St., Hollywood, Calif.
MONTREAL—Chairman, Sydney Sillitoe; Secretary, R. E. Hammond, 1261 Shearer St., Montreal, Que.
NEW ORLEANS—Chairman, G. H. Peirce; Secretary, D. W. Bowman, 8327 Sycamore St., New Orleans, La.
PHILADELPHIA—Chairman, H. J. Schrader; Secretary, R. L. Snyder, 103 Franklin Rd., Glassboro, N. J.
PITTSBURGH—Chairman, W. P. Place; Secretary, R. E. Stark, 90 Pilgrim Rd., Rosslyn Farms, Carnegie, Penna.
PORTLAND—Chairman, H. C. Singleton; Secretary, E. R. Meissner, United Radio Supply, Inc., 203 S. W. Ninth Ave., Portland, Ore.
ROCHESTER—Chairman, H. J. Klumb; Secretary, H. C. Sheve, Stromberg-Carlson Telephone Manufacturing Co., Rochester, N. Y.
SAN FRANCISCO—Chairman, F. E. Terman; Secretary, L. J. Black, 243-30th St., Oakland, Calif.
SEATTLE—Chairman, R. O. Bach; Secretary, Karl Ellerbeck, Pacific Telephone and Telegraph Co., 612 Northern Life Tower, Seattle, Wash.
TORONTO—Chairman, R. C. Poulter; Secretary, N. Potter, Canadian National Carbon Co., Ltd., 805 Davenport Rd., Toronto, Ont.
WASHINGTON—Chairman, Gerald C. Gross; Secretary, M. H. Biser, 3224-16th St., N. W., Washington, D. C.

Proceedings of the I·R·E

Published Monthly by
The Institute of Radio Engineers, Inc.

VOLUME 27 — *June, 1939* — NUMBER 6

Entered as second-class matter October 26, 1927, at the post office at Menasha, Wisconsin, under the Act of February 28, 1925, embodied in Paragraph 4, Section 412 of the Postal Laws and Regulations. Publication office, 450 Ahnaip Street, Menasha, Wisconsin. Subscription, $10.00 per year; foreign, $11.00.

THE INSTITUTE

The Institute of Radio Engineers serves those interested in radio and allied electrical-communication fields through the presentation and publication of technical material. In 1913 the first issue of the PROCEEDINGS appeared; it has been published uninterruptedly since then. Over 1500 technical papers have been included in its pages and portray a currently written history of developments in both theory and practice.

STANDARDS

In addition to the publication of submitted papers, many thousands of man-hours have been devoted to the preparation of standards useful to engineers. These comprise the general fields of terminology, graphical and literal symbols, and methods of testing and rating apparatus. Members receive a copy of each report. A list of the current issues of these reports follows:

Standards on Electroacoustics, 1938
Standards on Electronics, 1938
Standards on Radio Receivers, 1938
Standards on Radio Transmitters and Antennas, 1938.

MEETINGS

Meetings at which technical papers are presented are held in the twenty-one cities in the United States and Canada listed on the inside front cover of this issue. A number of special meetings are held annually and include one in Washington, D. C., in co-operation with the American Section of the International Scientific Radio Union (U.R.S.I.) in April, which is devoted to the general problems of wave propagation and measurement technique, the Rochester Fall Meeting in co-operation with the Radio Manufacturers Association in November, which is devoted chiefly to the problems of broadcast-receiver design, and the Annual Convention, the location and date of which is not fixed.

MEMBERSHIP

Membership has grown from a few dozen in 1912 to more than five thousand. Practically every country in the world in which radio engineers may be found is represented in our membership roster. Approximately a quarter of the membership is located outside of the United States. There are several grades of membership, depending on the qualifications of the applicant. Dues range between $3.00 per year for Students and $10.00 per year for Members. PROCEEDINGS are sent to each member without further payment.

PROCEEDINGS

The contents of each paper published in the PROCEEDINGS are the responsibility of the author and are not binding on the Institute or its members. Material appearing in the PROCEEDINGS may be reprinted or abstracted in other publications on the express condition that specific reference shall be made to its original appearance in the PROCEEDINGS. Illustrations of any variety may not be reproduced, however, without specific permission from the Institute.

Papers submitted to the Institute for publication shall be regarded as no longer confidential. They will be examined by the Papers Committee and Board of Editors to determine their suitability for publication. Suggestions on the mechanical form in which manuscripts should be prepared may be obtained from the Secretary.

SUBSCRIPTIONS

Annual subscription rates for the United States of America, its possessions, and Canada, $10.00; to college and public libraries when ordering direct, $5.00. Other countries, $1.00 additional.

The Institute of Radio Engineers, Inc.
Harold P. Westman, Secretary
330 West 42nd Street
New York, N.Y.

The Interpretation of Amplitude and Phase Distortion in Terms of Paired Echoes*

HAROLD A. WHEELER†, FELLOW, I.R.E.

Summary—*In picture-transmission systems, such as television and facsimile, the signal transients are noticeably distorted by small amounts of amplitude and phase distortion. There has been developed a simple method of estimating the effects of such distortion from inspection of the amplitude and phase curves. The distortion is regarded as made up of a pattern of echoes, each echo corresponding to a small amount of distortion of both kinds. The separate interpretation of amplitude and phase distortion requires pairs of echoes, those of each pair being equally displaced in time before and after the signal output. This is called the "method of paired echoes." Amplitude distortion corresponds to symmetrical "positive" pairs whereas phase distortion corresponds to skew-symmetrical "negative" pairs. A complete and exact theory is presented on the basis of a small amount of distortion. The method of paired echoes is most useful in the interpretation of phase curves and the determination of the tolerance of phase distortion.*

I. Introduction

THE selection of signals on the basis of their respective frequency bands requires band-pass filters. These cause distortion of the selected signal because the ideal selective characteristics can only be approximated in finite or dissipative networks, and practical networks are both finite and dissipative. The distortion may be regarded as the resultant of amplitude and phase distortion. These are distinct as concepts but are interdependent in that they are interrelated properties of any selective system.

Since any signal involves transient disturbances which convey its information, and since a transient has frequency components within every finite frequency band in the entire frequency spectrum, it follows that the very process of selection causes some distortion of the signal by the attenuation of some of its components. Such distortion is minimized by the selection of a frequency band sufficiently wide to include nearly all of the total energy of the frequency components. Whatever distortion remains from this cause, however, is amplitude distortion and is unavoidably associated with the attenuation in the selective system.

The amplitude and phase distortion remaining within the frequency band allotted to the signal can be reduced without limit by the choice of selective networks or by the use of auxiliary corrective networks. The usual procedure is to design the selective networks with the required attenuation and then to correct the phase distortion without adding amplitude distortion.

* Decimal classification: R148.1×R583. Original manuscript received by the Institute, November 1, 1938. Presented, Rochester Fall Meeting, Rochester, N. Y., November 15, 1938. Presented, New York Meeting, December 7, 1938.

† Hazeltine Service Corporation, Bayside, L. I., N. Y.

Amplitude distortion has received much more attention than phase distortion because it has been more important in the field of sound reproduction and also because it is so much more easily measured and studied. In some of the other fields of signaling, such as facsimile and television, phase distortion is not unimportant. The transients involved may be of very short duration, and they are detected by means which are sensitive to both phase and amplitude distortion. Either kind of distortion causes a confusion of the picture image which is readily perceptible by the eye. One of the most apparent forms taken by this distortion is the form of multiple images caused by echoes of the signal.

There has been an increasing need for a method of interpreting phase distortion, to be able to describe the distortion caused by given phase characteristics and to specify the tolerance of phase distortion on reasonable grounds. The method of paired echoes has been devised to meet this need.[1] It is so simple in its application that the effect of a nominal amount of phase distortion can be stated on inspection of the phase curve, in terms of the reproduced image. This method is fundamentally an adaptation of the Fourier integral, but in such a manner that every step has obvious physical significance and yields directly some of the desired information. It is particularly useful in getting a first approximation of the resulting distortion without any laborious computations.

The method of paired echoes is equally applicable to both amplitude and phase distortion. In its simplest form, here to be described, it is accurate only for a small amount of distortion, much less than one napier (8.7 decibels) or one radian (57 degrees) in the frequency band allotted to the signal. The total amount of attenuation in the neighborhood of the cutoff frequency is much greater than this, so this method is not useful for the study of the amplitude distortion caused by the cutoff characteristics. It is applicable to a small amount of amplitude distortion such as that arising in amplifiers which do not contribute materially to the large attenuation near the cutoff frequency.

The effect of amplitude distortion, separate from

[1] In correspondence with Mr. John R. Carson, the writer has since been informed of the independent development of a somewhat similar method of analysis by Mr. L. A. MacColl.

phase distortion, is relatively easy to determine first by the Fourier integral, which assumes the symmetric form including only the cosine terms.[2,3] It is then most convenient to use the method of paired echoes to study the effects of incremental amplitude and phase distortion. It is particularly useful for phase distortion because any other known method is so cumbersome as to be of little utility. Therefore this treatment is to be directed more especially to this case.

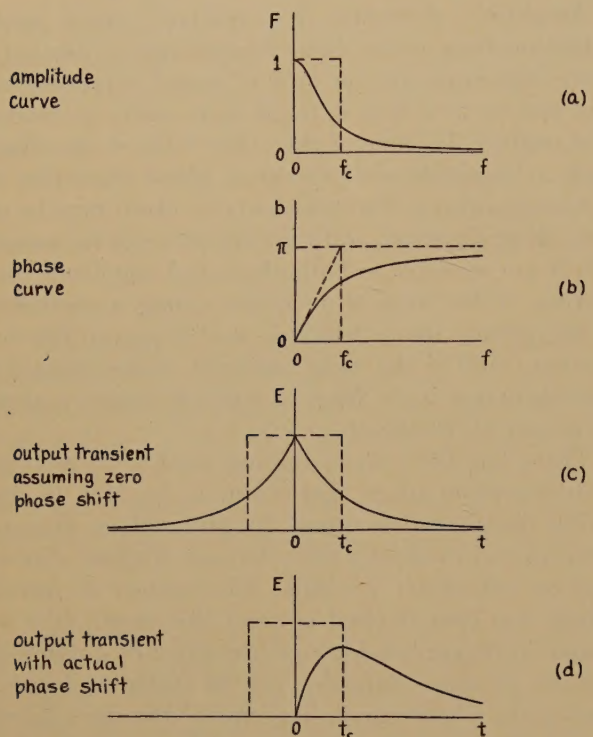

Fig. 1—A practical example of the effect of phase distortion on the output transient of an amplifier.

II. The Nature of Amplitude and Phase Distortion

As a further introduction, some relative characteristics of amplitude and phase distortion are to be pointed out with reference to a practical example. The circuit may be conceived as a two-stage resistance-coupled amplifier with shunt capacitance in each stage providing attenuation increasing with frequency. The amplitude characteristic $F(f)$ is shown in Fig. 1(a) and the phase $b(f)$ in Fig. 1(b). The signal is an instantaneous impulse. The mathematical derivations are given in Appendix A. First neglecting the phase shift, the amplitude characteristic is subjected to the Fourier integral, which yields the output signal transient $E(t)$ of Fig. 1(c). In this simple case, the actual output transient is readily obtained by integration, and is shown in Fig. 1(d). The latter differs from the former in that it includes the effects of the phase characteristics.

The nominal cutoff frequency f_c in Fig. 1(a) is the width of the dotted rectangle having the same area as the amplitude curve and the same height at zero frequency. This determines the cutoff time $t_c = 1/4f_c$, which is similarly related to each half of the output transient of Fig. 1(c). The nominal width of this symmetric transient is $2t_c = 1/2f_c$.

This example shows first the effect of a low-pass filter in widening the signal impulse, as in Fig. 1(c), caused entirely by the attenuation apart from the phase shift. This effect could be approximated with the aid of phase correction such that all frequency components, and therefore the symmetric transient, would merely be delayed uniformly in time. The resulting phase characteristic would be linear through the origin, instead of curved as in Fig. 1(b), and would have greater slope.

The actual phase shift of Fig. 1(b) is responsible for the difference between the symmetric transient of Fig. 1(c) and the actual output transient of Fig. 1(d). The latter is delayed and widened relative to the former. The delay is caused by the phase slope. The widening is caused by the phase distortion, that is, the departure of the phase curve from a straight line of uniform slope through the origin. In this case, the peak of the transient is delayed by t_c and its "center of gravity" is delayed by $2t_c$, the latter depending only on the phase slope at zero frequency. The curves of Fig. 1(c) and (d) have the same area, so the flattening and widening of the latter, as a result of phase distortion, is apparent in addition to the delay.

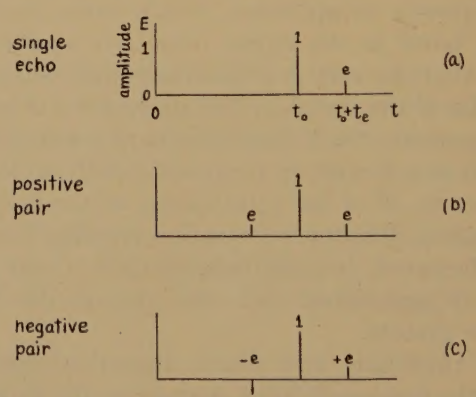

Fig. 2—The amplitude and time relations between signal and echoes.

[2] This subject is introduced and the same terminology is employed in the writer's previous paper,[3] especially in Section III and Appendix D thereof.

[3] H. A. Wheeler and A. V. Loughren, "The fine structure of television images," Proc. I.R.E., vol. 26, pp. 540–575; May, (1938). (Distortion introduced in the scanning process, the Fourier integral, relations between the amplitude characteristics and the shape of a transient pulse, bibliography.)

The uniform delay of the signal transient by the phase slope is not considered as distortion. The widening of the transient is caused symmetrically by the frequency-selective amplitude characteristics of the filter, which are essential in some form. The phase distortion, which is not essential, causes further widening and especially causes dissymmetry of the output transient. Any departure from symmetry in the reproduced image of a symmetrical object is the most obvious symptom of phase distortion.

III. The Amplitude and Phase Distortion Corresponding to a Single Echo

The method of paired echoes is here derived by reasoning from effect to cause, a procedure which is

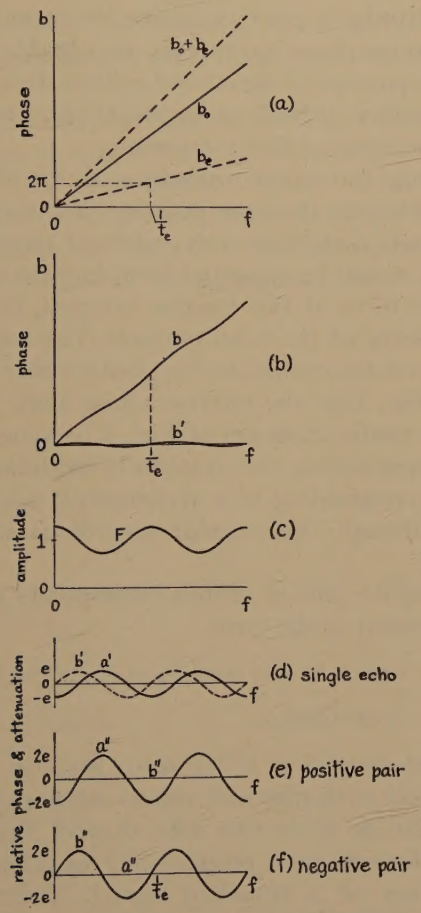

Fig. 3—The distortion of the frequency characteristics in a manner corresponding to small echoes.

increasingly common in electrical network theory. The starting point is a single echo much weaker than the main signal.[4,5]

[4] This single weak echo is the first approximation of the multiple-echo expressions of Guillemin,[5] pp. 497–498.

[5] E. A. Guillemin, "Communication Networks," vol. II, 1935, chap. XI, "The transient behavior of filters," pp. 461–507. (The Fourier integral, amplitude and phase distortion, echoes.)

Fig. 2(a) shows the amplitude and time relationship between a signal delayed by a certain length of time and an echo following slightly later. The signal amplitude is unity and the echo amplitude is e, much less than unity. The signal delay is t_0 and the further delay of the echo is t_e, both delays being free of distortion. No restrictions are placed on the signal characteristics, but it may be regarded as an instan-

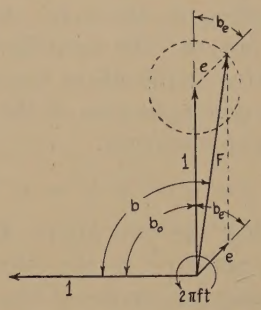

Fig. 4—The vector relations between the signal and echo components at each frequency.

taneous impulse occurring at zero time and being delayed accordingly. Such an impulse includes all frequency components in equal amplitude. In any case, each frequency component is treated individually on the basis of a steady state.

The delay of the signal and echo determines the corresponding values of phase shift at any frequency f:

$$b_0 = 2\pi f t_0; \qquad b_e = 2\pi f t_e. \tag{1}$$

These are plotted in Fig. 3(a), and are linear through the origin. The quantity more important in this discussion is b_e, the phase shift of the echo relative to the signal, depending on the relative delay t_e. The relative phase angle is 2π (one period) at a frequency equal to $1/t_e$, as indicated in dotted lines.

The signal and echo components at any frequency have the vector relations shown in Fig. 4. The entire diagram rotates at the frequency f, the angular displacement being $2\pi ft$. The relations within the diagram depend on the frequency but do not change with time during rotation. The horizontal unit vector is the input amplitude and the vertical unit vector is the main signal output with phase lag b_0. The obtuse vector e with additional phase lag b_e is the echo output.

The transmission factor expressing the resultant of signal and echo is the vector F, whose amplitude and phase lag are

$$F = 1 + e\cos b_e; \qquad b = b_0 + e\sin b_e \tag{2}$$

based on the first approximation valid for $e \ll 1$, that is, the echo much weaker than the signal. Letting a' and b' represent small values of relative attenuation

(in napiers) and relative phase lag (in radians), each much less than unity,

$$F = \exp(-a') = 1 - a'; \qquad b = b_0 + b' \tag{3}$$

in which

$$a' = -e \cos b_e = -e \cos 2\pi f t_e \tag{4}$$

$$b' = e \sin b_e = e \sin 2\pi f t_e. \tag{5}$$

These represent the distortion of amplitude and phase corresponding to the echo superimposed on the main signal output. The total distortion depends only on the relative amplitude of the echo if the total is defined as the quadratic sum of the amplitude and phase distortion components:

$$d = \sqrt{a'^2 + b'^2} = e. \tag{6}$$

This suggests that the two kinds of distortion are comparable and additive, so the tolerance of distortion should be stated in terms of the quadratic sum of both kinds.[6]

In the vector diagram of Fig. 4, the circular locus of the vector F is the same as the familiar impedance circle representing the input impedance of a transmission line with slightly unmatched resistance termination at the far end. Such a line is a perfect example of a system in which a weak echo is produced as described in the preceding discussion, by partial reflection of the signal at the far end.

Also this diagram is similar to that which shows the envelope of a carrier and a single sideband of modulation. In that case, however, the vector relations vary with time at the frequency of modulation whereas the relative positions here vary not with time but only with frequency.

In Fig. 3(b), the resultant phase curve b shows the wavy sinusoidal departure from the linear phase curve b_0 of the main signal in Fig. 3(a). The relative phase curve b' is the phase distortion corresponding to the presence of the small echo. It is noted that one cycle of fluctuation of this curve occupies a width along the frequency axis equal to $1/t_e$; that is, the frequency corresponding to 2π times the relative phase angle of the echo components.

The corresponding amplitude curve F is shown in Fig. 3(c). The relative amplitude and phase distortion are shown together in Fig. 3(d), in terms of attenuation a' (napiers) and phase b' (radians). Each oscillates between $+e$ and $-e$ while their quadratic sum is constant and equal to e, the relative amplitude of the echo.

A single echo corresponds to a combination of both amplitude and phase distortion, whereas it is desirable to be able to interpret each kind of distortion apart from the other. This is accomplished by the method of paired echoes here to be described.

IV. The Amplitude Distortion Corresponding to a Positive Pair of Echoes

Fig. 2(b) shows a pair of echoes of equal amplitudes, one before the output signal and the other after. This is called a positive pair of echoes, either in the form shown or if both amplitudes are negative. The essential characteristic of a positive pair is symmetry about the main signal. The product of the echo amplitudes is positive, hence the term "positive pair." Various physical systems are capable of yielding such a pattern of signal and echoes. It has physical significance as well as hypothetical, but that is outside the scope of this treatment.

Following the same procedure as for the single echo, it devolves that the positive pair corresponds to amplitude distortion only, without phase distortion. This would be expected from knowledge of the symmetric form of the Fourier integral, in view of the symmetry of the echo pattern. The relative attenuation corresponding to the positive pair is shown as a'' in Fig. 3(e), the relative phase angle b'' being zero. The vector diagram of Fig. 4 becomes similar to that representing the amplitude modulation of a carrier, corresponding to a symmetrical pair of sidebands, although the angular co-ordinates are not the same.

The positive pair of echoes corresponds to amplitude distortion of the form

$$\begin{aligned} a'' &= -e \cos -b_e - e \cos +b_e = -2e \cos b_e \\ &= -2e \cos 2\pi f t_e. \end{aligned} \tag{7}$$

The phase distortion b'' is zero, because the sine terms cancel with plus and minus signs of b_e and t_e.

If amplitude distortion like that of Fig. 3(e) is present, there exists a positive pair of echoes in the reproduction of a transient signal. This may be caused in any part of the system where such distortion is introduced, and all such effects are accumulative to give the final signal output transient. Naturally any compensative distortion causes cancellation of the corresponding echoes.

V. The Phase Distortion Corresponding to a Negative Pair of Echoes

Fig. 2(c) shows a pair of echoes of opposite amplitudes. This is called a "negative pair" of echoes

[6] Napiers and radians are comparable dimensionless units for the expression of attenuation and phase angle, respectively. It is unfortunate that these have separate names, because they are quantitatively identical, as is apparent in complex exponential expressions. One napier is equal to 8.7 decibels and one radian is equal to 57.3 degrees. Therefore one decibel is comparable with 6.6 degrees. The comparable units of attenuation and phase angle may be used interchangeably if desired. For example, an angle of 180 degrees may be expressed as 27.3 decibels.

because the product of the amplitudes is negative. The essential characteristic of a negative pair is skew-symmetry about the main signal.

The negative pair corresponds to phase distortion only, without amplitude distortion. This phase distortion is shown as b'' in Fig. 3(f), the relative attenuation a'' being zero. The vector diagram of Fig. 4 becomes similar to that representing the phase modulation of a carrier, corresponding to a skew-symmetrical pair of sidebands, although the angular co-ordinates are different.

The negative pair of echoes corresponds to phase distortion of the form

$$b'' = -e \sin -b_e + e \sin +b_e = 2e \sin b_e$$
$$= 2e \sin 2\pi f t_e. \qquad (8)$$

The amplitude distortion a'' is zero, because the cosine terms cancel with equal plus and minus coefficients.

If phase distortion like that of Fig. 3(f) is present, there exists a negative pair of echoes in the reproduction of a transient signal. If both amplitude and phase distortion are present, the corresponding positive and negative pairs of echoes are superimposed. Those on one side of the signal may cancel out while

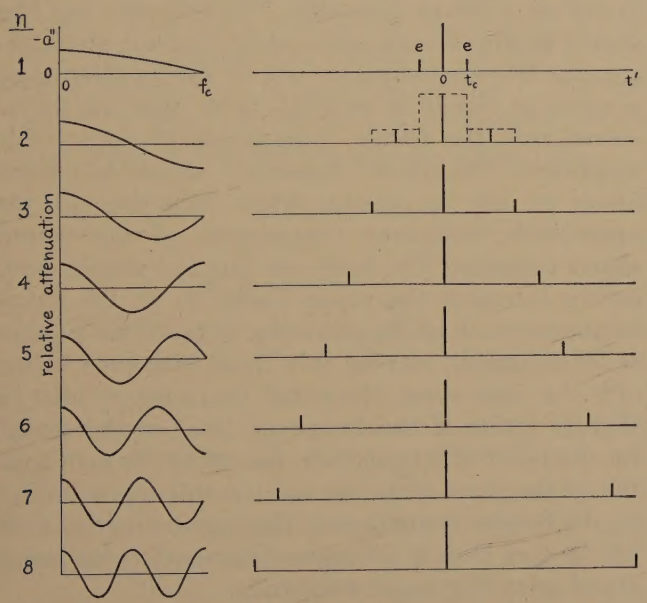

Fig. 5—Amplitude distortion and corresponding positive pairs of echoes.

those on the other side add up. The simplest example of this is the single echo with its corresponding amplitude and phase distortion shown in Fig. 3(d).

VI. The Interpretation of Amplitude and Phase Distortion in a Limited Frequency Band

In the derivation of the distortion corresponding to the various patterns of echoes, the attenuation or phase distortion curve has the same sinusoidal form over the entire frequency range, not only within a limited band. In signaling systems, however, all the appreciable frequency components of the signal transient must be within an allotted band. It is immaterial what distortion occurs outside of this band. If the

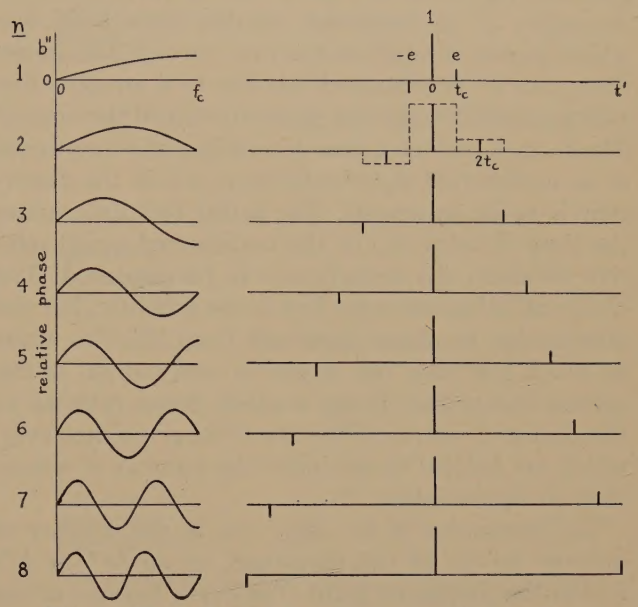

Fig. 6—Phase distortion and corresponding negative pairs of echoes.

distortion has, within the band, one of the forms described, that is sufficient to identify the corresponding pattern of echoes, just as if that form of distortion continued throughout the entire frequency range.

Any form of distortion curve which occurs within the limited frequency band occupied by the signal, can be analyzed into a Fourier series of distortion curves, each corresponding to a certain pair of echoes. The simpler forms of distortion curves can be closely approximated by one or two terms of such a series. In this manner, a small amount of amplitude or phase distortion can be readily interpreted in terms of a pattern of paired echoes. Usually this can be done in such a way that very few of the echoes are appreciable, so the detrimental effect of the distortion can be estimated on inspection of the phase curve.

Fig. 5. shows a family of attenuation curves and the corresponding positive pairs of echoes. Fig. 6 shows a similar family of phase curves and negative pairs of echoes.

In Figs. 5 and 6, a frequency band bounded by f_c is chosen, at least wide enough to include all the appreciable frequency components of the signal transient. The boundary f_c is termed the cutoff frequency,

although it may be chosen greater than the cutoff frequency of the system. Any given attenuation or phase curve, over this frequency band, is then resolved into its components.

The first step is to define the attenuation or phase distortion relative to a reference line which does not represent any distortion. The attenuation distortion a'' is measured relative to a level line which passes through the actual curve.[7] The phase distortion b'' is measured relative to a straight line which passes through the phase curve and the origin.[8] The former reference line determines the amplitude of an undistorted signal relative to which the distortion is to be measured. The latter (b_0) determines the time of delay (t_0) of the undistorted signal relative to which the distortion is to be measured. The choice of either reference line is not absolute, but the attenuation or phase departure from this line must be much less than one napier or one radian, in the system component being studied. Some rules as to the choice of reference line are to be given, however, which are helpful to minimize the number of echoes that are appreciable.

The parameter n for each row is the number of quarter waves in the distortion curve (a'' or b'') within the frequency band. The curve has one of the two forms

$$-a_n'' = 2e_n \cos \frac{n\pi f}{2f_c} = 2e_n \cos 2\pi f t_{en} \qquad (9)$$

$$b_n'' = 2e_n \sin \frac{n\pi f}{2f_c} = 2e_n \sin 2\pi f t_{en}. \qquad (10)$$

The time displacement of the echoes either side of the main signal output is then

$$t_{en} = \frac{n}{4f_c} = nt_c; \qquad t_c = \frac{1}{4f_c} \qquad (11)$$

in which t_c is called the cutoff time and is related to the width of the output signal transient. Twice this value ($2t_c$) is the nominal width (on the basis of height and area) of the narrowest transient that can be transmitted through a filter with nominal cutoff at f_c (on the same basis). This width is indicated by dotted rectangles on the second line of Fig. 5 and of Fig. 6.

Any given distortion curve of attenuation or phase is then resolved into its Fourier series of components like those shown in the left-hand column of Fig. 5 or 6. Each term of the series has a corresponding pair of echoes whose relative amplitude e_n is half the peak value of that component in (9) or (10) above, and whose time displacement t_{en} is given in (11) above. All of the echoes are plotted on a single chart to show the complete pattern.

To show the actual distortion of a signal output transient, there must be determined first what form the transient would have if the small distortion here considered were absent. This depends both on the form of the input signal transient and on the form of attenuation desired for selective purposes. If the input transient is symmetrical, the undistorted output is also. Having determined the form of the output transient in the absence of the undesired distortion, the effect of this distortion is shown by drawing in all the echoes of this same form and adding the ordinates. The resultant transient form includes the distortion effects.

Since amplitude distortion of all kinds at once is readily taken into account by the Fourier integral, symmetrical in the absence of phase distortion, the method of paired echoes is most valuable in the interpretation of phase distortion. The reference line (b_0) should be drawn with such a slope that the phase departure (b') approximates one of the Fourier components as closely as possible, or at least can be resolved into the fewest components of appreciable amplitude. The cutoff frequency f_c should be chosen about as low as possible while including all the appreciable frequency components of the output signal transient. The reference line (b_0) should preferably intersect the phase curve (b) at the cutoff frequency so all of the odd-order terms of the Fourier series disappear, leaving only those with even values of n. In some cases, the cutoff frequency f_c may be slightly inside of the frequency band of the signal, for the point of intersection, providing the continuation of the phase curve beyond f_c is still approximated by the Fourier components. This approximation need not be very close if the higher-frequency components are of relatively small amplitude.

Some general rules may be stated as to the distortion effects to be expected from a given curve of relative attenuation or phase. The echo amplitudes are proportional to the amount of distortion, and their time displacement from the main signal output is proportional to the number of peaks and valleys in the curve, or to the maximum slope. The center of gravity of the signal output transient is displaced in time by the amount of delay represented by the initial phase slope at the origin.

[7] The reference line for attenuation may be, instead of a level line, a curve representing a desired form of attenuation in that part of the system.

[8] This is the condition in a low-pass system. It may be modified to suit the different requirements found in any given band-pass example.

VII. A Practical Example of Phase Distortion Interpreted in Terms of Paired Echoes

Fig. 7(a) shows the amplitude curve and Fig. 7(b) the phase curve of a filter whose properties are illustrative of some practical circuits. The former curve has a gradual cutoff at the cutoff frequency f_c and the latter a maximum slope at the same frequency. The amounts are representative of a low-pass filter having about four sections and having much dissipation to secure gradual cutoff.

Fig. 8(a) shows the symmetrical transient output of such a filter, in response to an instantaneous impulse, assuming zero phase shift. This and Fig. 7(a) are neither exact because both have a small but negligible amplitude outside the limited range of the curve shown.[9]

The reference line for phase distortion, b_0 in Fig. 7(b), is chosen to intersect the phase curve b at the cutoff frequency f_c. The relative phase is shown separately as b', whose peak value is 1/2 radian. This corresponds to the second row of Fig. 6, $n=2$, with $e=-1/4$. Therefore there is a negative pair of echoes as shown in Fig. 8(b), each having one fourth the amplitude of the main signal output. The final form of the output transient is obtained by drawing in the echoes, each having the same shape as the main signal output, and summing the ordinates as shown in Fig. 8(c). It is plotted against t', the time relative to the uniform delay t_0 represented by the phase slope of the reference line b_0 in Fig. 7(b).

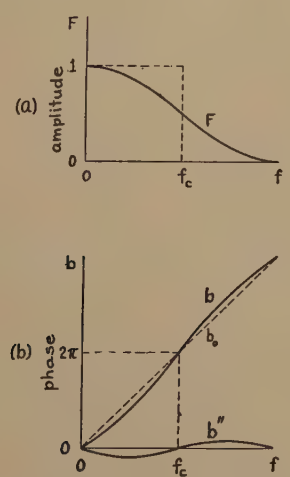

Fig. 7—The frequency characteristics of an illustrative example.

This example shows clearly the effect of phase distortion in disturbing the symmetry of the output transient, and in adding to its duration. The method of paired echoes establishes a convenient relation between the phase curve and the resulting distortion, in such a manner that the nature of the distortion can be seen by inspection of the curve.

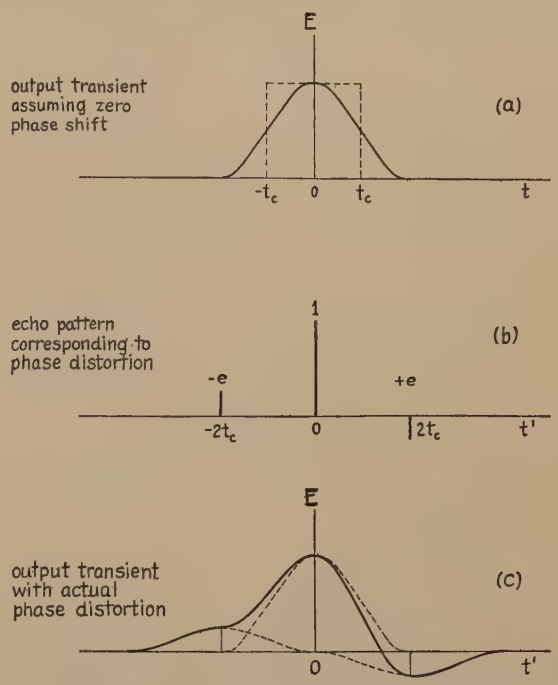

Fig. 8—The application of the method of paired echoes to evaluate the effects of the phase distortion shown in Fig. 7.

VIII. Echo Patterns Corresponding to Various Forms of Amplitude Distortion

It is desirable to gain familiarity with various forms of amplitude and phase distortion, and how they affect the shape of the output signal transient. It is with this aim that the examples of this and the following sections are to be described. They are selected with a view to demonstrating the variety of applications of the method of paired echoes, and also its limitations.

Figs. 9 to 11 show a number of amplitude curves with corresponding echo patterns. The echoes are related only to the small amount of amplitude distortion indicated for each example. The shape of the output transient depends also on the shape of the "undistorted" signal output. That is the shape the signal output would have if the amplitude curve and the input transient had the most desirable form. It is immaterial how the amplitude characteristics are divided between the frequency spectrum of the input transient and the frequency characteristics of the intervening system.

In the examples to be described, not only is the echo pattern shown but also the shape of the output transient is drawn. The latter is, in every case, based

[9] In Fig. 6 of footnote reference (3), the shape of these curves is described as the "cosine-squared" form. There it is shown that an amplitude curve of this shape leads to an output transient of substantially the same shape, or vice versa.

on an assumption as to the resultant amplitude curve of the input transient and the intervening system. In most cases, and unless otherwise stated, the conditions of Fig. 9(a) are taken as the standard of reference. The light curve F is the amplitude spectrum of the assumed "undistorted" output transient. It rep-

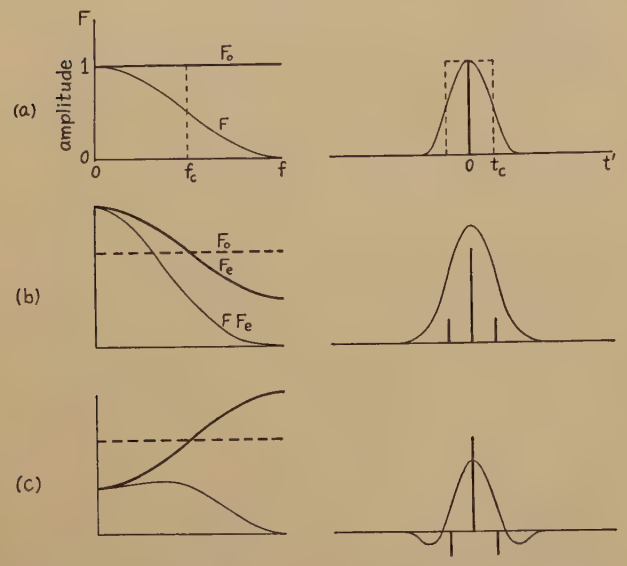

Fig. 9—First-order amplitude distortion and corresponding echo patterns.

resents [illegible]ial cutoff of the higher-frequency compone[illegible] shape of this curve may depend entirely on the shape of the input transient, with uniform transfer of all components through the system, according to the level heavy line F_0 in Fig. 9(a). Any distortion of the line F_0 would then represent the departure from uniform transfer through the system. An input transient of cosine-squared shape would have such attenuation of its higher-frequency components as to yield approximately the cosine-squared shape of curve F. On the other hand, the shape of this curve may represent only the desired gradual cutoff in the system. The input transient would then have to be a sharp impulse, which has components of uniform amplitude over the frequency range passed by the system.

In general, curve F in Fig. 9(a) represents the combined attenuation of higher-frequency components in the input transient and the intervening system, assumed for the purpose of defining a convenient shape of "undistorted" output transient. This curve, and therefore the output transient, have approximately the cosine-squared shape, as shown. The nominal cutoff frequency is f_c, equal to the width of a rectangle having the same height and area as the curve F. The "undistorted" output transient has the nominal width $2t_c$, which is the width of the dotted rectangle of the same height and area as the transient curve. This curve is centered at the time t_0, the uniform delay of the system in the absence of distortion, and is plotted against the time t' measured relative to t_0.

The level line F_0 in Fig. 9(a) indicates that the distortion is zero relative to the standard of reference which is curve F. In the following examples, as in Fig. 9(b), the curve F_e shows, relative to F_0, a "small" amount of amplitude distortion. It is this distortion whose effect is shown by the echo pattern in each case. The modification of curve F is shown also as FF_e, distorted in accordance with the factor F_e. This modified curve is the over-all amplitude curve of the input transient and intervening system, so it is the amplitude spectrum of the output transient drawn in for example.

With this introduction, Fig. 9(b) and (c) shows the echo patterns for the simplest case of amplitude distortion. It is the case of $n=1$ in Fig. 5. The peak distortion is $\pm 1/2$ radian (drawn approximately to scale) so the relative amplitude of each echo is 1/4. The positive pair of echoes has positive polarity in Fig. 9(b) and negative in (c). The former corresponds to more gradual cutoff at a lower frequency, curve F, so the output transient becomes wider. The latter corresponds to sharper cutoff at a higher frequency, so the output transient becomes narrower and its sides steeper.

The simple example of Fig. 9 is given mainly to illustrate the scheme of presenting amplitude distortion. Echo pairs of odd order ($n=1, 3$, etc.) are not needed and usually are better avoided in the study of distortion in the frequency band between zero and the nominal cutoff frequency. If there are appreciable components at higher frequencies, then odd-order pairs may be needed, but then it is usually better to select a higher value for the cutoff frequency. In these examples, the higher-frequency components are small so their distortion is of minor importance, but theoretically the curve F_e has to represent the actual distortion out to $2f_c$.

Fig. 10 shows the echo patterns for the most useful simple case of amplitude distortion, the case of $n=2$ in Fig. 5. The amplitude curve slopes downward in (a) and upward in (b), relative to the desired shape. The effect is similar to that of Fig. 1(b) and (c), respectively. Fig. 10(c) remains to be described in Section X.

The examples of Fig. 10 show the great advantage of using only the even-order pairs of echoes. The echoes being further separated, the corresponding transients overlap much less. The dotted rectangles of Fig. 10(a) show the nominal width of the tran-

sients, $2t_c = 1/2f_c$. The separation of the echoes is equal to this nominal width. In the case of the "cosine-squared" gradual cutoff here assumed as the standard of reference, the overlapping is confined to the space between the peaks in the echo pattern. Therefore the curve of the resultant output transient passes through the echo peaks. This relation makes the echo pattern especially valuable as an aid in visualizing the distortion of the output transient. The echo pattern of Fig. 10(b), even before drawing the curve, shows that one napier increase of amplitude in the pass band causes adjacent reversed pulses whose relative amplitude is 1/4.

The presence of sharp discontinuities in the curve of relative distortion (F_e) corresponds to the sum of many echo components. Fig. 11 shows such an example, having a step of $\pm 2c$ at the nominal cutoff frequency. This distortion curve is resolved into a Fourier series (see Appendix B) of odd-order cosine terms. Each of these terms has its corresponding pair of echoes. The resulting echo pattern is shown. There is a transient oscillation on each side which is damped hyperbolically, that is, the echoes decay in amplitude in the inverse ratio of their separation from the center. The first echo on each side has an amplitude of $2c/\pi$. The diagrams are drawn for $c = \pm 1/2$ radian, or a step of one radian.

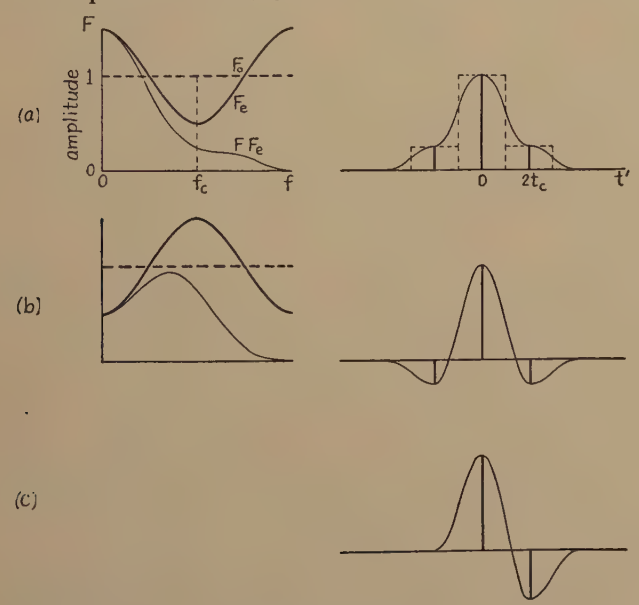

Fig. 10—Second-order amplitude distortion and corresponding echo patterns.

Carrying this example to the extreme, it becomes a complete sharp cutoff at f_c. This extreme is beyond the scope of the method of paired echoes, but is shown in Fig. 11(c) for comparison.[10] It also has oscillations damped hyperbolically. They are of greater amplitude but otherwise similar to those of Fig. 11(a) and the reverse of those of (b).

Further examples of amplitude distortion are deferred to Section X.

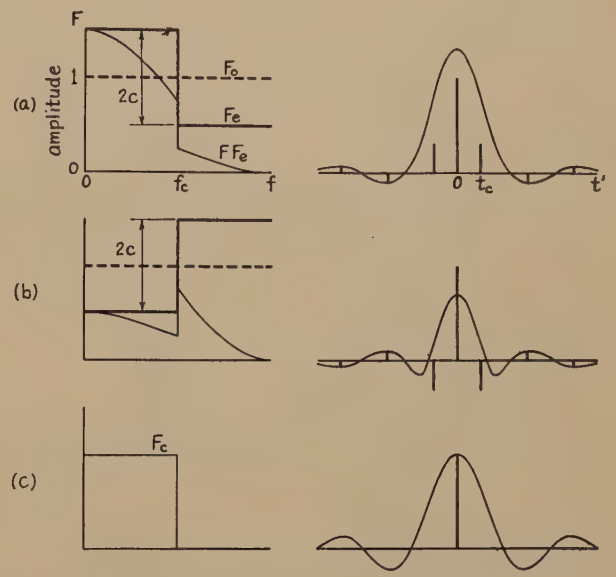

Fig. 11—The amplitude step and corresponding echo patterns.

IX. Echo Patterns Corresponding to Various Forms of Phase Distortion

The standard of reference in the case of phase distortion is less arbitrary. This is one reason why the method of paired echoes is more useful as applied to phase distortion than as applied to amplitude distortion. The main reason, however, is the greater difficulty of applying other methods to phase distortion.

A straight line through the origin is the standard of reference. This represents uniform delay of all signal components, that is, phase displacement proportional to the frequency. It is arbitrary to the extent that its slope is not uniquely determined. The slope is so chosen that the straight line has some points in common with the actual phase curve, and perhaps as many points as possible. The echo pattern depends on the chosen slope in the same manner as any equation depends on the choice of co-ordinate axes. Therefore the slope is chosen with the aim of securing the simplest echo pattern, unless there is some other objective in view.

It is generally preferable to choose the slope so the straight line and the phase curve intersect at the cutoff frequency. Alternatively, the straight line may may be drawn first, and then the nominal cutoff frequency chosen at an intersection which occurs near the cutoff frequency. The advantage of this relation

[10] Its response to a step of driving force is given by Guillemin, footnote reference (5). Its response to an impulse is given in Appendix D of footnote reference (3).

is the avoidance of odd-order pairs of echoes. This assures more space between echoes with less overlapping, as described above. It is also likely to minimize the number of echoes required to approximate the distortion.

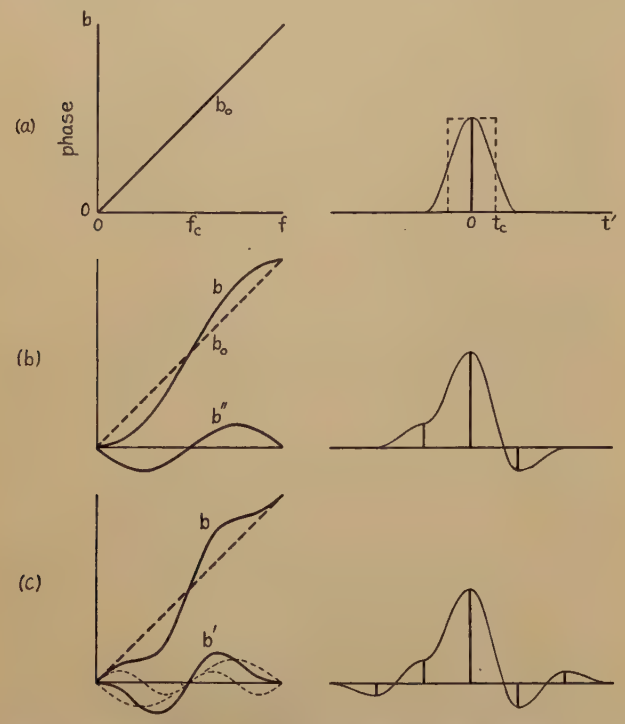

Fig. 12—Second-order and fourth-order phase distortion and corresponding echo patterns.

The reference line b_0 in Fig. 12(a) has a slope corresponding to a uniform delay t_0. It is relative to this delay that the distortion is to be determined, so it is to be plotted in terms of the relative time t'. The slope of this line and the choice of the nominal cutoff frequency together determine what echo pattern is obtained for a given phase curve. In order also to show a sample wave form of the output transient, the "cosine-squared" amplitude curve of Figs. 7(a) and 9(a) is asumed unless otherwise noted. The resulting "undistorted" output transient is shown in Fig. 12 (a), with the nominal width $2t_c$ indicated by the dotted rectangle.

Fig. 12(b) shows the simple case of $n=2$ in Fig. 6, exemplified also in Figs. 7 and 8. The actual phase curve is b, and the relative phase distortion is b'' from which the pair of echoes is determined. If the peak distortion is $\pm 1/2$ radian, the amplitude of each echo is 1/4 as shown.

It is a usual property of filters to have maximum phase slope at the cutoff frequency, so these examples are chosen with this property. The introductory example of Fig. 1, however, differs from most filters in this respect. It has such gradual cutoff that the phase slope is maximum at zero frequency. Therefore the tendencies of the phase distortion in Figs. 1 and 9(b) are opposite. In Fig. 1(d), the output transient has maximum slope on its entering edge, while in Fig. 12(b) it has maximum slope on its trailing edge. The example of Fig. 1 could have its phase distortion analyzed in terms of paired echoes, but many echoes would be required, closely spaced, in view of the appreciable frequency components of the higher frequencies causing the sharp rise of the entering edge. The resulting curve of output transient would be rough because each component would have the pointed shape of Fig. 1(c). It is apparent that the method of paired echoes is more useful where the higher-frequency components are small beyond the nominal cutoff frequency f_c and negligible beyond $2f_c$.

Fig. 12(c) shows an example having two pairs of echoes, with maximum phase slope at the cutoff frequency and a lesser maximum at zero. The tendency is toward this shape when simple phase correction is used, such as the m-derived filter with m greater than one. The pairs of echoes are those of $n=2$ and 4 in Fig. 6. The peak values of the components of the phase distortion b' are respectively 1/2 and 1/4 radian, so the amplitudes of the echoes are, respectively, 1/4 and 1/8. These echoes are the first two pairs of the next example, which has many pairs.

In Fig. 12(c), the phase curve would in practice tend to level off at higher frequencies. The difference between this and the upward trend shown at $2f_c$ is not important, since it occurs only at the higher frequencies of the very weak signal components. An exact analysis would require very weak odd-order echoes to take this difference into account.

Since the tendency is toward a maximum slope of the phase curve occurring at the cutoff frequency, it is interesting to pass to the limit of infinite slope. This amounts to a step in the phase curve, as shown in Fig. 13(a). Even though this is an extreme case requiring an infinite series of echoes for its exact interpretation, it leads to only a nominal amount of distortion of the signal transient, comparable with that of Fig. 12(c). The echo pattern is derived in Appendix B by resolving the relative phase curve b' into its Fourier series of sine terms. It represents an oscillation with hyperbolic damping. That is, the echo amplitudes are inversely proportional to their separation from the center. If the step in the phase curve has a height of $2c'$, the peak value of the phase distortion is $\pm c'$ and each echo of the first pair ($n=2$) has the amplitude c'/π. The transient curve is drawn for peak distortion of $\pm 1/2$ radian and echo amplitude of $1/2\pi$ in the first pair.

This case of a step in the phase curve is of unu-

sual value in comparing the effect of small distortion, treated in terms of paired echoes, with that of large distortion, treated directly by means of the Fourier integral. In Fig. 13(b), the phase curve b has a step of π radians, which is greater than can be treated by the simple use of paired echoes. However, it may be regarded not as phase distortion but rather as a reversal of amplitude. A secondary reference curve of phase is taken as b_0'. The upper part of the phase curve is lowered into the new reference curve, relative to which the phase distortion disappears.

The step taken out of the phase curve is replaced by a reversal in the amplitude curve. The modified amplitude curve is shown in Fig. 13(c) for this example. The new curve F having much less net area than the original, the nominal cutoff frequency is reduced to $f_c' = (2/\pi)f_c$. This means a widening of the output transient to a nominal width of $2t_c' = (\pi/2)2t_c = \pi t_c$. Therefore, in this case, the simplest effect of the step in the phase curve is the widening of the output transient.

Since the distortion can be expressed entirely in terms of amplitude distortion, as in Fig. 13(c), it

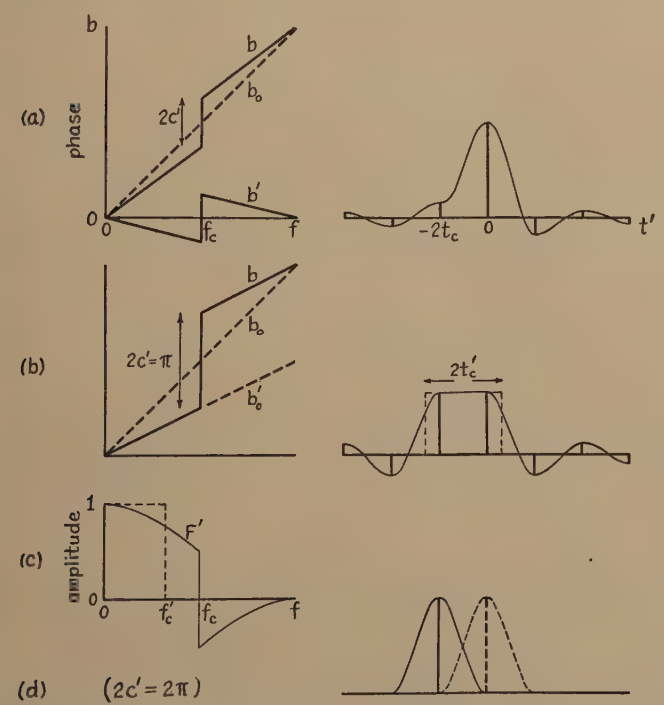

Fig. 13—The phase step and corresponding echo patterns.

follows that the output transient must be symmetrical. However, its center of symmetry is located not by the primary reference curve b_0 but rather by the secondary reference curve b_0' of Fig. 13(b). The difference of their slopes determines a phase difference of $\pi/2$ or 1/4 period at the cutoff frequency f_c, which is a time difference of t_c. Therefore the center of the symmetrical pulse has a delay which is less than that of the primary reference curve by the amount of t_c.

The shape of the output transient is derived from the amplitude curve F of Fig. 13(c) with the aid of the symmetric Fourier integral in Appendix B. This incidentally determines the echo spectrum because the location of the echoes is known on the same basis

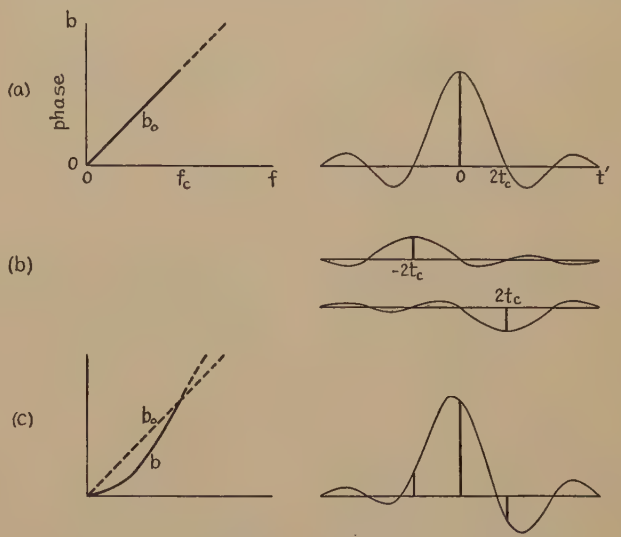

Fig. 14—The combined effects of sharp cutoff and phase distortion.

as in Fig. 13(a). Merely increasing the amount of distortion does not change the positions of the echoes, although it disturbs their skew-symmetry, as remains to be shown further in Section XI. In this case, the "center" component of the output signal is reduced and the next preceding echo becomes equal to it. Their amplitude is $2/\pi$ as compared with unit amplitude of the center component in Fig. 13(a).

The same procedure is applicable to a step of any multiple of π in the phase curve. Fig. 13(d) illustrates a step of 2π. This is really not distortion at all, because a phase shift of 2π cannot be detected. This is merely a logical extension of the preceding case. The output transient has twice the displacement from the "center," which is $2t_c$. The center component has disappeared, as have all the echo components except the one which has become the single remaining component. The center component would appear as shown in dotted lines, if the phase distortion were absent.

The step in the phase curve represents distortion only of the frequency components beyond the nominal cutoff frequency f_c at which the step occurs. If such components were absent, the reference phase slope would be chosen to coincide with the phase curve in the pass band, and no phase distortion could be detected. This appears clearly in Fig. 13(c), where

the reversal of amplitude would have no effect in the absence of higher-frequency components.

In general, the output transient may have any form, symmetrical or not, before taking into account the phase distortion under consideration. Fig. 14 illustrates the method of paired echoes as applied to

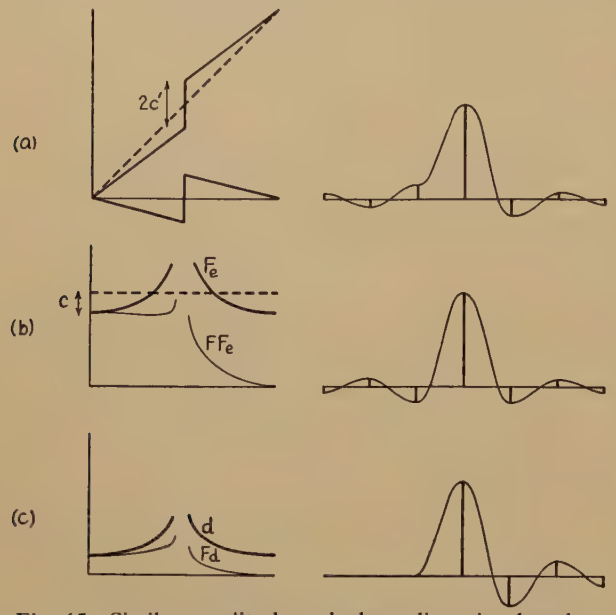

Fig. 15—Similar amplitude and phase distortion based on hyperbolic damping of the echoes.

an extended transient with oscillations on both sides. The amplitude curve is assumed uniform ($F=1$) below the cutoff frequency f_c, and zero above. The amplitude curve and therefore the undistorted output transient are those of Fig. 11(c), the latter being shown for reference also in Fig. 14(a). Simple phase distortion and the corresponding echo pattern are shown in Fig. 14(c), and are similar to those of Fig. 12(b). The curve of the output transient (c) is obtained by adding together the undistorted curve (a) with the echo curves (b) of the same shape. In spite of the complex shape of the undistorted transient and the echoes, the resulting curve in this case passes through the points of all the components of the echo pattern.

Further examples of phase distortion, with the similar examples of amplitude distortion, are to be described in the next section.

X. Similar Forms of Amplitude and Phase Distortion

There are some related forms of amplitude and phase distortion which, if they are both present in equal amounts, cancel out on one side of the output transient and add together on the other side. In practice, it is more common for the output transient to trail off after the main pulse, than for it to precede the main pulse. This is especially true of filters which do not have phase correction.[11,12] Therefore, forms of distortion which lead to this result are of special interest, because they seem more likely to occur in practice.

The simplest examples of similar amplitude and phase distortion are those of Figs. 10(b) and 12(b) each having a single pair of echoes. If the distortion of each kind is small, so echoes of echoes are negligible, the two echo patterns may be superimposed by simple addition. The result is shown in Fig. 10(c), where the preceding echoes are canceled and the trailing echoes are added. This degenerates into a single echo instead of a pair of echoes.

Just as in the case of a single echo, there appears a theorem that echo patterns appearing entirely on one side are the result of combined amplitude and phase distortion in equal amounts. The equality of amounts is true, in general, only if the echoes are much weaker than the main signal. The similar forms of amplitude and phase distortion to be described are merely those which, in small amounts and in combination, lead to patterns of single echoes on

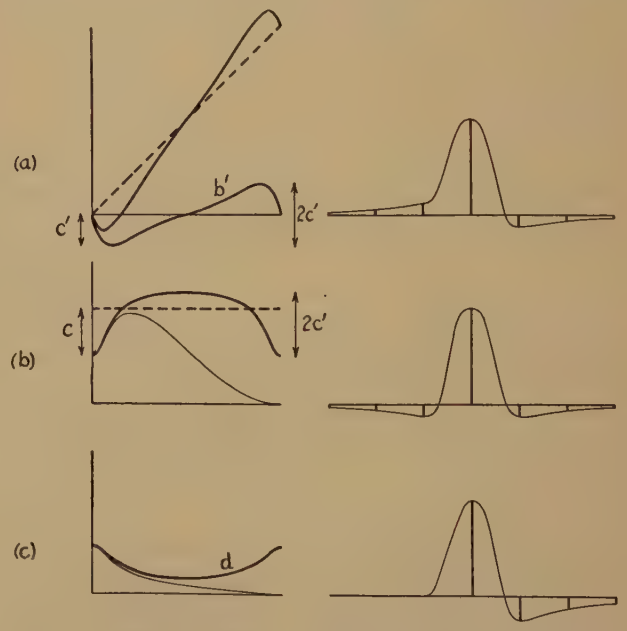

Fig. 16—Similar amplitude and phase distortion based on exponential damping of the echoes.

one side, instead of pairs of echoes on both sides. The examples are chosen to result in echoes on the trailing side only. They are selected to indicate a variety of

[11] Carson and Zobel[12] show the indicial admittance of constant-k filters; the response to an impulse is indicated by the slope of the indicial admittance.

[12] J. R. Carson and O. J. Zobel, "Transient oscillations in electric wave filters," *Bell Sys. Tech. Jour.*, vol. 2, pp. 1–52; July, (1923).

forms and to give information of value in the study of tolerances.

The next example of similar amplitude and phase distortion is based on a step in the phase curve, described with reference to Fig. 13(a) and shown for comparison in Fig. 15(a). The step causes transient oscillations before and after the signal, with hyperbolic damping. They are skew-symmetrical, since caused by phase distortion. There is developed in Appendix B the form of amplitude distortion which leads also to oscillations with hyperbolic damping, but symmetrical instead of skew-symmetrical. It has a narrow, sharp peak at the cutoff frequency. This form of amplitude distortion and its echo pattern are shown in Fig. 15(b). The combination of this amplitude distortion with the step in the phase curve causes the preceding oscillations to cancel out, leaving only the trailing oscillations with double amplitude as shown in Fig. 15(c). The total distortion d is also shown, which is the quadratic sum of amplitude and phase distortion.

Fig. 16 is derived in Appendix B on the basis of exponential damping of the echoes on either side. This could be secured by a resonant peak or valley in the amplitude curve, at either the cutoff frequency or zero. A valley at zero frequency is the case shown, as in Fig. 16(b). The phase curve and its echo pattern are shown in Fig. 16(a) and the amplitude in (b). The one-sided echo pattern in (c) results from the combination of (a) and (b). This is the type of distortion caused by attenuation of very low frequencies, as in the coupling condenser of a resistance-coupled amplifier. If the valley of the amplitude curve is below the reference line and the ratio of damping from one echo to the next is 1/2, the corresponding maximum of amplitude distortion is $c=1/2$ and of phase distortion is $c'=1/3$, the echoes of the first pairs have an amplitude of 1/8, and the first echo in Fig. 16(c) has an amplitude of 1/4 as shown.

An especially interesting case is that of Fig. 17, in which there are any number of echoes of the same amplitude. The phase and amplitude curves are derived in Appendix B. They are shown in Fig. 17(a) and (b) for the case of four echoes on each side, of alternating polarity. The amplitude curve is shown in terms of relative attenuation $-a'$, or departure from unity amplitude. The total number of peaks and valleys in the pass band (zero to f_c) is equal to the number of echoes on each side. The amplitude distortion yields also a zero-order echo as indicated. The combined effect of this phase and amplitude distortion is the one-sided echo pattern of Fig. 17(c), by which there is shown a curve of total distortion d, which is the quadratic sum of amplitude and phase distortion. The dotted curves on the left side show the envelopes of the distortion curves for any number of echoes. If the envelope curves have a minimum spread equal to 1/4, the echoes of each pair have an

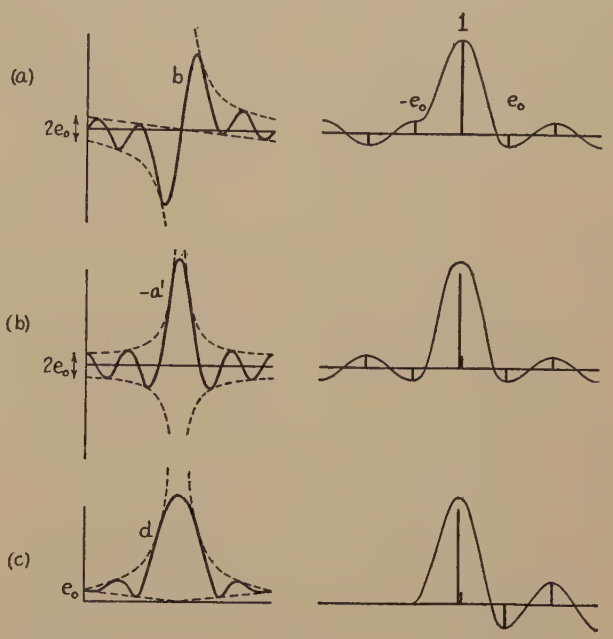

Fig. 17—Similar amplitude and phase distortion based on a number of equal echoes.

amplitude of 1/8, while the single echoes of Fig. 17(c) have an amplitude of 1/4.

The three examples of Figs. 15 to 17 illustrate three forms of damping of the echoes; hyperbolic, exponential, and none at all. The first requires a discontinuity in the distortion curves which may be roughly approximated in practice, but is mainly of theoretical interest. The second requires a peak or valley of the shape of a resonance curve, which is commonly found in practice. The third requires alternating peaks and valleys such as might be found in a circuit of many elements, perhaps including networks for the compensation of a large amount of distortion.

There are four variations of each example, which may be identified with reference to the amplitude curves. The distortion may appear as a peak or a valley, which may be at zero frequency or at the nominal cutoff frequency. If it is a peak, the second echo after the signal ($n=4$) has positive amplitude, and conversely, if a valley, negative. The transient has its natural frequency equal to the frequency at which the peak or valley occurs. If it is at zero frequency, the echoes on each side are all of the same polarity as in Fig. 16, but if it is at the cutoff frequency, they are of alternating polarity as in Figs.

15 and 17. In practice, a peak or valley at zero frequency, or a peak at the cutoff frequency, are common, but a valley at the cutoff frequency is unusual.

The phase distortion is here treated in terms of its angular magnitude, rather than in terms of its slope or time of delay. The slope of the relative phase curve is the departure of the phase slope from its reference value, namely, the slope of the reference curve. The phase distortion in terms of slope has some direct significance worthy of mention. The

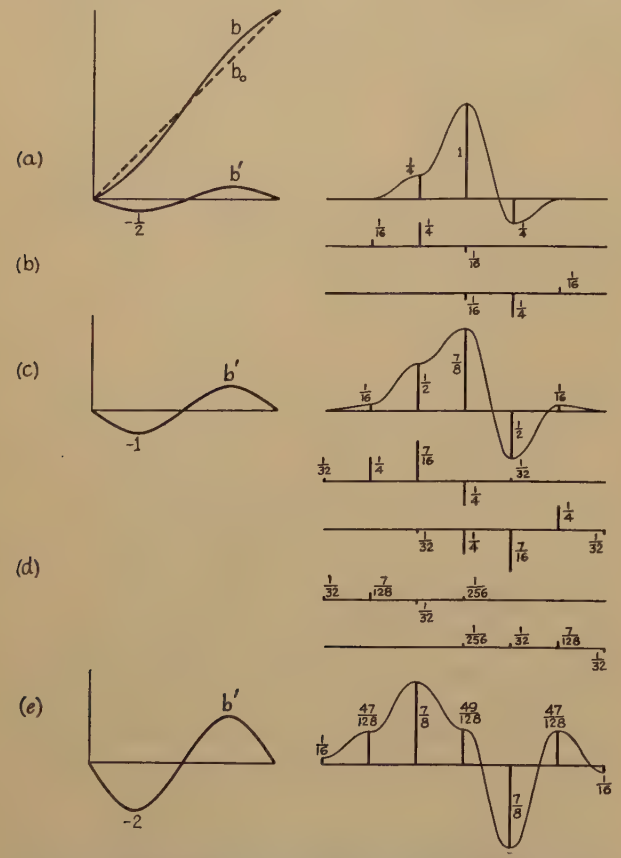

Fig. 18—The evaluation of large distortion by successive applications of the method of paired echoes.

phase slope at the origin determines the delay of the "center of gravity" of the output transient, because the phase angle of the low-frequency components depends mainly on the center of gravity. If it differs much from the average slope, the output transient has very unsymmetrical distortion.

XI. The Evaluation of Large Distortion by Successive Applications of the Method of Paired Echoes

The method of paired echoes is theoretically valid only for small distortion, much less than one napier or one radian, because of the simplifying assumptions in its derivation. The simple addition of the effects of amplitude and phase distortion is likewise limited in its application. There remains to be shown how much error is incurred in its use on moderately large distortion, and also how its use may be extended to very large distortion.

The application of this method to a large amount of amplitude distortion is of doubtful utility. The successive applications to be described are likely to be more laborious than the simple application of the symmetric Fourier integral, which is not difficult and is adapted for any shape of distortion curve. Therefore the application to large distortion is to be illustrated on phase distortion, where the utility is greater and extreme distortion such as the cutoff characteristic is absent.

A large amount of distortion may be subdivided into small parts, and each part treated individually. Each part may be made small enough to fall within the scope of the method of paired echoes. Then the distortion of the respective parts may be combined, just as if it occurred in different parts of the system. In terms of echo patterns, each individual echo caused by one part of the distortion is spread out into a complete pattern of echoes caused by another part of the distortion. If the two parts are alike, this shows the effect of doubling the amount of distortion of any form. If the echoes of each pattern are very small, as assumed in deriving the method, the subechoes are so much smaller as to be negligible. They became appreciable, however, if the total distortion is comparable with one napier or one radian, or larger. It is in such cases that successive applications of the method are needed to yield the echoes of lesser magnitudes.

Fig. 18 shows an example of the successive applications in the case of a simple form of phase distortion, that of Fig. 12(b). Fig. 18(a) shows this form of phase distortion with a peak value of 1/2 radian, and its pattern of one pair of echoes, each with an amplitude of 1/4.

Double this amount of distortion is evaluated by a second application of the method. In the first application, the original signal had only the central component of unit amplitude. This became three components as in Fig. 18(a). In the second application, these three components are taken as the input signal. The distortion superimposes two echoes of this signal, each having similar three components as in Fig. 18(b). The sum of the signal (a) and the pair of echoes (b) is the signal output (c) corresponding to phase distortion with peak value of one radian as shown.

The result of two successive applications of the method is not very different from the result of a

single application on the basis of double the amount of distortion. The pattern of Fig. 18(c) has five components of amplitudes 1/16, 1/2, 7/8, −1/2, and 1/16. A direct application of the method would have yielded three components of amplitudes 1/2, 1, and −1/2. The maximum difference is 1/8, which is of secondary importance. It is concluded that the method gives directly a rough approximation for phase distortion of peak value up to one radian. The approximation can be shown to be very close (within 1/32) for a peak value up to 1/2 radian, as in Fig. 18(a). Therefore, the practical utility of the method in its simplest form is not limited to extremely small distortion.

The third successive application is based on the pattern of Fig. 18(c) as the input signal. Each echo in this pattern is likewise expanded in a similar pattern as shcwn in (d). The resulting signal output transient is obtained by the addition of (c) and (d) to secure the pattern of (e). (Not all of the lesser and more remote echoes are shown.) This corresponds to a peak distortion of 2 radians as indicated. This amount is entirely beyond the scope of a single application of the method, because one of the echoes becomes the main component and there is great departure from skew-symmetry of the echo pattern.

Successive applications of the method appear to be useful and not too laborious in evaluating fairly large distortion. The result is merely a more complex pattern of echoes, not all related in pairs. The method is still independent of the shape of the "undistorted" output transient. The original spacing of echoes, in this case, is retained in the final pattern. This is generally true where the relative phase angle is zero at the nominal cutoff frequency, so only even-order echoes are present.

Theoretically, the echo pattern or the Fourier components of phase distortion or both have the form of an infinite series. This exact theory is outside the scope of this treatment because it departs from the simplicity of the method of paired echoes.

XII. The Tolerance of Distortion in Picture Transmission

It is relatively easy to specify the tolerance in terms of permissible amplitude of echoes, which appear as spurious lines, edges, or shadows in a picture. This manner of specification may be sufficient in some cases, since any actual distortion in terms of attenuation and phase can be resolved into its echo pattern by the method of paired echoes.

There are some objects which are unusually sensitive to distortion of the frequency characteristics. These are objects which have repetitive lines or edges close together in the horizontal direction. The resulting signal has its power distribution unusually concentrated in the higher part of the frequency range, whereas the average power distribution is very much concentrated in the extreme lower part. Objects of this type might be disregarded for the reason that their probability of occurrence is very small, except in resolution charts designed to be sensitive to distortion. However, it is well to note how the nature of such an object increases the effect of some echo patterns more than that of others.

If several vertical lines are spaced equally by such a pitch that each line image is augmented by the echoes of other lines, the sharpness of definition is augmented, which in itself is not objectionable. If there are many echoes, however, the undesirable echoes in the image, outside of the group of lines, are also augmented. The relative accentuation of the echoes, which are small for one line alone, is much greater than that of the line images. The fewer the echoes of each line, or the greater their rate of damping, the less they can accumulate outside the group of line images. If the echoes in the pattern for one line have hyperbolic damping, as in Fig. 15, the augmentation of the image lines increases indefinitely with the number of lines in the group. This case can only be approximated in practice, where there is always a definite limit on this process of building up by echo summation. The exponential damping in Fig. 16 or the limited number of echoes in Fig. 17 is possible in practice, with a limit on the amount of augmentation. The amplitude step of Fig. 11 is a special case of hyperbolic damping, in which the augmentation of the desired image lines increases by a limited amount with the number of lines, but that of the echo lines increases gradually without limit. This case is approximated in practice by a sharp cutoff, which is known to cause great accentuation of the echo lines adjacent to a group of lines such as used in resolution charts.

Though useful, the statement of tolerance in terms of echoes is indirect. Some general rules are desired to link the echo amplitudes with the amplitude and phase distortion. It is shown at the end of Appendix B, that the total distortion (the quadratic sum of the amplitude and phase distortion in napiers and radians) is related with the quadratic sum of the echo amplitudes. The quadratic mean of the total distortion, taken over the frequency range, is equal to the quadratic sum of the echo amplitudes,

$$\sqrt{\overline{d^2}}=\sqrt{\overline{a'^2+b'^2}}$$
$$=\sqrt{2e_1^2+2e_2^2+\cdots+2e_1'^2+2e_2'^2+\cdots}. \qquad (12)$$

The mean-squared distortion over the frequency range is $\overline{d^2}$. The echo amplitudes are e_1, e_1', etc.

It appears that the echoes are individually weaker if the amount of distortion is divided among a larger number of echoes. A large amount of distortion may be tolerable if it is divided among a large number of

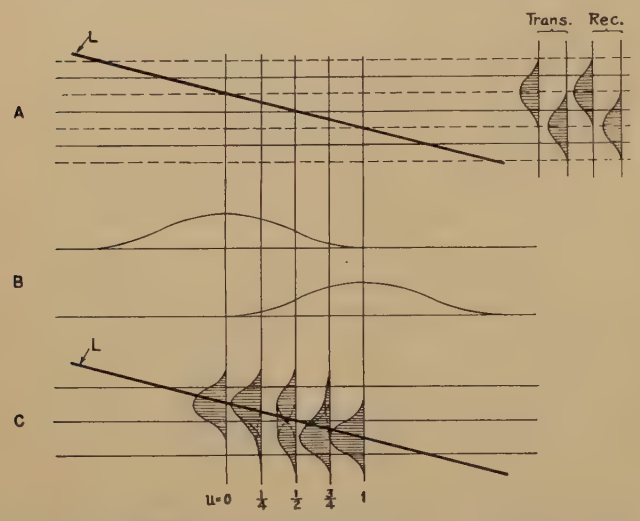

Fig. 19—The distortion of a line image, which is inherent in the scanning process.

echoes, each one sufficiently weak. This is exemplified in Fig. 17, in which there are a large number of echoes of the same amplitude. The amount of distortion is large in terms of amplitude and phase, and in terms of their quadratic sum. An equal amount of distortion concentrated in one echo would be much more detrimental. It is impossible to state definitely that a given amount of distortion is excessive unless it is known how it is to be divided among the echo components.

It is possible to state that a small amount of distortion is definitely permissible if that amount is tolerable concentrated in a single echo. In this case, the tolerance of distortion is of the order of 0.1 napier or radian. This small a value for the entire system is chosen because the single echo may be separated from the desired signal sufficiently to fall in a different region of the picture. An echo as weak as 0.01 might be visible in the picture under extreme conditions of a very bright object on a very dark background.[13]

The tolerance of distortion is related with the amplitude characteristics of the entire system, including the frequency distribution of components in the picture input signal. The latter being indefinite, it cannot be counted on with certainty but may be included if only the reasonable probability of distortion is to be evaluated. It is logical that weaker components, such as near the cutoff frequency, would be subject to greater tolerance of relative attenuation and phase shift. It can be stated with confidence that the tolerance is inversely proportional to the relative amplitude of signal components, assuming that spurious components are equally visible at all frequencies. This assumption is not far from the facts, although components of very low and very high frequencies are somewhat less apparent in the image.

To take into account the amplitude characteristics, the distortion in terms of attenuation and phase is multiplied by the amplitude factor. The product Fd is called the "weighted distortion." Tolerance should be stated in terms of weighted distortion. Therefore the echo relations are not sufficient; they do not take into account the shape of the signal pulse which comprises each echo component. The amplitude factor implicitly takes this into account. Nearly all of the output transient curves shown herein are based on the cosine-squared shape of pulse whose amplitude factor F has approximately the cosine-squared shape shown in Fig. 9(a). If the corresponding distortion d is to be interpreted with reference to these transient curves, it should be multiplied by

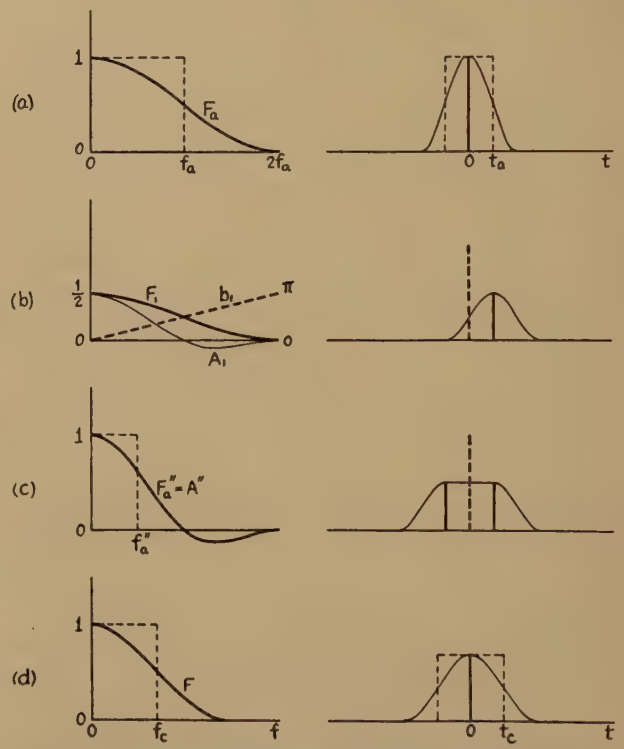

Fig. 20—The symmetrical cases of distortion in the scanning process, and the corresponding frequency characteristics.

[13] The relative illumination of light and dark areas might differ in a ratio as great as thirty to one. An echo of the light area, of relative amplitude 0.01, if it appeared in the dark area, would have a relative brightness thirty times as great (0.3). This would be visible under these conditions if the echo were sufficiently far from the light object in the picture image.

the weighting factor F. This is shown by way of illustration in Figs. 15(c) and 16(c), in light lines under the curves of total distortion. Conversely, having specified the tolerance in terms of weighted distortion, the actual tolerance of attenuation and phase distortion is the specified tolerance multiplied by the inverted amplitude factor, $1/F$.

In picture-transmission systems using the scanning process, this process introduces distortion which is variable with picture conditions. For example, a nearly horizontal thin line is not reproduced with uniform width along its length. This effect is illustrated in Fig. 19, which does not need further description here.[14] The width of reproduction is variable between one and two times the width of a scanning line, which is equal to the pitch of scanning lines. The average width is $\sqrt{2}$ times the pitch.

If a vertical line were reproduced in the same manner, it would appear as if subjected to a variable amount of attenuation and phase distortion. Figs. 19 to 22 are the basis for deriving in Appendix C the

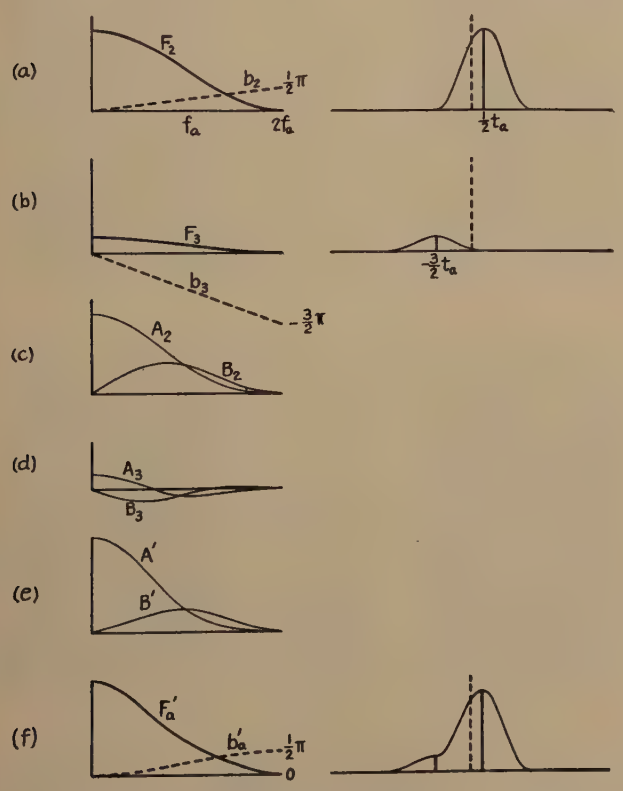

Fig. 21—The unsymmetrical cases of distortion in the scanning process, and the corresponding frequency characteristics.

amount of variable distortion represented. Since this range of distortion is inherent in the reproduction of horizontal lines by the scanning process, the reproduction of vertical lines need not be held within a closer range.

[14] See figure 3 of footnote reference (3).

Fig. 22(b) shows the range of weighted amplitude distortion which corresponds to that inherent in the scanning process. The uppermost curve, with maximum amplitude at higher frequencies, corresponds

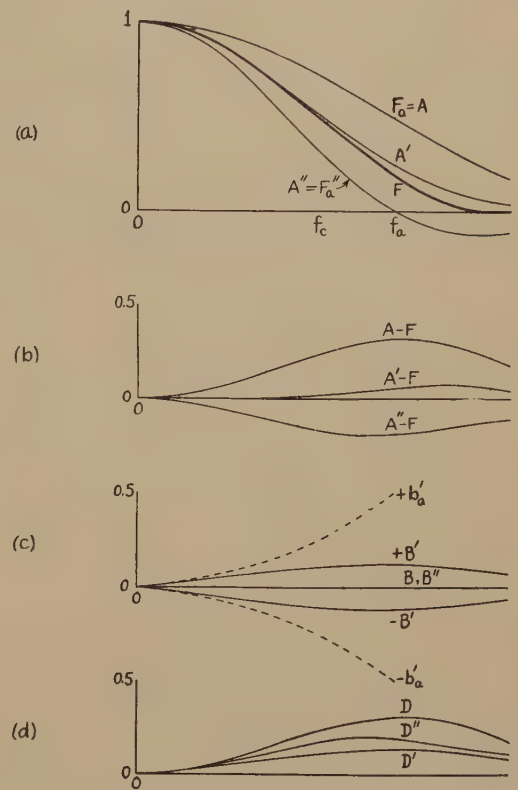

Fig. 22—The range of weighted amplitude and phase distortion corresponding to the distortion inherent in the scanning process.

to the narrowest image and sharpest reproduction. The lowest curve corresponds to the widest image. Fig. 22(c) shows the range of weighted phase distortion representing the departure from symmetrical reproduction. Maximum phase shift is found with minimum departure from normal amplitude, and vice versa, so the total weighted distortion (quadratic sum) shown in Fig. 22(d) does not vary greatly. Its value, as shown, is within 0.3, while its quadratic mean value is somewhat less.

Before concluding the discussion of tolerance, it is desirable to have an example of the visual effect of echo distortion in the reproduced image. Such an example is to be given on the basis of two vertical white lines as the object to be reproduced. Fig. 23(a) shows the signal transient corresponding to the horizontal scanning of such lines. The distortion of such lines may be approximated by dividing each line into several parts, each regarded as an instantaneous impulse. In Fig. 23(b) to (e), each line is replaced by two impulses as shown, and the output transient is built up from these impulses.

Fig. 23(b) shows the effect of merely the gradual cutoff of Fig. 9(a), while (c) shows the added effect of the phase distortion of Fig. 12(b). (It is noted that the echoes between the lines cancel out.) Fig. 23(d) shows the effect of merely the sharp cutoff of Fig. 11(c), while (e) shows the added effect of the same phase distortion, as in Fig. 14(c). Even the last case is not so extreme as to be far from some of the practical experience.

The output transients shown are based on such a cutoff frequency that the norminal width of reproduction ($2t_c = 1/2f_c$) is equal to the width of each of the vertical lines. Therefore the distortion shown

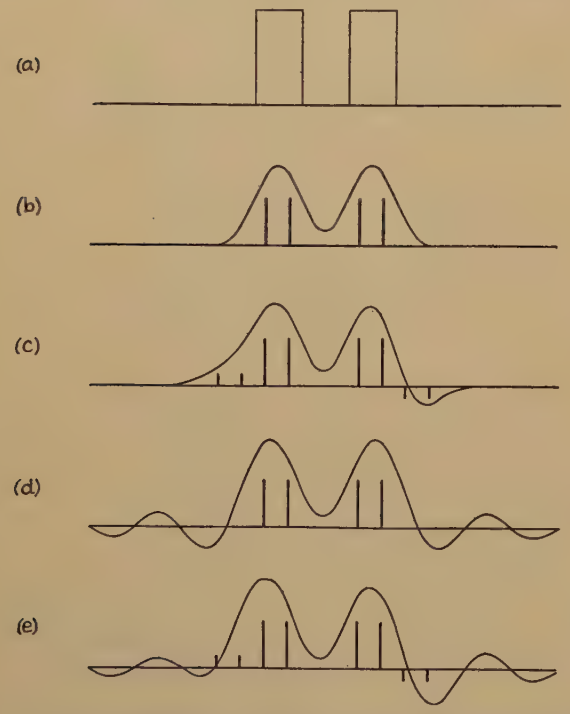

Fig. 23—The distortion of a pair of vertical lines by various combinations of cutoff and phase characteristics.

is that which is effective in the marginal reproduction of lines so close that they can just be distinguished clearly. (The width of each line is $\sqrt{2}$ times the pitch of scanning.)

In order to show the visual effect of such distortion, the half-tone plates of Fig. 24 are given. They correspond to the output transients of Fig. 23(a), (b), and (e). The gray background illumination is taken as one third of white, so the shadow in the last case is nearly black. These conditions are intended to show the extreme effects of such distortion rather than the most probable effects. The plates should be viewed from such a distance that the fine lines disappear in the gray background. (The distance need not be so great if the plate is viewed from one side at an angle instead of from the front.)

These plates illustrate several properties of images under various conditions. The lines are a sample from the charts used to check the resolving power. In (b) it appears that the gradual cutoff by itself gives an image slightly blurred but entirely free of shadows

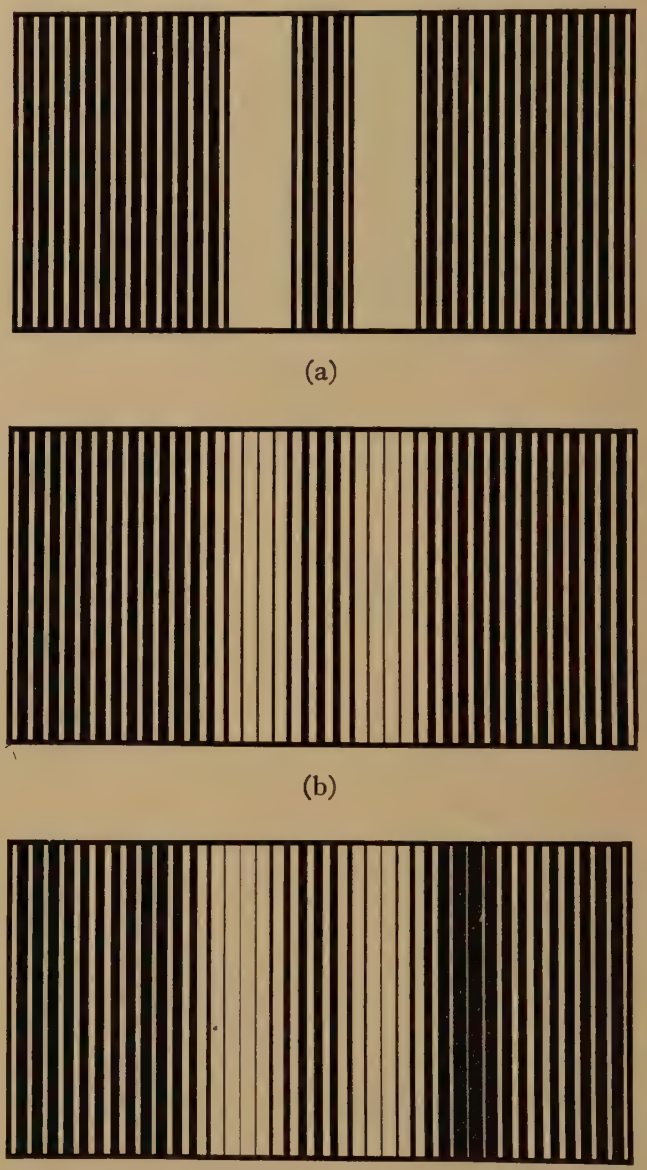

Fig. 24—Half-tone representations of the vertical lines of Fig. 23(a), (b), and (c).

or echoes. The opposite extreme in (c) shows less blurring but a deep shadow and several other echoes. They are the combined effect of sharp cutoff and phase distortion. The sharp cutoff alone tends to sharpen the reproduction at all edges. The phase distortion tends to blur the left edges and sharpen the right edges. Both together produce distortion

which is noticeable but might be tolerable during the infrequent appearance of such sharply defined objects.

If echoes of such great amplitude (about one half as strong as the signal) were to appear much farther from the signal, they would not contribute to the sharpness of reproduction. Also they would be so obvious as to be intolerable. This illustrates the decreasing tolerance of echoes of higher order, farther from the signal, such as might accompany a great delay of the signal. On the average, an echo one tenth as strong as the signal (such as those on the left side) and not too far from the signal should not be objectionable. It would seldom be obvious because the fine details of the signal seldom utilize a major part of the available contrast between black and white, and the background is seldom so plain and dark that weak echoes are obvious.

With the various factors in view, it is submitted that excellent reproduction (the best possible by the scanning process) would not be impaired noticeably by a tolerance of 0.1 as the weighted total distortion of the system. If amplitude and phase tolerance must be expressed independently, the weighted peak value of each may be stated as 0.1 napier or radian. The actual tolerance is greater at the higher frequencies, in proportion to the inverse amplitude factor $1/F$. Somewhat greater tolerance is permissible with a reasonable probability of excellent reproduction. The amplitude tolerance is expressed relative to the most desirable characteristics. The phase tolerance is expressed relative to the straight line (through the origin) relative to which the amount of weighted distortion is the least.

XIII. Conclusion

Amplitude and phase distortion may be expressed in terms of a pattern of echoes. The relations are simple if the amount of distortion is small. The separate evaluation of amplitude and phase distortion requires pairs of echoes equally displaced before and after the signal output, hence the "method of paired echoes." Amplitude distortion leads to symmetrical positive pairs, phase distortion to skew-symmetrical negative pairs. (These are analogous to the sidebands produced by amplitude or phase modulation of a carrier.) Any combination of distortion can be evaluated as the sum of positive and negative pairs.

The evaluation of distortion effects in terms of echoes is useful with reference to picture transmission. The method of paired echoes is especially useful as applied to a small amount of phase distortion, where previous methods have been of little value. It is fundamentally a simplified application of the Fourier integral.

Some forms of amplitude and phase distortion are similar in that their echo patterns are the same except for the difference between positive and negative pairs. If similar forms are combined in equal small amounts, the echoes on only one side remain, those on the other side being canceled out. Such similar forms are often found together in practice.

Since the method of paired echoes is valid only for a small amount of distortion, a large amount requires successive applications of the method. The total distortion is divided into parts which are small enough to come within the scope of the method. A single application deals fairly accurately with distortion up to 1/2 unit (napier or radian), and approximately up to one unit.

The tolerance of distortion depends on how it is divided among the echo components. It should be expressed in terms of "weighted distortion," the weighting factor being the relative amplitude. The scanning process inherently causes an amount of weighted distortion variable within 0.3 unit.

In general, the echoes may be farther from the signal, and therefore more detrimental. The tolerance in terms of weighted distortion is stated to be about 0.1 unit. It is probably much more in practice if it is divided among several echoes, of which the strongest are nearest the signal.

Acknowledgment

The writer acknowledges with his appreciation the constructive suggestions of his associates and the valuable assistance of Messrs. E. T. Joss and W. D. Frere in the preparation of this material.

Appendix A. The Derivation of Output Transients in a Simple Example

Fig. 1(a) shows the amplitude curve and 1(b) the phase curve of a simple example comprising a two-stage amplifier having in each stage a parallel connection of resistance R and capacitance C. The complex relative transfer ratio is

$$\overline{F}(f) = \frac{1}{(1 + j2\pi fCR)^2}. \tag{13}$$

The relative amplitude is

$$F(f) = \frac{1}{1 + (2\pi fCR)^2} \tag{14}$$

and the phase angle is

$$b = 2 \text{ antitan } 2\pi fCR. \tag{15}$$

The area under the amplitude curve determines the nonimal cutoff frequency

$$f_c = \int_0^\infty F(f) \cdot df = \frac{1}{4CR} \cdot \tag{16}$$

In terms of the cutoff frequency, the relative amplitude and the phase angle are

$$F(f) = \frac{1}{1 + \left(\frac{\pi f}{2f_c}\right)^2}; \quad b = 2 \text{ antitan} \frac{\pi f}{2f_c} \cdot \tag{17}$$

Assuming zero phase angle, the signal transient $E(t)$ in response to an instantaneous unit impulse is obtained by the the Fourier integral of the symmetric form[15,16]

$$E(t) = 2\int_0^\infty F(f) \cos 2\pi ft \cdot df = 2\int_0^\infty \frac{\cos 2\pi ft \cdot df}{1 + \left(\frac{\pi f}{2f_c}\right)^2}$$

$$= 2f_c \exp - \left| 4f_c t \right| . \tag{18}$$

This is plotted in Fig. 1(c). The nominal width of this transient is the width of a rectangle of equal height at the center and of equal area. The height is $2f_c$ and the area is unity. Therefore the nominal width is

$$2t_c = \frac{1}{2f_c} = 2CR. \tag{19}$$

The expression of the transient in terms of its nominal width is

$$E(t) = \frac{1}{2t_c} \exp - \left| \frac{t}{t_c} \right| . \tag{20}$$

The actual transient in response to the unit impulse is readily derived by a solution of the circuit, or by operational methods directly from the transfer ratio. The actual transient is

$$E(t) = \frac{t}{C^2R^2} \exp - \frac{t}{CR} = \frac{t}{t_c^2} \exp - \frac{t}{t_c} \cdot \tag{21}$$

This curve is plotted in Fig. 1(d). The area is unity, as in Fig. 1(c), but the peak is less in the ratio $2/\epsilon$. Therefore the nominal width is greater in the inverse ratio, $\epsilon/2$. The peak is delayed by t_c and the center of gravity is delayed by $2t_c$ The latter is the delay represented by the phase slope at zero frequency, which is one-half period (π) at f_c or one period at $2f_c$. But one period at $2f_c$ is equal to $2t_c$ from (19) above. The peak is delayed less than the center of gravity because the phase slope is less at higher frequencies.

[15] See equation (36) on page 569 of footnote reference (3). The definite integral is given by Peirce,[16] page 63, number 490.

[16] B. O. Peirce, "A Short Table of Integrals," 1899, 1910, 1929. (Definite integrals, pp. 62–65. Infinite series, pp. 88–96.)

Appendix B. The Derivation of Echo Patterns of Many Pairs

Fig. 11 shows the echo patterns caused by a step in the amplitude characteristics. In Fig. 11(a), the relative amplitude F_e exceeds the unit reference level F_0 by the amount c in the nominal pass band (0 to f_c). It is less by the same amount at higher frequencies (f_c to $2f_c$). Since c is assumed much less than unity, this step may be expressed as follows in terms of attenuation a' (napiers) relative to the reference level:

$$\begin{aligned} -a' &= c \qquad (0 < f < f_c) \\ -a' &= -c \quad (f_c < f < 2f_c). \end{aligned} \tag{22}$$

The step of attenuation is $2c$.

In resolving the step into a Fourier series, it must be appreciated that the amplitude characteristics are inherently symmetrical about zero frequency; that is, they are the same at equal positive and negative frequencies. Therefore only cosine terms are available. This step is expressed by one of the well-known Fourier series as follows:

$$-a' = \frac{4c}{\pi}\left(\cos\frac{\pi f}{2f_c} - \frac{1}{3}\cos\frac{3\pi f}{2f_c} + \frac{1}{5}\cos\frac{5\pi f}{2f_c} - \cdots\right). \tag{23}$$

The angle in each cosine term identifies the term with one pair of echoes in Fig. 5. Its coefficient determines the amplitude of that pair of echoes. Expressing the series in terms of paired-echo coefficients,

$$-a' = 2e_1\cos\frac{\pi f}{2f_c} + 2e_3\cos\frac{3\pi f}{2f_c} + 2e_5\cos\frac{5\pi f}{2f_c} + \cdots . \tag{24}$$

Therefore, there is a pair of echoes for each odd-numbered order, and the amplitudes of the echoes are

$$e_1 = 2c/\pi; \quad e_3 = -2c/3\pi; \quad e_5 = 2c/5\pi; \quad \cdots . \tag{25}$$

The echoes alternate in polarity and decay hyperbolically either side of the main signal in the center. The diagrams are drawn for a step of one napier: $c = 1/2$, $e_1 = 1/\pi$, etc.

Fig. 11(b) has opposite attenuation so the echo pattern is merely inverted.

Fig. 11(c) is derived directly by the symmetric Fourier integral.[17] The formula for the output transient shown is

[17] See Appendix D of footnote reference (3).

$$E(t) = \frac{\sin 2\pi f_c t}{2\pi f_c t} = \frac{\sin \pi t/2t_c}{\pi t/2t_c}. \tag{26}$$

The latter expression follows from the fact that $2t_c = 1/2f_c$. This transient also has hyperbolic damping, like the echo pattern. At the points where echoes appear in (a) and (b), at odd multiples of t_c, the numerator is ± 1, so the curve has the amplitude values $2/\pi$, $-2/3\pi$, $2/5\pi$, etc. These are interesting as the extreme case of the amplitude step, whereas the method of paired echoes is applicable to a relatively small step.

Fig. 13(a) shows the echo patterns caused by a small step in the phase characteristics. The phase slope is the same on both sides of the step. The amount of the step is $2c'$. The step is expressed relative to the reference line b_0, in terms of the relative phase angle b', as follows:

$$\begin{aligned} b' &= -c'f/f_c \qquad (0 < f < f_c) \\ b' &= 2c' - c'f/f_c \quad (f_c < f < 2f_c). \end{aligned} \tag{27}$$

Since the phase characteristics are inherently skew-symmetrical about zero frequency, only sine terms are available. This step is expressed by another well-known Fourier series as follows:

$$b' = -\frac{2c'}{\pi}\left(\sin\frac{\pi f}{f_c} - \frac{1}{2}\sin\frac{2\pi f}{f_c} + \frac{1}{3}\sin\frac{3\pi f}{f_c} - \cdots\right). \tag{28}$$

The angle in each sine term identifies it with one pair of echoes in Fig. 6. This series is expressed in terms of paired-echo coefficients:

$$b' = 2e_2 \sin\frac{2\pi f}{2f_c} + 2e_4 \sin\frac{4\pi f}{2f_c} + 2e_6 \sin\frac{6\pi f}{2f_c} + \cdots. \tag{29}$$

There is a pair of echoes for each even-numbered order, and their amplitudes are

$$e_2 = -c'/\pi; \quad e_4 = c'/2\pi; \quad e_6 = -c'/3\pi; \cdots. \tag{30}$$

In the figure, the step is one radian, so $c' = 1/2$, $e_2 = -1/2\pi$, etc. As in Fig. 11, the echoes alternate in polarity and decay hyperbolically. These properties are characteristic of a step at the cutoff frequency, in either amplitude or phase.

Fig. 13(b) shows the output transient for a phase step of π radians, too large to be treated simply in terms of paired echoes. It amounts to a reversal of polarity at the nominal cutoff frequency, so it can be treated as amplitude distortion. The new reference of phase is the line b_0' which coincides with the phase characteristic in the nominal pass band. The difference of delay between b_0 and b_0' must be taken into account.

The resulting amplitude curve F' is shown in Fig. 13(c), and is defined as follows:

$$\begin{aligned} F' &= \cos^2 \pi f/4f_c = \frac{1+\cos \pi f/2f_c}{2} \qquad (0 < f < f_c) \\ F' &= -\cos^2 \pi f/4f_c = -\frac{1+\cos \pi f/2f_c}{2} \quad (f_c < f < 2f_c). \end{aligned} \tag{31}$$

The resulting output transient is obtained by the symmetric Fourier integral as follows:[18]

$$\begin{aligned} E(t) &= 2\int_0^{2f_c} F' \cos 2\pi f t \cdot df \\ &= 2f_c \frac{\sin 2\pi f_c t}{2\pi f_c t} + f_c \frac{\sin(\pi/2 - 2\pi f_c t)}{\pi/2 - 2\pi f_c t} \\ &\quad + f_c \frac{\sin(\pi/2 + 2\pi f_c t)}{\pi/2 + 2\pi f_c t} - 2f_c \frac{\sin 4\pi f_c t}{4\pi f_c t} \\ &\quad - f_c \frac{\sin(\pi - 4\pi f_c t)}{\pi - 4\pi f_c t} - f_c \frac{\sin(\pi + 4\pi f_c t)}{\pi + 4\pi f_c t}. \end{aligned} \tag{32}$$

The first line of terms gives the transient caused by the reversal at f_c while the second line gives that caused by the gradual cutoff toward $2f_c$. The fractions are given in the form for easy computation of indeterminate values; that is, where both numerator and denominator are zero. Where any denominator is zero, that fraction has unit value. Combining terms and substituting $2f_c = 1/2t_c$, this expression becomes

$$\begin{aligned} E(t) &= \frac{1}{2t_c}\frac{\sin \pi t/2t_c}{\pi t/2t_c} + \frac{1}{\pi t_c}\frac{\cos \pi t/2t_c}{1-(t/t_c)^2} \\ &\quad - \frac{1}{2t_c}\frac{1}{1-(t/t_c)^2}\frac{\sin \pi t/t_c}{\pi t/t_c}. \end{aligned} \tag{33}$$

These three terms, respectively, decay as the first, second, and third powers of the time (t/t_c) found in the denominators. The first term has the slowest rate of decay (hyperbolic) and is related most closely with the reversal at f_c. The expressions simplify greatly at multiples of t_c, as follows:

$t/t_c = 0$	± 1	± 2	± 3	± 4	± 5
$2t_c E(t) = 2/\pi$	$2/\pi$	$2/3\pi$	$-2/3\pi$	$-2/15\pi$	$2/5\pi$.

(34)

It is noted that the odd-multiple values decay hyperbolically.

Fig. 13(b) shows a plot of this transient, with echo lines drawn where echoes would be located in (a). It is shown in Section XI that large distortion in terms

[18] Equations (48) and (49) on page 573 of footnote reference (3) give the same derivation but without the reversal.

of echoes retains the same spacing of echoes. They merely lose the skew-symmetry which is characteristic of the paired echoes. The center of the transient in (b) is shifted to the left because the phase slope b_0' relative to b_0 represents less delay by the amount of t_c.

The nominal cutoff frequency f_c' in Fig. 13(c) is reduced to $(2/\pi)f_c$ by the reduction of net area occasioned by the reversal. Therefore, the nominal width of the output transient is correspondingly increased from $2t_c$ to $2t_c' = (\pi/2)2t_c$. The displacement off-center and the widening of the output transient are the results of the phase distortion.

Figs. 15 to 17, described in Section X, show similar forms of amplitude and phase distortion; that is, forms which lead to similar echo patterns. The method of attack differs in that the echo patterns are given and the forms of distortion are to be found.

Fig. 15 is characterized by even-order echoes of alternating polarity and hyperbolic damping. This pattern already being found in Fig. 13(a), as to phase distortion, it is duplicated in Fig. 15(a). It shows a phase step at the cutoff frequency. There remains to be found the amplitude distortion giving the same echo pattern after the signal, and the same but inverted pattern before the signal.

This form of phase distortion is expressed above in (28) as a Fourier series of sine terms. The similar amplitude distortion is expressed by a series of cosine terms having the same coefficients, because these determine the echo pattern. Therefore, the amplitude distortion, in terms of relative attenuation a', is given by the series,

$$-a' = -\frac{2c'}{\pi}\left(\cos\frac{\pi f}{f_c} - \frac{1}{2}\cos\frac{2\pi f}{f_c} + \frac{1}{3}\cos\frac{3\pi f}{f_c} - \cdots\right). \tag{35}$$

The sum of this series is known:[19]

$$-a' = -\frac{2c'}{\pi}\log\left|2\cos\frac{\pi f}{2f_c}\right| = -\frac{c}{\log 2}\log\left|2\cos\frac{\pi f}{2f_c}\right|. \tag{36}$$

This is plotted as $(F_e - 1)$ in Fig. 15(b). The amplitude reference dimension c is related to the phase dimension c' as follows:

$$c = \frac{\log 4}{\pi}c' = 0.44\,c'. \tag{37}$$

[19] See number 814 on page 96 of footnote reference (16).

The coefficient of the first term in each series is $2e_2$, twice the amplitude of the first echo on either side ($n = 2$). Therefore the dimensions are related with the paired-echo amplitudes as follows:

$$e_2 = -c'/\pi = -c/\log 4;\quad c' = -\pi e_2;\quad c = -e_2\log 4. \tag{38}$$

In Fig. 15(c), the one-sided echo pattern is caused by the combination of the two similar forms of distortion, the first echo having the amplitude $2e_2$. The figures are drawn for a phase step of one radian, so $c' = 1/2$, $c = 0.22$, $e_2 = -1/2\pi$, etc.

Fig. 15(c) shows also the quadratic sum of the phase distortion and the amplitude distortion:

$$d = \sqrt{a'^2 + b'^2}. \tag{39}$$

This is plotted as a thick line, while the thin line just below shows the weighted distortion Fd.

Fig. 16 is characterized by even-order echoes of like polarity and exponential damping. None of the preceding examples has either of these properties, although they are common in practical circuits. The amplitude distortion is to be found first, as it is of simpler form.

Fig. 16(b) has a pattern of paired echoes whose amplitudes are in geometric progression, corresponding to exponential damping:

$$e_2 : e_4 : e_6 : \cdots = 1 : r : r^2 : \cdots \tag{40}$$

in which the ratio r is less than unity and in this case is positive. This relation determines the Fourier series, which expresses the amplitude distortion,

$$-a' = 2e_2\left(\cos\frac{\pi f}{f_c} + r\cos\frac{2\pi f}{f_c} + r^2\cos\frac{3\pi f}{f_c} + \cdots\right). \tag{41}$$

The sum of this series is known:[20,21]

$$-a' = 2e_2\frac{\cos\pi f/f_c - r}{1 + r^2 - 2r\cos\pi f/f_c} = 2e_2\frac{(1-r) - 2\sin^2\pi f/2f_c}{(1-r)^2 + 4r\sin^2\pi f/2f_c} = -2e_2\frac{(1+r) - 2\cos^2\pi f/2f_c}{(1+r)^2 - 4\cos^2\pi f/2f_c}. \tag{42}$$

The second and third forms, respectively, are convenient for positive and negative values of the ratio r near unity, or for evaluation near the frequencies zero and f_c. In the present case, r is positive and e_2 is negative, so the peak value of a' at zero frequency is

[20] See number 6.833 on page 139 of footnote reference (21).

[21] E. P. Adams, "Smithsonian Mathematical Formulae," 1922. (Trigonometry: finite series, pp. 81–83. Infinite series: Fourier's series, pp. 137–140.)

$$c = \frac{-2e_2}{1-r}. \tag{43}$$

The curves in (b) are plotted for $c=1/2$, $r=1/2$, $e_2=-1/8$, etc.

Fig. 16(a) shows the similar form of phase distortion. It is expressed by a series of sine terms with the same coefficients:

$$b = 2e_2\left(\sin\frac{\pi f}{f_c} + r\sin\frac{2\pi f}{f_c} + r^2\sin\frac{3\pi f}{f_c} + \cdots\right). \tag{44}$$

The sum of this series is also known:[22]

$$\begin{aligned} b &= 2e_2\frac{\sin \pi f/f_c}{1+r^2-2r\cos \pi f/f_c} \\ &= 2e_2\frac{\sin \pi f/f_c}{(1-r)^2+4r\sin^2 \pi f/2f_c} \\ &= 2e_2\frac{\sin \pi f/f_c}{(1+r)^2-4r\cos^2 \pi f/2f_c}. \end{aligned} \tag{45}$$

The extreme values occur where

$$\sin \pi f/f_c = \frac{1-r^2}{1+r^2}; \quad \cos \pi f/f_c = \frac{2r}{1+r^2}. \tag{46}$$

The peak dimension c' in the figure is

$$c' = \frac{-2e_2}{1-r^2} = \frac{c}{1+r}. \tag{47}$$

It is noted that the spread of b' from peak to valley, $2c'$, is equal to that of the amplitude curve in (b).

Fig. 16(c) shows the quadratic sum of the phase distortion in (a) and the amplitude distortion in (b):

$$\begin{aligned} d = \sqrt{a'^2+b'^2} &= \frac{2e_2}{\sqrt{1+r^2-2r\cos \pi f/f_c}} \\ &= \frac{2e_2}{\sqrt{(1-r)^2+4r\sin^2 \pi f/2f_c}} \\ &= \frac{2e_2}{\sqrt{(1+r)^2-4r\cos^2 \pi f/2f_c}}. \end{aligned} \tag{48}$$

This is plotted as a thick line, while the thin line shows the weighted distortion.

Fig. 17 is characterized by even-order echoes of alternating polarity and equal amplitudes (no damping). Any number of echo pairs may be assumed. The limits to be derived are independent of the number. The amplitude distortion is to be found first.

Fig. 17(b) shows the symmetrical pattern of echoes, including one of zero order which serves to simplify the expressions. Since all the amplitudes are the same, they are denoted simply $\pm e_0$. The number of echoes on each side is m, the total number of echoes being $2m+1$. The Fourier series expressing the corresponding amplitude distortion is a finite series in this case:

$$\begin{aligned} -a' = e_0\cos\frac{0\pi f}{f_c} - 2e_0\cos\frac{\pi f}{f_c} + 2e_0\cos\frac{2\pi f}{f_c} - \cdots \\ \pm 2e_0\cos\frac{m\pi f}{f_c}. \end{aligned} \tag{49}$$

The first term is constant, e_0. The sum of this series is[23]

$$-a' = e_0(-1)^m\frac{\cos(2m+1)\dfrac{\pi f}{2f_c}}{\cos\dfrac{\pi f}{2f_c}}. \tag{50}$$

This is plotted in (b) for $m=4$, and the echo pattern is given for $e_0=-1/8$. The peak value at the cutoff frequency ($f=f_c$) is

$$a' = (2m+1)e_0. \tag{51}$$

The more interesting characteristic of Fig. 16(b) is the envelope of the amplitude distortion a'. If the envelope is denoted $\pm a''$, the relative attenuation may be expressed

$$-a' = \pm a''\cos(2m+1)\frac{\pi f}{2f_c}. \tag{52}$$

This envelope is independent of the number of echoes ($2m+1$)

$$\pm a'' = \frac{e_0}{\cos \pi f/2f_c} = e_0\sec \pi f/2f_c. \tag{53}$$

It is plotted in dotted lines. The minimum spread is $2e_0$ at zero frequency.

Fig. 17(a) shows the similar phase distortion. It is expressed by the finite Fourier series of sine terms in place of cosine terms:

$$\begin{aligned} b' = e_0\sin\frac{0\pi f}{f_c} - 2e_0\sin\frac{\pi f}{f_c} + 2e_0\sin\frac{2\pi f}{f_c} - \cdots \\ \pm 2e_0\sin\frac{m\pi f}{f_c}. \end{aligned} \tag{54}$$

The first term is zero. The sum of this series is[24]

$$b' = e_0\frac{(-1)^m\sin(2m+1)\dfrac{\pi f}{2f_c} - \sin\dfrac{\pi f}{2f_c}}{\cos\dfrac{\pi f}{2f_c}}. \tag{55}$$

[22] See number 6.830 on page 139 of footnote reference (21)

[23] See numbers 2 and 11 on pages 81 and 82 of footnote reference (21).

[24] Adams, footnote reference (21), page 81, number 1, adapted to alternating signs just as number 2 is transformed to number 11, page 82.

This is plotted in (a) for $m=4$, and the echo pattern is given for $e_0=-1/8$.

The phase envelope of Fig. 17(a) is unsymmetrical so it requires two separate expressions, one positive and the other negative at zero frequency:

$$b_+''=e_0\frac{1-\sin \pi f/2f_c}{\cos \pi f/2f_c}=e_0 \tan\left(\frac{\pi}{4}-\frac{\pi f}{4f_c}\right)$$
$$b_-''=e_0\frac{-1-\sin \pi f/2f_c}{\cos \pi f/2f_c}=-e_0 \tan\left(\frac{\pi}{4}+\frac{\pi f}{4f_c}\right). \quad (56)$$

These envelopes are plotted in dotted lines. The minimum spread is $2e_0$ at zero frequency.

Fig. 17(c) shows the quadratic sum of the phase distortion and the amplitude distortion. It is easily derived from the preceding expressions:

$$d=\sqrt{a'^2+b'^2}=\frac{e_0}{\cos\dfrac{\pi f}{2f_c}}\sqrt{1+\sin^2\frac{\pi f}{2f_c}-2(-1)^m\sin\frac{\pi f}{2f_c}\sin(2m+1)\frac{\pi f}{2f_c}}. \quad (57)$$

The envelope is the most interesting characteristic, and it has the same form as for the phase distortion b' in (a). It is plotted in dotted lines in (c).

In Section XII, there is stated the relation between the total distortion and all the echoes, assuming a small amount of distortion. The amplitude distortion is expressed in terms of its Fourier series of cosine terms, and the phase in terms of sine terms:

$$-a'=2e_1\cos\frac{\pi f}{2f_c}+2e_2\cos\frac{2\pi f}{2f_2}+\cdots \quad (58)$$

$$b'=2e_1'\sin\frac{\pi f}{2f_c}+2e_2'\sin\frac{2\pi f}{2f_c}+\cdots. \quad (59)$$

The sum of the squares of these two series, averaged over a frequency range whose width is f_c or a multiple thereof, is known to be

$$\overline{d^2}=\overline{a'^2+b'^2}=2e_1^2+2e_2^2+\cdots$$
$$+2e_1'^2+2e_2'^2+\cdots. \quad (60)$$

The two first terms, $2e_1^2$ and $2e_1'^2$, come from two echoes of the first order, whose amplitudes are e_1+e_1', and e_1-e_1'. The sum of the squares of these two amplitudes is

$$(e_1+e_1')^2+(e_1-e_1')^2=2e_1^2+2e_1'^2 \quad (61)$$

which is equal to the sum of the two first terms in the preceding series. The same applies to the terms of higher orders.

Therefore there is a general rule that the mean-squared total distortion is equal to the sum of the squares of the amplitudes of all the echoes. The rule is general if the mean is taken over a frequency band of width f_c, which may be zero to f_c, the nominal pass band.

Appendix C. The Derivation of the Distortion Inherent in the Scanning Process

Fig. 19 shows the mechanism of scanning a nearly horizontal line in a system for picture transmission.[25] The transverse intensity distribution depends on the position of this line relative to the scanning lines, so the distortion has a random variation within limits. If a vertical line were reproduced with similar intensity distribution, it could be resolved into the corresponding frequency characteristics depending on the transverse distribution in the horizontal direction. This could be done directly by means of the Fourier intergal, but the general form involving phase angle would be needed. It is simpler to treat separately the two parts contributed by the two scanning lines involved. That is the procedure to be followed.

Fig. 20(a) shows the transverse distribution as a time transient, corresponding to the first point ($u=0$) on the line in Fig. 19. The nominal time width of the transient $2t_a$ corresponds to the width of a scanning line, equal to the pitch of scanning lines. It has the cosine-squared distribution whose frequency characteristic is very closely approximated by the cosine-squared amplitude curve F_a. Its nominal cutoff frequency is $f_a=1/4t_a$. Since this transient is symmetrical about the center line, the phase shift is zero in the frequency characteristics.

The other point where the distribution is symmetrical is the third point ($u=1/2$) on the line in Fig. 19. The contribution of one scanning line is shown as a time transient in Fig. 20(b) and of both scanning lines in (c). Referring to (b), the pulse is similar to (a) but half as intense, and is displaced in time by t_a, half the width. This displacement does not affect the amplitude curve, which is drawn as $F_1=(1/2)F_a$. It introduces a phase angle proportional to the frequency, the phase slope corresponding to the time t_a. The phase angle is denoted b_1, and the slope is $2\pi t_a=\pi/2f_a$.

In order to add the frequency characteristics of the two parts of the transient, only one part being shown in (b), it is necessary to resolve the amplitude

[25] See Fig. 3 of footnote reference (3).

curve into its cosine (parallel) and sine (perpendicular) components with reference to the time origin. The cosine component of one part is

$$A_1 = F_1 \cos b_1 \tag{62}$$

plotted in (b). The sine component need not be computed, because it cancels out in the frequency characteristics of the two parts, whose resultant is symmetrical.

The frequency characteristics of the other part are the same as (b), but for a reversal of the time displacement. The phase angle is negative, so the sine component cancels that of the first part. The cosine components add together. Their sum is plotted in (c) as F_a'', which is, in the absence of a sine term, the same as the cosine coefficient,

$$A'' = 2A_1 = F_a \cos b_1. \tag{63}$$

Since

$$F_a = \cos^2 \pi f/4f_a = \frac{1 + \cos \pi f/2f_a}{2} \tag{64}$$

and

$$b_1 = \pi f/2f_a \tag{65}$$

it follows that

$$F_a'' = A'' = \cos^2 \frac{\pi f}{4f_a} \cos \frac{\pi f}{2f_a}. \tag{66}$$

The symmetrical transient is shown in (c), which is the resultant of the two parts. It is twice as wide as (a), so the nominal cutoff frequency f_a'' is half as great as f_a.

The average width of reproduction of the line in Fig. 19 is known to be $\sqrt{2}$ times the pitch of scanning lines ($2t_a$).[26] The extremes are one and two times the pitch, as in Figs. 20(a) and (c). The mean shape of the transverse distribution is approximated by the cosine-squared shape shown in (d), with a width[27] of $2t_c = 2t_a\sqrt{2}$. The nominal cutoff frequency of the latter is $f_c = 1/4t_c$, and its amplitude curve is closely approximated by the cosine-squared curve F.

Returning to the expression of the transverse distribution in terms of frequency characteristics, Fig. 21 shows the case of the second point in Fig. 19 ($u = 1/4$). (The fourth point, $u = 3/4$, is the same but reversed with respect to time.) The major part is contributed by the nearer scanning line as shown in (a), the minor part by the other line as shown in (b). Their relative intensities are

$$\tfrac{1}{2}(1 \pm 1/\sqrt{2}) = 0.85 \text{ and } 0.15. \tag{67}$$

[26] See Appendix A of footnote reference (3).

[27] It is on this basis that the nominal cutoff frequency of the system has been specified in footnote reference (3).

The amplitude and phase characteristics of each part are determined as described with reference to Fig. 20(b). Those of the major part (a) are

$$\begin{aligned} F_2 &= \frac{1 + 1/\sqrt{2}}{2} \cos^2 \pi f/4f_a \\ b_2 &= \pi f/4f_a. \end{aligned} \tag{68}$$

Those of the minor part (b) are

$$\begin{aligned} F_3 &= \frac{1 - 1/\sqrt{2}}{2} \cos^2 \pi f/4f_a \\ b_3 &= -3\pi f/4f_a. \end{aligned} \tag{69}$$

The cosine and sine coefficients of (a), as shown in (c), are respectively

$$\begin{aligned} A_2 = F_2 \cos b_2 &= \frac{1 + 1/\sqrt{2}}{2} \cos^3 \frac{\pi f}{4f_a} \\ B_2 = F_2 \sin b_2 &= \frac{1 + 1/\sqrt{2}}{2} \cos^2 \frac{\pi f}{4f_a} \sin \frac{\pi f}{4f_a}. \end{aligned} \tag{70}$$

Those of (b), shown in (d), are, respectively,

$$\begin{aligned} A_3 = F_3 \cos b_3 &= \frac{1 - 1/\sqrt{2}}{2} \cos^2 \frac{\pi f}{4f_a} \cos \frac{3\pi f}{4f_a} \\ B_3 = F_3 \sin b_3 &= -\frac{1 - 1/\sqrt{2}}{2} \cos^2 \frac{\pi f}{4f_a} \sin \frac{3\pi f}{4f_a}. \end{aligned} \tag{71}$$

The resultant cosine and sine coefficients of (c) and (d) together, as shown in (e), are

$$A' = A_2 + A_3; \qquad B' = B_2 + B_3. \tag{72}$$

The two parts together make the transient of Fig. 21(f). Its amplitude and phase characteristics are, respectively,

$$F_a' = \sqrt{A'^2 + B'^2}; \quad b_a' = \text{antitan } B'/A'. \tag{73}$$

Fig. 22 shows the relative distortion inherent in the transverse distribution caused by scanning lines. The standard of reference is the pulse shape and the frequency characteristics of Fig. 20(d), the amplitude curve F being shown and the phase angle being zero. The distortion components are to be expressed not in terms of attenuation and phase, but in terms of the departure of cosine and sine coefficients from their "undistorted" values.

The curve F of Fig. 22(a) is the standard of reference for cosine coefficients, and zero is for sine coefficients. The cosine coefficients of the different transients are plotted on the same scale. Their departure from F are plotted in (b). The sine coefficients are zero except for the case of Fig. 21, and these are plotted in Fig. 22(c) on the same scale as (a) and (b).

The quadratic sum of cosine and sine distortion coefficients is plotted in Fig. 22(d) for the several cases:

$$D = \sqrt{(A - F)^2 + B^2}\ ; \quad \text{etc.} \tag{74}$$

The phase distortion b_a' is plotted in dotted lines in Fig. 22(c). It is increasingly greater than the sine coefficient at higher frequencies, but its effect is not proportional to its value. The amplitude of the higher-frequency components is less, so more phase shift is required to cause the same amount of distortion as appears in the picture image. The cosine and sine distortion coefficients are a weighted measure of the attenuation and phase distortion; they are approximately equal to the latter multiplied by the weighting factor F which is the relative amplitude-frequency characteristic of the system.

Additional Bibliography

(1) S. P. Mead, "Phase distortion and phase distortion correction," *Bell Sys. Tech. Jour.*, vol. 7, pp. 195–224; April, (1928). (Facsimile transmission.)

(2) C. E. Lane, "Phase distortion in telephone apparatus," *Bell Sys. Tech. Jour.*, vol. 9, pp. 493–521; July, (1930). (Examples of phase distortion and correction, oscillograms.)

(3) J. C. Steinberg, "Effects of phase distortion on telephone quality," *Bell Sys. Tech. Jour.*, vol. 9, pp. 550–566; July, (1930).

DISCUSSION

Charles R. Burrows:[1] This timely paper presents a novel line of thought that should be fruitful in the study of distortion in television systems. The main purpose of this note is to present the general solution of which the method of paired echoes is a special case. This follows directly from an exact solution due to L. A. MacColl which allows the evaluation of the magnitude of the approximations in the method of paired echoes. A paragraph is appended which discusses the paradox of the output preceding the input in the absence of phase distortion. It is hoped that this will increase the application of the method presented in the paper.

While the method of paired echoes is presented as an approximate method for small distortions it may readily be extended to a method that is rigorous for any transmission characteristic. With this extension the method becomes an analysis of the output signal as a sum of echoes of the input signal, or, if desired, the output signal of any transmission characteristic which may be chosen as a standard of reference.

This may be proved by writing the input signal as a Fourier integral,

$$g(t) = \int_{-\infty}^{\infty} f(\omega) e^{i\omega t} d\omega \tag{1}$$

and the transmission characteristic

$$F(\omega) = A(\omega) e^{iB(\omega)} \tag{2}$$

so that the output will be

$$G(t) = \int_{-\infty}^{\infty} f(\omega) A(\omega) e^{i[\omega t + B(\omega)]} d\omega. \tag{3}$$

The amplitude and phase characteristics of the transmission network are then expressed as the Fourier series

$$A(\omega) = \frac{a_0}{2} + \sum_{n=1}^{\infty} a_n \cos nc\omega = \frac{1}{2} \sum_{n=-\infty}^{\infty} a_n e^{inc\omega},\ a_{-n} = a_n \tag{4}$$

and

$$B(\omega) = -b_0\omega + \sum_{m=1}^{\infty} b_m \sin mc\omega \tag{5}$$

[1] Bell Telephone Laboratories, Inc., Deal, N.J.

over a frequency range that includes all the components of the input signal.[2] ($c \geqq 1/2f_a$, where f_a is the highest frequency of the components of the input signal.) Making use of the following expansion in Bessel functions,[3]

$$e^{iz\sin\theta} = \sum_{k=-\infty}^{\infty} J_k(x) e^{ik\theta} \tag{6}$$

the output may be expressed as

$$G(t) = \frac{1}{2} \int_{-\infty}^{+\infty} f(\omega) e^{i\omega(t-b_0)} \sum_{n=-\infty}^{\infty} a_n e^{inc\omega} \prod_{m=1}^{\infty} \sum_{k=-\infty}^{\infty} J_k(b_m) e^{mkc\omega i} d\omega. \tag{7}$$

If the reader will write out a few terms of the indicated series it will be evident that this expresses the output signal as an infinite sum of signals of the same shape as the input signal.[4] The principal signal is retarded by the time b_0. The echoes occur both before and after the principal signal by multiples of the time c.

To apply this method when the coefficients a_n and b_n of the amplitude and phase-characteristic components are not small it is expedient to consider first the effect of the amplitude characteristic with the linear term of the phase characteristic and then the components of the phase characteristic in the order of their amplitudes. Hence

$$F(\omega) = F_0(\omega) F_1(\omega) F_2(\omega) \cdots \tag{8}$$

where

$$F_0(\omega) = \frac{1}{2} \sum_{n=-\infty}^{\infty} a_n e^{inc\omega - b_0\omega} \tag{9}$$

and

$$F_m(\omega) = e^{ib_m \sin mc\omega} = \sum_{k=-\infty}^{\infty} J_k(b_m) e^{ikmc\omega},\quad m > 0. \tag{10}$$

The output of the first part of the network having the characteristic $F_0(\omega)$ is

$$G_0(t) = \sum_{n=-\infty}^{\infty} \frac{a_n}{2} g(t - b_0 + nc) \tag{11}$$

which is a sum of "echoes" of the same wave shape as the input signal. The principal component has the amplitude $a_0/2$ equal to the constant term of the amplitude characteristic and is delayed by the time b_0. This is flanked by "paired echoes" of amplitude $a_1/2$ spaced c seconds before and after the principal component. Another pair of echoes of amplitude $a_2/2$ are spaced $2c$ seconds before and after the principal component, etc.

When this signal has been transmitted through that part of the network having the characteristic $F_1(\omega)$ it has the form[5]

$$G_1(t) = \sum_{k=-\infty}^{\infty} J_k(b_1) G_0(t + kc). \tag{12}$$

Here again the output is a sum of a number of components of the same shape as the input but this time the input wave shape is the output of the first part of the network. This process may be repeated until all of the b_m's that are not small have been used.[6] The remaining b's may be treated all at once so that the final output

$$G(t) = G_h(t) + \sum \frac{b_m}{2} [G_h(t + mc) + G_h(t - mc)] \tag{13}$$

where $G_h(t)$ is output wave shape before this last operation and

[2] It is not necessary that the sinusoidal components of $A(\omega)$ and $B(\omega)$ be harmonically related. Any predominate cosine components of $A(\omega)$ or sine components of $B(\omega)$ may be removed from them and the remaining functions expanded as cosine and sine series respectively. In this case these components must be added to the sums in (4) and (5) wherever they occur.

[3] This follows directly from expressions 9.181 and 9.103 of E. P. Adams, "Smithsonian Mathematical Formulae and Tables of Elliptic Functions" Smithsonian Institution of Washington, Washington D. C., (1922).

[4] Here m is taken as 1 and the sum is written for all values of k. This is multiplied by a similar sum with $m = 2$, another with $m = 3$, etc., through all values of m. Finally the result is multiplied by the sum in n. The integration is performed by recognizing that each term is the same as the input signal except for amplitude and time delay.

[5] This exact solution for a phase characteristic of a single sine term and the one corresponding to (11) for a single cosine term in the amplitude characteristic were derived in unpublished memoranda by L. A. MacColl of the Bell Telephone Laboratories in 1931 which were available to the writer of this discussion.

[6] The general term is $G_m(t) = \sum_{k=-\infty}^{\infty} J_k(b_m) G_{m-1}(t + kmc)$.

TABLE I

	$b_1=1/2$		$b_1=1$			$b_1=2$			
	Paired Echoes Applied Directly	Exact Solution	Paired Echoes		Exact Solution	Paired Echoes			Exact Solution
			Direct	2 steps		Direct	2 steps	3 steps	
4th leading echo	+0.00	+0.0002	+0.0	+0.0000	+0.0025	+0.0	+0.00	+0.0000	+0.0340
3rd leading echo	+0.00	+0.0025	+0.0	+0.0000	+0.0196	+0.0	+0.00	+0.0625	+0.1284
2nd leading echo	+0.00	+0.0619	+0.0	+0.0625	+0.1149	+0.0	+0.25	+0.3672	+0.3528
1st leading echo	+0.25	+0.2423	+0.5	+0.5000	+0.4401	+1.0	+1.00	+0.8750	+0.5767
Principle component	+1.00	+0.9385	+1.0	+0.8750	+0.7652	+1.0	+1.00	+0.3828	+0.2239
1st following echo	−0.25	−0.2423	−0.5	−0.5000	−0.4401	−1.0	−1.00	−0.8750	−0.5767
2nd following echo	+0.00	+0.0619	+0.0	+0.0625	+0.1149	+0.0	+0.25	+0.3672	+0.3528
3rd following echo	−0.00	−0.0025	−0.0	−0.0000	−0.0196	−0.0	−0.00	−0.0625	−0.1284
4th following echo	+0.00	+0.0002	+0.0	+0.0000	+0.0025	+0.0	+0.00	+0.0000	+0.0340

the summation is over all the b's that haven't been treated previously.

The following definition of the Bessel functions allows an evaluation of the error introduced by the assumption that b is small either in the above or in the paper under discussion:

$$J_k(b) = \left(\frac{b}{2}\right)^k \left(\frac{1}{k!} - \frac{b^2}{2^2 1!(k+1)!} + \frac{b^4}{2^4 2!(k+2)!} - \frac{b^6}{2^6 3!(k+3)!} + \cdots\right). \quad (14)$$

For the principal component, $k=0$, $b^2/4$ is neglected in respect to unity; for the main echoes, $k=1$, $b^2/8$ is neglected in respect to unity. Echoes of the order of $b^2/4$ are neglected in their entirety. The last equation allows the evaluation of the approximation inherent in Fig. 18 of the paper. The exact solution is compared with the method of paired echoes as used in the paper in Table I. It shows that for a phase term of 1/2 radian the method of paired echoes ignores a reduction in the principal component of 0.6 decibel, gives an error of 0.2 decibel in the main echoes, and ignores secondary echoes 23.6 decibels below the principal component. This confirms Wheeler's statement that the method of paired echos gives results of sufficient accuracy for television purposes when applied to a small phase distortion. For larger phase terms it is easier to use the exact solution given by (12) using (14) or a table of Bessel functions than to apply the approximate method a number of times.

The method of paired echoes as presented in the paper is exact for amplitude distortion.[7] The limitation to small amplitudes is unnecessary.

Fig. 1c of the paper shows a finite output occurring before the input signal when there is no phase distortion. This paradox is readily explained when it is realized that the phase of Fig. 1(b) accompanies the amplitude characteristic in the simple network under consideration.[8] In order to obtain a network without phase distortion, all-pass networks may be added. Each all-pass network adds a phase shift that is proportional to frequency at low frequencies. In order to equalize the phase for all frequencies, an infinite number of these all-pass networks is required so that the resulting network with no phase distortion has infinite delay. If the phase is corrected over only a finite frequency range the output signal will differ from Fig. 1(c) in such a way that it is identically zero for negative times numerically greater than the delay.

C. W. Carnahan:[9] This paper is a substantial contribution to the growing collection of approximate methods for calculating the transient behavior of networks. Methods hitherto used for sound communication systems have assumed ideal characteristics which are rarely found in practice. Deviations of the actual characteristics from the ideal are generally of no importance in sound work, but in television, where a finer analysis of transients is required, these deviations are usually large enough to make of doubtful value any close scrutiny of a solution obtained by assuming ideal shapes. Mr. Wheeler has removed this last difficulty with his method of paired echoes, and has given us not only the means for handling characteristics with irregularities, but a physical interpretation of these irregularities of such simplicity that it should go a long way towards divesting the Fourier integral method of its mathematical strait jacket.

Wheeler's present paper applies his method to the problem of network analysis. One hopes that this will be extended to the equally urgent problem of network synthesis. One would like, for instance, in the case of a low-pass filter for television use, to determine in advance the optimum characteristics of the filter with regard to phase and amplitude distortion. Here the interdependence of the two types of distortion is emphasized, as a result of the rule that the responses of any physically realizable network must be zero prior to the application of a suddenly applied input. Many of the examples shown by Wheeler in his paper probably violate this rule, since they were used only for the purpose of illustration, and were not drawn from specific networks. The rule itself is not a part of the logical structure of the Fourier-integral method, but acts to select out of the infinity of characteristics pairs that possibly may be realized in physical networks. In the low-pass filter problem, one might start with a known filter characteristic, make a change in its amplitude characteristic, and then find the compensating pair of negative echoes due to the phase which would approximately cancel the response prior to zero time. This would also require choosing a definite time delay or reference phase slope. By surveying a sufficient number of characteristics in this manner, the selection of an optimum set with regard to total distortion, delay time, economical distortion compensation, etc., should be possible.

[7] From the equations in this discussion it is evident that when the amplitude distortion is large the amplitude characteristic must be analyzed as a ratio and not as the logarithm of this ratio (nepers or decibels).

[8] For a clear presentation of the relationship between amplitude and phase characteristics see H. W. Bode, U.S. Patent No. 2,123,178.

[9] Hygrade Sylvania Corporation, St. Marys, Pa.

Analysis of Load-Impedance Modulation*

HANS RODER†, MEMBER, I.R.E.

Summary—*A new type of modulation for television transmitters which was proposed recently is investigated. The relations referring to the operation of the network, of the modulator, and of the radio-frequency amplifier tubes are derived as well as the expressions for the sideband attenuation characteristic.*

It is concluded from the results that the claims made for the new modulation system are exaggerated. The modulator tubes are required to have a very high emission. This fact will limit the application of the new type of modulation to modulator tubes having thoriated-tungsten filaments and consequently to relatively small power, since at present tubes of this type are built for low or medium output power only. The efficiency of the new modulation system is essentially the same as that of grid-bias modulation. Contrary to expectations, the band width is not materially greater than that which is attainable with grid-bias modulation. This is due to the sideband clipping taking place in the quarter-wave line connecting the modulator tubes with the remainder of the network. The modulation characteristic is straighter than is customarily obtainable with grid-bias modulation; this is achieved by working the modulator grids in the positive region only, a mode of operation which requires high driving power and modulator grids capable of dissipating that power. The output capacitance of the modulator tubes is substantially smaller than the output capacitance of a grid-bias-modulated amplifier, but so is also the damping effect contributed by the internal resistance of the modulator. In consequence, the beneficial effect is frustrated which the reduction of the output capacitance otherwise would have upon the sideband transmission characteristic.

Introduction

THE design and operation of a new and very interesting type of modulation system has been described by W. N. Parker,[1] but unfortunately an analysis of it was not included. However, for a transmitter development engineer the analysis is of great interest because it will enable him to design new equipment and to determine whether or not the new method is superior to previous, more conventional systems.

An analysis will be presented here in as short a space as possible and a comparison will be made versus the more orthodox grid-bias modulation system. The new method will be referred to as plate-load-impedance modulation, since the power-amplifier tank looks out into a variable impedance. Despite the apparent simplicity of the system, the analysis is by no means very brief and simple.

Nomenclature

Terms not found in this tabulation are shown in Fig. 1.

I_1 = fundamental radio-frequency component of modulator-tube plate current, root-mean-square

I_{10} = maximum value of I_1, occurring at modulation peak, root-mean-square

I_0 = direct-current component of modulator-tube plate current

μ = amplification factor of modulator tube

R_p = plate resistance of modulator tube

E_m = radio-frequency plate swing, root-mean-square, for 1 modulator tube

$R_0 = 2E_m/I_1$ = resistance represented by modulator tubes

Z_m, Z_T, Z_z, Z_a = surge impedances, see Fig. 1

θ = electrical length of Z_m transmission line

$Z_0 = Z_m \sin\theta$

R = input resistance of antenna transmission-line system, seen when looking in from junction

P_a = antenna power, at modulation peak

P_0 = maximum modulator plate dissipation, per tube, occurring during modulation cycle

E_g = radio-frequency voltage allowed to develop between grid and filament of modulator tubes (per tube)

$a = E_g/E_m$

E_0 = bias voltage on grids of modulator tubes

$\omega_0/2\pi$ = carrier frequency

δ = ratio of video frequency over carrier frequency (percentage frequency deviation)

R_m = internal resistance of modulation generator network

I_m = constant input current of modulation generator network

C = output capacitance of modulator tubes

X_{c0} = reactance of C at carrier frequency

f_b = band width (between carrier and $\frac{1}{2}\sqrt{2}$ value)

Analysis

The analysis is divided into three parts, the network, the modulator, and the calculation of the sideband attenuation.

A. The Network

The nomenclature is illustrated in Fig. 1. All voltages and currents are root-mean-square values of fundamental harmonic frequency. We assume for our analysis first, the input impedance R of the antenna system, when seen from AA', shall be constant and purely resistive, and second, the voltage $2E_m$ shall be essentially sinusoidal. This will be true for all practi-

* Decimal classification: R148. Original manuscript received by the Institute, August 8, 1938.

† Formerly, General Engineering Laboratory, General Electric Company, Schenectady, N. Y.; now, Telefunken Laboratories, Berlin, Germany.

[1] W. N. Parker, "A unique method of modulation for high-fidelity television transmitters," PROC. I.R.E., vol. 26, pp. 946–962; August, (1938).

cal purposes, because the Z_m line will act similarly to a tank circuit. The MM's are the output terminals of the modulator. The ratio

$$R_0 = \frac{2E_m}{I_1} \tag{1}$$

is the variable radio-frequency resistance represented by the modulator tubes. C is the output capacitance of the modulator. When looking from the junction AA' towards the modulator, the impedance seen should be purely ohmic. To achieve this, the following tuning conditions must be fulfilled: first, one has to make the electrical length of the Z_m line somewhat shorter than a quarter-wave line, such that

$$\frac{Z_m}{X_c} = \operatorname{ctg} \theta \tag{2}$$

and, second, one has to add a capacitance C_1 at the inner end of the Z_m line, making $C_1 = C$. (The insertion of C_1 can be omitted if the power-amplifier tank is slightly detuned.) We put for brevity

$$Z_0 = Z_m \sin \theta = X_c \cos \theta \tag{3}$$

and find now

$$\frac{1}{Z_r} = \frac{R_0}{Z_0^2} - j\frac{1}{X_c}. \tag{4}$$

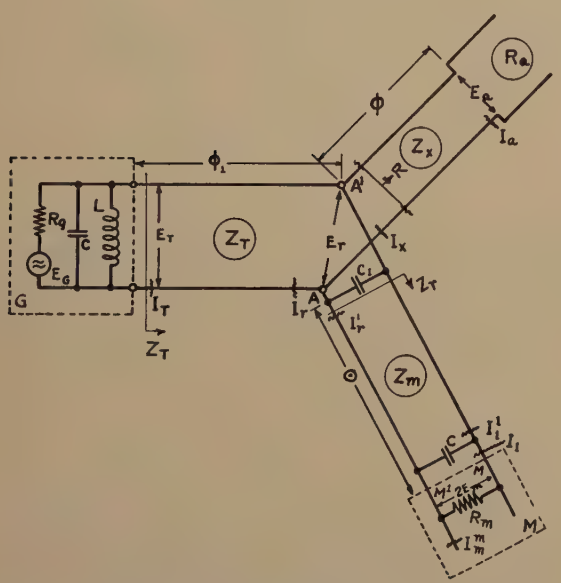

Fig. 1—Schematic diagram for plate-load-impedance modulation.

The input impedance seen when looking out from the terminals of the voltage E_T becomes

$$Z_i = Z_T^2\left(\frac{1}{R} + \frac{R_0}{Z_0^2}\right), \tag{5}$$

since the Z_T line is a one-fourth wave long. It is thus seen that the tank load impedance consists of the fixed portion Z_T^2/R and the variable portion

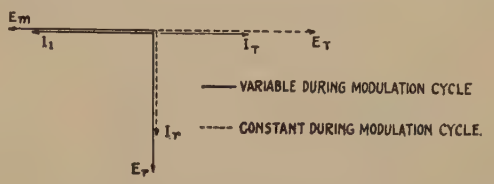

Fig. 2—Phase relations between currents and voltages.

$(Z_T/Z_0)^2 R_0$. The Z_m line, with its input and output capacitances C_1 and C, respectively, behaves now like a quarter-wave line of surge impedance Z_0. Next, we can readily derive the following relations:

$$E_r = jZ_0 I_1 = j\frac{Z_0}{R_0} 2E_m \tag{6}$$

$$E_T = -Z_T\left(\frac{Z_0}{R} + \frac{R_0}{Z_0}\right) I_1 \tag{7}$$

$$E_T = jI_r Z_T \tag{8}$$

$$I_T = j\frac{E_r}{Z_T}. \tag{9}$$

It is seen from (8) that I_r is constant. The quarter-wavelength section between the tank and the junction simply serves to convert from the constant voltage E_T into the constant current I_r.

Fig. 2 is a vector diagram showing the mutual phase relations.

Writing now absolute magnitudes in place of vectors we derive from (1) and (7)

$$E_m = \frac{1}{2}\left(\frac{E_T}{Z_T} Z_0 - \frac{Z_0^2}{R} I_1\right). \tag{1}$$

This equation represents the *dynamic load line* for the modulator tube which is a straight-line relation.

The network efficiency of the system becomes (from (10))

$$\eta = \frac{\dfrac{E_r^2}{R}}{\dfrac{E_r^2}{R} + 2E_m I_1} = \frac{Z_0 I_1}{RI_r} = \frac{I_x}{I_r}. \tag{11}$$

The efficiency is proportional to I_x which is the current flowing through R. I_x becomes equal to I_r, and the network efficiency equal to 100 per cent, if E_m becomes zero. This condition is not quite attainable (because it would require making $R_0 = 0$), but values up to 90 per cent can be obtained (if E_0 is operated in the positive region only). This means that the network efficiency is about 45 per cent at carrier level

and the over-all efficiency is 27 per cent if the efficiency of the power amplifier is 60 per cent. This efficiency is about equal to that obtainable with a class B amplifier, or with a bias-modulated stage.

The loss of the modulator tube is

$$\text{plate loss for } \textit{two} \text{ tubes} = I_1^2 R_0 = \frac{E_T}{Z_T} E_r - \frac{E_r^2}{R} \cdot \quad (12)$$

As E_r varies from zero to maximum during the modulation cycle, the loss goes through a maximum. This occurs when

$$E_r = \frac{1}{2} R \frac{E_T}{Z_T} \cdot$$

By substitution into (12) we obtain the

$$\text{maximum loss per tube} = P_0 = \frac{1}{8} R \left(\frac{E_r}{Z_T}\right)^2 = \frac{1}{8} R I_r^2 \cdot \quad (13)$$

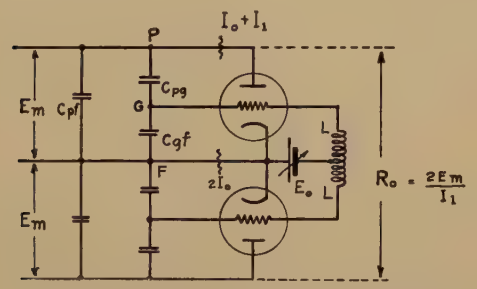

Fig. 3—Output capacitance of the modulator.

The input power supplied by the tank circuit is

$$P_{\text{input}} = E_r I_r.$$

The input power increases in linear proportion with the antenna current. The power supplied to the antenna is E_r^2/R; the difference (equation (12)) is dissipated on the plates of the modulator tubes.[2]

For design purposes we are not so much interested in the maximum loss P_0 as we are interested in knowing the modulator plate loss at carrier level, that is, with no modulation, as well as in knowing the plate loss for sustained 100 per cent modulation.

We put

I_{10} = value of I_1 at modulation peak

P_a = value of antenna power at modulation peak

$P_a = (I_{10} Z_0)^2/R$

$\eta_{\max}$ = network efficiency at modulation peak.

We find from (11) that

$$\eta_{\max} = \frac{1}{2} \sqrt{\frac{P_a}{2P_0}} \cdot$$

At carrier level, $I_1 = \frac{1}{2} I_{10}$ and from (12)

plate loss at *carrier* level, for one tube

$$= \frac{1}{4}\left[\frac{E_T}{Z_T} Z_0 I_{10} - \frac{1}{2} P_a\right]$$

$$= \tfrac{1}{4}\sqrt{2P_a P_0}\,(2 - \eta_{\max}). \quad (14)$$

For sustained 100 per cent modulation we find

$$E_r = \tfrac{1}{2}\eta_{\max} R I_r (1 + \sin vt),$$

where v is the modulation (or video) frequency. The loss during one complete modulation cycle is:

average plate loss for 100 per cent modulation, for one tube

$$= \int_{vt=0}^{vt=2\pi} \frac{1}{2} \frac{E_r}{R} (RI_r - E_r) d(vt)$$

$$= \tfrac{1}{2}\sqrt{2P_0 P_a}\,(1 - \tfrac{3}{4}\eta_{\max}). \quad (15)$$

Comparing (14) and (15) we find that the loss is always greatest with no modulation. The same condition holds true for grid-bias modulation.

B. The Modulator

1. Output Capacitance. The modulator consists of two tubes working in push-pull with respect to radio frequency. The grids work in parallel with respect to the modulation frequency. The arrangement is shown in Fig. 3. Both grids are joined by a wire connection whose center tap is tied to the filaments through the source of modulation voltage E_0. The inductance of this wire connection between grids is called $2L$. The radio-frequency impedance between grid and filament becomes

$$Z_{gf} = j\omega L \frac{1}{1 - \left(\frac{\omega}{\omega_0}\right)^2}$$

where ω_0 is the frequency at which L and C_{gf} will resonate with each other. A portion of the total plate swing E_m will lie across grid and filament. The ratio a of the two voltages is given by the relations

$$a = \frac{E_g}{E_m} = \frac{Z_{gf}}{Z_{gf} - j\dfrac{1}{\omega C_{pg}}} \cdot$$

The effective capacitance C between PP is readily computable if L is known. In many cases L is very small. We then have for *two* tubes, as shown in Fig. (3),

$$C = \tfrac{1}{2}(C_{pf} + C_{pg}). \quad (16)$$

This may be contrasted to the output capacitance found in a neutralized push-pull output stage for grid-bias modulation. Here we have for each tube

$$C = 2C_{pg} + C_{pf}. \quad (17)$$

[2] Figure 5 of reference 1.

Hence, for the same number of tubes, the output capacitance is about twice as high as for plate-load-impedance modulation. In practice, however, the ratio is usually smaller than 2:1 on account of the unavoidable stray capacitances which are present for either type of system.

2. Tube Operation. For computing the operation of the tubes we shall make use of idealized $i_p - e_p$ relations. We put

$$i_p = \frac{1}{R_p}(e_p + \mu e_g)$$

which is valid only for positive values of i_p and e_p and is limited to the region where $e_p > e_g$. In the region where $e_p < e_g$, the plate current is independent of e_g and given by the relation ("diode" characteristic)

$$i_p = \frac{1+\mu}{R_p} e_p. \qquad (18)$$

We thus obtain the idealized $i_p - e_p$ diagram shown in Fig. 4, upper half.

If the tubes are operating, we have

$$e_p = \sqrt{2}\, E_m \sin x,$$
$$e_g = E_0 + \sqrt{2}\, aE_m \sin x.$$

Upon substitution

$$i_p = \frac{1}{R_p}((1+\mu a)\sqrt{2}\, E_m \sin x + \mu E_0). \qquad (19)$$

In the region where $e_p < e_g$ (equation (18))

$$i_p = \frac{1+\mu}{R_p}\sqrt{2}\, E_m \sin x.$$

These relations are shown in Fig. 4, lower half.

For computing the direct current and the fundamental radio-frequency component of i_p we must distinguish between three different conditions.

1. The region where $e_p < e_g$ (Equation (20)).

$$I_0 = \frac{1}{2\pi}\int_0^\pi i_p dx = \frac{1+\mu}{\pi R_p}\sqrt{2}\, E_m \qquad (21)$$

$$\sqrt{2}\, I_1 = \frac{1}{\pi}\int_0^\pi i_p \sin x dx = \frac{1+\mu}{R_p}\frac{\sqrt{2}}{2} E_m. \qquad (22)$$

2. The region where E_0 is positive (equation (19)).

In this region the flow of plate current is limited to the positive half cycle of e_p,

$$I_0 = \frac{1}{2\pi}\int_0^\pi i_p dx$$
$$= \frac{1}{R_p}\left[\frac{(1+\mu a)\sqrt{2}\, E_m}{\pi} + \frac{\mu E_0}{2}\right] \qquad (23)$$

$$I_0 = \frac{2}{\pi}\left[\sqrt{2}\, I_1 + \frac{\mu E_0}{R_p}\left(\frac{\pi}{4} - \frac{2}{\pi}\right)\right]$$

$$\sqrt{2}\, I_1 = \frac{1}{\pi}\int_0^\pi i_p \sin x dx$$

$$\sqrt{2}\, I_1 = \frac{1}{R_p}\left(\frac{1+\mu a}{2}\sqrt{2}\, E_m + \frac{2}{\pi}\mu E_0\right). \qquad (24)$$

In deriving (23) and (24) we have used (19) as if it were valid all the way down to $e_p = 0$. In other words,

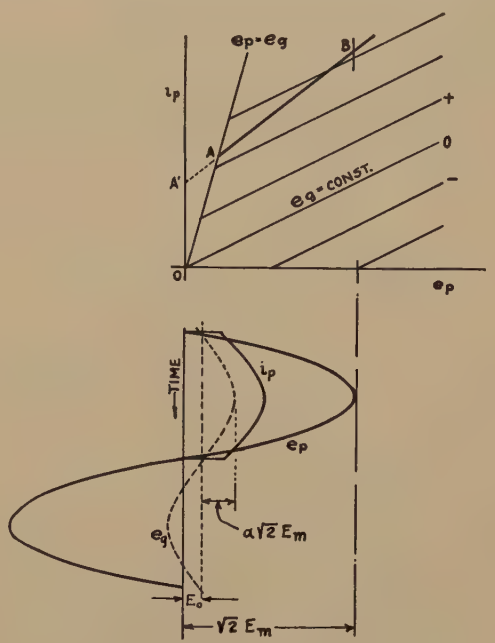

Fig. 4—Operation of modulator tubes.

(23) and (24) refer to an operating line $OA'B$ instead of OAB (Fig. 4, upper diagram). This error should not be very large, particularly in the case of I_1.

3. The region where E_0 is negative (equation (19)).

Operating conditions are to some extent similar to grid-bias modulation in this case, which, therefore, will not be discussed here.

The energy dissipated on the plate of each tube is:

$$\text{plate loss} = E_m I_1.$$

3. Modulation Characteristic. The most important and interesting operating condition of plate-load-impedance modulation is obtained if $1+\mu a = 0$. This requires to give L (Fig. 3) a suitable value such that a becomes equal to $-1/\mu$ and $\mu E_g = -E_m$. Thus the voltage E_g, which is allowed to develop between grid and filament, is in phase opposition to the plate voltage and will cancel the control effect which the plate voltage normally has upon the plate current. The radio-frequency plate current becomes, from (24),

$$I_1 = \frac{\sqrt{2}}{\pi}\frac{\mu}{R_p}E_0.$$

Hence, I_1 depends upon E_0 only, and not upon E_m; that is, not upon the network. According to (6), E_r and I_1 are directly proportional. Consequently, we have, in this case, a linear relation between the modulation voltage E_0 and the antenna current. The plate current i_p consists of square lumps of current whose height is $\mu E_0/R_p$, and whose duration is half a radio-frequency cycle. The voltage E_0 is positive throughout the full modulation cycle.

We now draw the diagram of Fig. 5 in which we plot I_1 versus E_0 (equation (24)) and also the load line I_1 versus E_m (equation (10)). We plot, furthermore, (22) into the $E_m - I_1$ diagram. Now, I_1 cannot

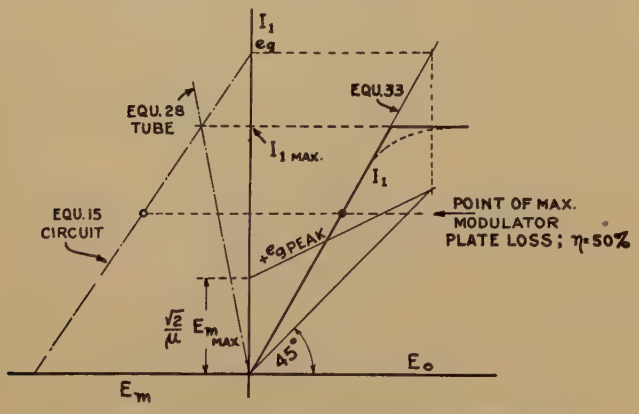

Fig. 5—Modulation characteristic, I_1 versus E_0.

rise above the point where the two lines, (10) and (22), intersect. At that point e_p becomes smaller than e_g, resulting in E_0 losing control over I_1. The modulation characteristic, I_1 versus E_0, becomes the broken straight line shown in Fig. 5. Actually, the break is a more gradual one (dotted in Fig. 5) for the reasons previously outlined. The curve thus drawn is the equivalent of the lower curve in Fig. 8 of Parker's paper.

It is highly unconventional to operate a triode with positive bias, as is done for the modulators in the case of positive E_0 operation. Since the grids draw current all the time, the required driving power of video frequency is appreciable. The plate dissipation should be adjusted conservatively in order to allow for this additional grid dissipation.

C. Sideband Attenuation Between Modulator and Antenna

The next step in our study will be to investigate as to how the system is capable of transmitting the wide frequency band required for television.

Referring to Fig. 1, we must now consider the complete mechanism of generating modulated radio frequency. The modulator M represents the sideband generator, while the power amplifier G supplies the radio-frequency carrier plus the power lost in the modulator. The sidebands travel through the transmission lines Z_m, Z_x, and Z_a to the antenna. A certain fraction of sideband energy, however, will pass along the line Z_T to generator G, despite the fact that the current I_r and the voltage E_T are not modulated magnitudes. The reason for this is evident from two facts: first, both E_r and I_T are modulated magnitudes and second, the electrical length of transmission line Z_T differs from $\frac{1}{2}\pi$ at sideband frequencies. The sideband components of I_T must pass through the generator network G, while the output voltage E_T and the generator voltage E_G must remain unmodulated carrier voltages. This is evidently impossible, unless either LC is a very "stiff" tank, representing a short circuit at modulation frequencies, or R_g, i.e., the "regulation" of the power-amplifier tubes, is zero.

We shall introduce now modulated currents and voltages by putting

$$\omega = \omega_0(1 + \delta), \tag{25}$$

where,

$$\delta = \frac{\omega - \omega_0}{\omega_0} = \frac{\text{video frequency}}{\text{carrier frequency}}. \tag{26}$$

δ is a small quantity; thus terms including δ^2 and higher powers of δ can be neglected in general.

1. The Z_T Line. When looking back towards the tank from the E_T terminals, we see the impedance

$$\frac{1}{Z_g} = \frac{1}{R_g} + j\sqrt{\frac{C}{L}}\,2\delta \tag{27}$$

wherein $\omega_0 L = 1/\omega_0 C = \sqrt{L/C}$. This impedance, when seen from the terminals AA', becomes

$$Z_{gT} = \frac{Z_g \cos\phi_1 + jZ_T \sin\phi_1}{Z_T \cos\phi_1 + jZ_g \sin\phi_1} Z_T. \tag{28}$$

The electrical length ϕ_1 is at sideband frequencies

$$\phi_1 = \tfrac{1}{2}\pi(1 + \delta).$$

Since δ is a small quantity, we may write

$$\cos\phi_1 = -\tfrac{1}{2}\pi\delta,$$
$$\sin\phi_1 = 1,$$

and (28) becomes

$$Z_{gT} = Z_T \frac{\dfrac{Z_T}{R_g} + j\delta\left(\dfrac{1}{2}\pi + 2Z_T\sqrt{\dfrac{C}{L}}\right)}{1 + j\dfrac{1}{2}\pi\delta\dfrac{Z_T}{R_g} - \pi Z_T\sqrt{\dfrac{C}{L}}\,\delta^2}. \tag{29}$$

The last two terms in the denominator (29) are usually very small in comparison with 1. If R_g or $\sqrt{L/C}$ is zero, (29) becomes

$$Z_{gT} = -jZ_T \frac{1}{2\pi\delta}. \tag{30}$$

Thus, the line Z_T always reflects an impedance across the junction terminals AA'. It is desirable that this impedance be as large as feasible. This can be achieved by making Z_T as large and R_g or $\sqrt{L/C}$ as small as possible.

2. The Z_x and Z_a Line. Let R_a be the input resistance of the antenna transmission line.

If R equals R_a, then no quarter-wave matching line is required and we have simply

$$I_x = I_a = \frac{E_r}{R}.$$

If R and R_a are not equal, a quarter-wave matching section is required. The surge impedance of this section becomes

$$Z_x = \sqrt{RR_a}. \tag{31}$$

Between input and output currents and voltages we have the relation, respectively,

$$E_a = E_r \frac{1}{-\frac{1}{2}\pi\delta + j\frac{Z_x}{R_a}} \tag{32}$$

$$I_x = I_a\left(-\frac{1}{2}\pi\delta + j\frac{R_a}{Z_x}\right). \tag{33}$$

The input impedance becomes

$$\frac{E_r}{I_x} = Z_x \frac{-\frac{1}{2}\pi\delta + j\frac{Z_x}{R_a}}{-\frac{1}{2}\pi\delta\frac{Z_x}{R_a} + j} = Z_x\left(\frac{Z_x}{R_a} + j\frac{1}{2}\pi\delta\right). \tag{34}$$

3. The Z_m Line. At the inner end of the Z_m line we have

$$I_r' = I_x + E_r\left(\frac{1+\delta}{-jX_{c0}} + \frac{1}{Z_{gT}}\right) \tag{35}$$

and at the outer end

$$I_1 = I_1' + j2E_m\frac{1+\delta}{X_{c0}}. \tag{36}$$

X_{c0} is the reactance of C or C_1 at carrier frequency. We have, furthermore, the relations

$$2E_m = E_r\cos\theta + jI_r'Z_m\sin\theta \tag{37}$$

$$I_1' = I_r'\cos\theta + j\frac{E_r}{Z_m}\sin\theta \tag{38}$$

with

$$\theta = \theta_0(1+\delta). \tag{39}$$

Finally, we have to derive a relation between I_1 and E_r, but before we can proceed we must know more about the behavior of the modulator as a sideband generator.

4. Equivalent Network of the Modulator. The current I_1 is not an independent magnitude. It depends upon both the voltage drop E_m and the modulation voltage E_0. Only E_0 is an independent magnitude. Therefore, we shall break up I_1 into two components; one of which depends upon E_m only, while the other one depends upon E_0 only.

For positive E_0 we obtain from (24), after introducing modulated magnitudes,

$$I_1^c + I_1^m\sin vt = \frac{1+\mu a}{2R_p}(E_m^c - E_m^m\sin vt) = \frac{2}{\pi}\frac{\mu}{R_p}(E_0^c + E_0^m\sin vt).$$

The exponent c indicates carrier components; the exponent m, modulation vector components. $v/2\pi$ is the video frequency. E_m^m has a negative sign, because during modulation E_m drops if I_1 increases. The modulator acts as a generator for the sidebands. The internal resistance of this generator is, by definition,

$$R_i = -\frac{dE_m^m}{dI_1^m} = +\frac{2R_p}{1+\mu a} = \frac{1}{2}R_m. \tag{40}$$

For the currents, we have

$$I_1^m + \frac{E_m^m}{R_i} = I_m^m$$

$$I_m^m = \frac{\sqrt{2}}{\pi}\frac{\mu}{R_p}E_0^m. \tag{41}$$

Thus, for the generation of sidebands, the modulator behaves like a constant-current generator, whose internal resistance, for one pair of tubes, is $2R_i = R_m$ as shown in Fig. 1. The feeding current I_m^m depends only upon the independent magnitude E_0^m.

If $1+\mu a = 0$, the internal impedance R_m becomes infinite. In this case, the generator does not exert damping upon the circuit. This is quite undesirable, because a damping resistor R_m will contribute to a better sideband characteristic.

5. Sideband Attenuation Formulas. We are now going to express the output voltage E_r in terms of

the independent modulated input current I_m^m. From Fig. 1,

$$I_m^m = I_1 + \frac{2E_m}{R_m} = I_1' + 2E_m\left(\frac{1}{R_m} + j\frac{1+\delta}{X_{c0}}\right).$$

After substituting the expressions for I_1', I_r', and $2E_m$ which were derived above and after introducing (2), (3), and (39), one obtains the following relation after a lengthy manipulation:

$$\begin{aligned} I_m^m = \frac{E_r}{Z_0}\Big[&+ j\cos\delta\theta_0 - \frac{Z_m}{R_m}(\sin\delta\theta_0 + \delta(\cos\theta_0)\sin(\theta_0+\delta\theta_0)) \\ &- j\operatorname{ctg}\theta_0((1+2\delta)\sin\delta\theta_0 + \delta^2(\cos\theta_0)\sin(\theta_0+\delta\theta_0)) \\ &+ Z_0\left(\frac{I_x}{E_r} + \frac{1}{Z_{gT}}\right)\left(-\frac{\sin\delta\theta_0}{\sin\theta_0}\right. \\ &\left. + j\left(\frac{Z_m}{R_m} + j\frac{Z_m}{X_{c0}}\delta\right)\sin(\theta_0+\delta\theta_0)\right)\Big]. \end{aligned} \tag{42}$$

In this expression, we have the dependent magnitude E_r as a function of the independent magnitude I_m^m. The bracketed term represents the attenuation for a frequency deviation of δ per cent in both amplitude and phase angle. Equation (42) represents the exact expression for the sideband attenuation of the complete network. For numerical calculations, we shall limit ourselves to the following conditions:

$$\text{no } Z_x \text{ line; i.e., } \quad R_a = R$$

$$R_g \text{ very small; i.e., } \quad \frac{1}{Z_{gT}} = j\frac{1}{Z_T}\frac{1}{2}\pi\delta.$$

For $\sin\delta\theta_0$ and $\cos\delta\theta_0$ we substitute the first terms of their respective power series. We thus obtain from (42) after some additional manipulation a simplified expression, which is easier to handle and still yields only a small error,

$$\begin{aligned} I_m^m = \frac{E_r}{Z_0}\Big[&j\left(1+\frac{Z_0^2}{RR_m}\right) \\ &+ \delta\left\{-\left(\frac{\theta_0}{\sin\theta_0}+\cos\theta_0\right)\left(\frac{Z_0}{R_m}+\frac{Z_0}{R}\right)\right. \\ &\left. -\frac{1}{2}\pi\frac{Z_0^2}{Z_T R_m} - j\theta_0\operatorname{ctg}\theta_0\left(1-\frac{Z_0^2}{RR_m}\right)\right\} \\ &+ \delta^2\left\{-\theta_0\cos^2\theta_0\left(\frac{Z_m}{R_m}+\frac{Z_m}{R}\right)\right. \\ &-\frac{1}{2}\pi\frac{Z_0 Z_m}{Z_T R_m}\theta_0\cos\theta_0 - j\left(\frac{1}{2}\pi\frac{Z_0}{Z_T}\left(\frac{\theta_0}{\sin\theta_0}+\cos\theta_0\right)\right. \\ &\left.\left. +\operatorname{ctg}\theta_0(2\theta_0+\sin\theta_0\cos\theta_0)\right)\right\}\Big]. \end{aligned} \tag{43}$$

An important case is the one in which $(1+\mu a)=0$ and R_m becomes infinite. Neglecting the δ^2 term in (43) as well as the j component of the coefficient of δ, we get for the band width the following approximate relation:

$$f_b = f_c\frac{R}{Z_0}\frac{\sin\theta_0}{\theta_0+\sin\theta\cos\theta_0}. \tag{44}$$

Band width f_b is defined as the spacing between the carrier frequency f_c and that sideband at which the attenuation is $\sqrt{2}$ times the value at carrier frequency.

Equations (42), (43), and (44) permit the calculation of the band width for the transmission-line-modulation system.

Paragraph added in proof: Without having to refer to these formulas, it is evident that the Z_m line has about the same sideband clipping effect as has a tank circuit in the case of grid-bias modulation. The claim made in the original paper of the tank decrement limitation being removed is thus unfounded. The Z_m line is in fact equivalent to a π-type filter section.

For comparison purposes we shall need the corresponding formulas for grid-bias modulation. These may be given here without proof. We assume a single tuned tank. The band width is

$$f_b = \frac{1}{2}f_c\sqrt{\frac{L}{C}}\left(\frac{1}{R_m}+\frac{1}{R}\right). \tag{45}$$

L and C are the inductance and capacitance of the tank, respectively. R is the useful resistance (in parallel to L and C), i.e., the coupled-in antenna resistance plus any loss resistance of the tank. It can be shown, that a grid-bias-modulation stage has an equivalent network identical with that shown for the modulator M in Fig. 1. R_m is the internal resistance of the modulation generator. It is found to be

$$R_m = 1.05(2R_p) \text{ approximately} \tag{46}$$

per tube. In other words, for two tubes in push pull with each tube having an R_p of 2000 ohms, R_m becomes about 8400 ohms.

Comparison Between Load-Impedance Modulation and Grid-Bias Modulation

We shall first apply the above-derived analysis to Parker's arrangement and shall later compare it against a corresponding grid-bias modulation system. Mr. Parker's kind co-operation in supplying the necessary circuit data is gratefully acknowledged.

Data given: The modulator consists of four Eimac 450 TL tubes whose constants are as follows:

$R_p = 2000$ ohms

$\mu = 13$

Maximum direct plate current—500 milliamperes

Maximum plate dissipation—450 watts
$C_{pf}=1$ micromicrofarad
$C_{pg}=4$ micromicrofarads
Carrier frequency—50 megacycles
Output power at modulation peak = 4000 watts
$R=52$ ohms
No Z_x line used
$Z_m=500$ ohms estimated
θ of Z_m about 30 degrees, corresponding to 50 centimeters length
$Z_T=70$ ohms
$E_{0\ max}$ = about 150 volts

The E_0 operation is positive through the full modulation cycle and sufficient radio-frequency grid voltage is allowed to develop on the grid such that $1+\mu a=0$.

We find from the above data that

$$Z_m/ctg\theta=290 \text{ ohms}$$
$$Z_0=Z_m \sin\theta=250 \text{ ohms}$$
$$X_c=Z_m/ctg\,\theta=290 \text{ ohms}$$
$$C=11 \text{ micromicrofarads at 50 megacycles.}$$

This value of total output capacitance which was calculated from the above given data leaves 6 micromicrofarads for stray capacitance after subtracting the output capacitance of the four tubes. The figure of stray capacitance appears quite reasonable for the actual arrangement. From

$$P_a=(I_{10}Z_0)^2/R$$

we get

$$I_{10}=1.83 \text{ amperes (for two tubes)},$$
$$\tfrac{1}{2}I_{10}=0.915 \text{ ampere (for one tube)}.$$

Because

$$I_{10}=\frac{E_T}{Z_T}\frac{R}{Z_0}$$

we find

$$\frac{E_T}{Z_T}=I_r=\frac{Z_0}{R}I_{10}=8.8 \text{ amperes}$$

$$E_T=Z_TI_r=616 \text{ volts}$$

$$E_{m\ max}=\frac{1}{2}\frac{E_T}{Z_T}Z_0=1100 \text{ volts}$$

$$P_0=\tfrac{1}{4}I_{10}E_{m\ max}=504 \text{ watts for two tubes}.$$

Plate dissipation, carrier level, for one tube = 252 watts. From (24)

$$I_{10}=\frac{\sqrt{2}}{\pi}\frac{\mu}{R_p}E_{0\ max},$$

thus

$$\frac{\mu}{R_p}=g_m=13.6 \text{ ma/volt for two tubes}.$$

The manufacturer's data give a g_m of about from 6 to 7 milliamperes per volt per tube.

When computing the band width, we must remember that $1+\mu a=0$ and R_m is infinitive. Formula (44) yields

$$f_b=5.40 \text{ megacycles}.$$

If the exact formula, (42), is used, we find +5.7 and −5.3 megacycles for the band width.

Leaving now I_{10} constant, we vary R. We obtain a curve of power output versus band width, which is

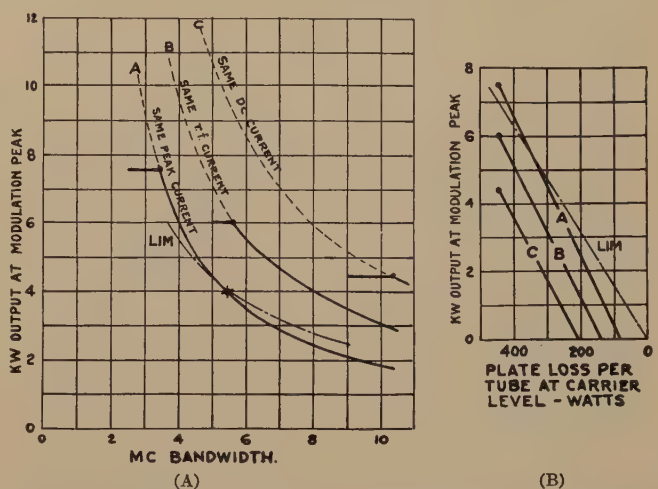

(A) (B)

Fig. 6—Comparison of plate-load-impedance modulation (LIM) versus grid-bias modulation.
Plate-load-impedance modulation:
Two tubes Eimac 450 TL for carrier.
Four tubes Eimac 450 TL for modulator.
Grid-bias modulation:
Two groups of three tubes Eimac 450 TL in push-pull.
In Fig. 6(B), plate loss for plate-load-impedance modulation refers to one modulator tube.
Curve A: Grid-bias-modulation plate-current peak (at modulation peak) per tube is the same as plate-load-impedance-modulation plate-current peak.
Curve B: Ditto, but plate radio-frequency current at modulation peak is the same.
Curve C: Ditto, but plate direct current at modulation peak is the same.

Plate Current	Plate-load-impedance modulation	Grid-bias modulation		
		A	B	C
Peak current	2.04	2.04	2.60	3.2
Radio-frequency current (r-m-s)	0.915	0.72	0.915	1.13
Direct current	1.02	0.65	0.825	1.02

plotted in Fig. 6 (A). In Fig. 6 (B), we plot the plate loss per tube at carrier level.

In the above numerical analysis of Parker's arrangement it will be noted that I_{10} per tube is about 915 milliamperes (corresponding to I_0 about equal to 820 milliamperes) while the plate dissipation is 252 watts. The rated plate-current value for the Eimac

450 TL is equal to 450 milliamperes, while the dissipation is 450 watts. Thus, he uses about twice the rated plate current, but only 56 per cent of the rated plate dissipation. The tube filament is thoriated tungsten with high emission, making this mode of operation perfectly safe, as far as the plate circuit is concerned. This throws an interesting light on the type of tube required for plate-load-impedance-modulation service: the tube should have very high plate current, but need not have a very large anode. Furthermore, it should be capable of dissipating substantial power on the grid. In choosing the Eimac 450 TL for his modulator, Parker undoubtedly selected a tube which is well suited for this type of service.

Thoriated-tungsten-filament tubes are available for carrier powers in the order of from 1 to 2 kilowatts. For higher power, one has to resort to water-cooled tubes with tungsten filament. These tubes represent high-impedance devices because their filaments do not have the large excess emission which is characteristic of thoriated tungsten. In plate-load-impedance modulation a high modulator impedance is converted to a low impedance by the inversion action of the Z_m line and thereby a matching problem is presented which becomes extremely difficult to solve. For instance, when using two suitable 20-kilowatt water-cooled tubes for modulators to generate a peak power of 40 kilowatt, one will find an output impedance R in the order of from 4 to 8 ohms. Since Z_a will be in the order of from 50 to 100 ohms, a step-up transformer would be required (Z_x line). The sideband loss in this transformer would be so unreasonably great as to rule out plate-load-impedance modulation entirely. Thus, unless special tubes are developed, plate-load-impedance modulation seems to be limited to the power range for which tubes with thoriated-tungsten filaments are available.

Finally we come to the controversial subject of comparing load-impedance modulation with grid-bias modulation. In grid-bias modulation the wave shape of the plate current at modulation peak is a half sine wave. In plate-load-impedance modulation the wave shape of the modulator plate current is a square-topped wave. On the basis of equal radio-frequency currents, grid-bias-modulation peak current will be 28 per cent higher than the plate-load-impedance-modulation peak current, while at the same time the direct current for plate-load-impedance modulation is 25 per cent higher than the direct current for grid-bias modulation. In case of emission-limited tubes, that is, for tubes with tungsten filaments, it would be logical to base the comparison upon equal peak currents. However, with thoriated-tungsten filaments, the filament emission is so extremely high that a consideration of peak currents is immaterial and in this case, the comparison should be based only on input direct current and plate loss. Furthermore, we must consider that in plate-load-impedance modulation the modulator supplies the sidebands only, while in grid-bias modulation the tubes have to supply carrier plus sidebands.

An acceptable solution seems to be therefore to place ourselves in the position of a man who has a certain number of tubes available and has to decide whether he will design a plate-load-impedance-modulation or a grid-bias-modulation system utilizing these tubes. Let us assume that we have, say, six tubes, type Eimac 450 TL.

If we choose plate-load-impedance modulation, we have to reserve two tubes for supplying the carrier. These tubes can be operated class C with an estimated efficiency of about 60 per cent at the plate loss of 450 watts per tube, yielding useful output, 1000 watts; tank loss, 360 watts; plate loss, 900 watts; input, 2260 watts; and efficiency, 60 per cent. The tank must have very large C, for reasons outlined previously; hence, its losses will be relatively high. The remaining four tubes are assumed to constitute a modulator equivalent to the one just previously analyzed. The plate loss of the modulator tubes is 252 watts per tube. This rating is very conservative but is preferably not exceeded in view of the additional losses on the grids. The peak value, the direct-current, and radio-frequency component of the plate current are tabulated in the legend of Fig. 6 and the curve of output versus band width (for variable R) is plotted in Fig. 6 (A).

If choosing grid-bias modulation we would utilize the tubes in groups of three in push-pull. We get a total output capacitance of 22.5 micromicrofarads if we assume, in addition to the tube-output capacitance (equation (17)) a distributed capacitance of 6 micromicrofarads per tube (i.e., the same value as for plate-load-impedance modulation). We now can compute the curves "band width versus peak output" and "plate loss versus peak output" taking the load resistance R as the independent variable. These curves are shown in Fig. 6. Three sets of curves are shown having, respectively, the same peak current, the same direct current, or the same radio-frequency current as the curve for plate-load-impedance modulation. Taking for instance curve A we note that at 4 kilowatts peak output, the input of the plate-load-impedance-modulation arrangement is 2260 watts, while that of the grid-bias-modulation arrangement is 2680 watts. Thus, at that point plate-load-impedance mod-

ulation is more efficient than grid-bias modulation, but the fact must not be overlooked that for plate-load-impedance modulation additional energy is dissipated on the modulator grids. If the requirement "equal peak currents" is dropped it will be noted when considering curves B and C that by means of grid-bias modulation more power and greater band width may be obtained from our six tubes without exceeding the dissipation limit than is possible with plate-load-impedance modulation. Thus, if we need only 1 kilowatt carrier and about 5 megacycles band width, we may use either plate-load-impedance modulation or grid-bias modulation, our preference depending upon other items such as efficiency, tube life, grid dissipation, ease of adjustment, etc. However, if we want to get the utmost in power and band width from the tubes, then grid-bias modulation appears preferable.

Additional comparative calculations have been made, based on equal current I_{10} for grid-bias modulation and plate-load-impedance modulation. The results will not be given here because of lack of space. In no case was it found that plate-load-impedance modulation was substantially superior to grid-bias modulation in power or band width. In many cases, it was inferior.

One point which is in favor of plate-load-impedance modulation has not yet been mentioned. In grid-bias modulation, even with perfect tubes, the modulation characteristic shows a certain amount of curvature. In plate-load-impedance modulation the modulation characteristic is, at least theoretically, a straight line (Fig. 5). Parker's curves show that the actual curve has good linearity.

We may now summarize our results:

1. The output capacitance in plate-load-impedance modulation is substantially smaller than in grid-bias modulation. This advantage, however, is practically canceled because in plate-load-impedance modulation with positive E_0 operation the generator does not exert any damping upon the circuit. In grid-bias modulation, the circuit damping contributed by the generator, is quite effective.
2. Power output and band width in plate-load-impedance modulation are comparable or somewhat inferior to those obtainable with grid-bias modulation if low-impedance, high-current tubes are available for the modulator. If high-impedance tubes have to be used, plate-load-impedance modulation is decidedly inferior in output and band width in comparison to grid-bias modulation. This fact limits plate-load-impedance modulation to relatively low carrier power.
3. Positive E_0 operation yields a practically straight modulation characteristic which cannot be obtained in grid-bias modulation. This advantage, however, is confronted by the necessity of operating the grids with positive bias during the full modulation cycle and thereby dissipating a large amount of valuable video-frequency energy on the grid.

Oscillations in Certain Nonlinear Driven Systems*

DONALD L. HERR†, STUDENT MEMBER, I.R.E.

Summary—*The development of the theory of nonlinear oscillating systems has given rise to some rather intractable nonlinear differential equations. The formerly used isoclyne method of solution is inadequate for the solution of the equation of the nonlinear system producing relaxation oscillations under the influence of an impressed periodic force. In this paper, using the specific example of a triode oscillator with impressed sinusoidal electromotive force, differential analyzer solutions of the governing differential equation, are given. A brief study of the phenomena of automatic synchronization and frequency demultiplication is made on the basis of the nonlinear theory.*

I. Introduction

As pointed out by van der Pol[1] in 1934, the analytical investigation of systems producing relaxation oscillations under the influence of an impressed periodic force had at that time hardly begun. The intractable nature of the nonlinear differential equations governing such systems affords a ready explanation for the slow progress encountered. Within recent years, however, with the increased development and use of mechanical means for the solution of mathematical problems, the mechanical solution of these equations is made possible. This paper presents differential-analyzer solutions of the equation of oscillation in certain nonlinear driven systems. These solutions, which have been obtained with the Moore School differential analyzer,[2,3] illustrate the phenomena of automatic synchronization and frequency demultiplication. The nonlinear theory of oscillating systems, as summarized by van der Pol several years ago, has served as the basis of the work described herein.

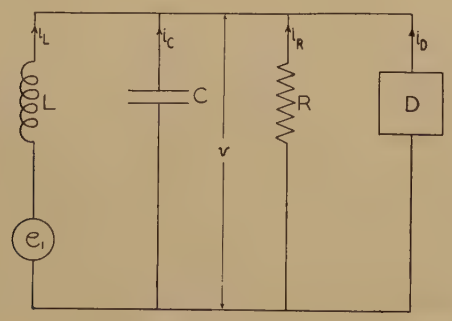

Fig. A—The fundamental circuit.

II. Derivation of the General Equation

The development of the general equation governing certain simple nonlinear systems with periodic impressed force follows. Similar derivations have appeared previously,[1] but because of certain points of physical reasoning contained therein it seems desirable to repeat the development. For the sake of specific example and because of its practical importance, consider the system depicted in Fig. A. Here D is a nonlinear electrical device, such as a vacuum tube, having a parallel LCR oscillatory circuit located in its anode circuit; e_1 is an impressed electromotive force whose presence may be due to induction from another system or it may be an actual generator at the location indicated.

In the following analysis the total current through D (total plate current of a triode in this case) is assumed to be a function of the single variable

$$(v_a + \mu v_g),$$

where v_a is the plate voltage, v_g is the grid voltage, and μ the amplifying factor of the tube. Grid current is neglected. Denote by v the varying part of the plate potential and by i_D the variable part of the plate current. Further, assume that, over the portion of the characteristic of the tube in which operation is to occur,

$$i_D = -\alpha v + \beta v^2 + \gamma v^3,$$

where α, β, and γ are constants, having respectively the dimensions $(R)^{-1}$, $(RV)^{-1}$, $(RV^2)^{-1}$, (R) denoting resistance and (V) denoting voltage.

By Kirchhoff's first law, the currents indicated on Fig. A are related by

$$i_L + i_C + i_R + i_D = 0.$$

Since

$$v = \frac{1}{C}\int i_C dt_1 = Ri_R = L\frac{di_L}{dt_1} - e_1,$$

where t_1 denotes time in seconds, it follows that

$$\frac{d^2v}{dt_1^2} + \frac{1}{C}\frac{d}{dt_1}\left\{\left(\frac{1}{R} - \alpha\right)v + \beta v^2 + \gamma v^3\right\} + \frac{v}{LC} = -\frac{1}{LC}e_1. \tag{1}$$

* Decimal classification: R140. Original manuscript received by the Institute, May 5, 1938. Revised manuscript received by the Institute, March 6, 1939.

† Formerly, Moore School of Electrical Engineering, University of Pennsylvania, Philadelphia, Penna.; now, Massachusetts Institute of Technology, Cambridge, Mass.

[1] Balth. van der Pol, "Nonlinear theory of electric oscillation," and appended bibliography, Proc. I.R.E., vol. 22, pp. 1051–1086; September, (1934).

[2] V. Bush, "A differential analyzer, a new machine for solving differential equations," *Jour. Frank. Inst.*, vol. 212, p. 447; October, (1931).

[3] Irven Travis, "Differential analyzer eliminates brain fag," *Machine Design*, p. 15; July, (1935).

Simplify (1), after the manner of van der Pol, by the substitutions

$$\frac{1}{C}\left(\alpha - \frac{1}{R}\right) = \alpha',$$

$$\frac{2\beta}{C} = \beta',$$

$$\frac{3\gamma}{C} = \gamma',$$

$$\frac{1}{LC} = \omega_0^2.$$

There results

$$\frac{d^2v}{dt_1^2} - (\alpha' - \beta' v - \gamma' v^2)\frac{dv}{dt_1} + \omega_0^2 v = -\omega_0^2 e_1. \qquad (2)$$

For practical reasons, assume the impressed electromotive force to be

$$e_1 = K^2 E_1 \sin n\omega_1 t_1,$$

where

$$K^2 = \frac{n^2\omega_1^2}{\omega_0^2},$$

and $n\omega_1$ is the periodicity of e_1.

For further simplicity, make the substitutions

$$\frac{\gamma' v^2}{\alpha'} = y^2,$$

$$\beta'(\alpha'\gamma')^{-1/2} = b,$$

$$\alpha'\omega_0^{-1} = \epsilon,$$

$$\omega_0 t_1 = t.$$

Then (2) becomes

$$\frac{d^2y}{dt^2} - \epsilon(1 - by - y^2)\frac{dy}{dt} + y = -\sqrt{\frac{\gamma'}{\alpha'}}\, K^2 E_1 \sin Kt. \qquad (3)$$

Finally, letting

$$E = -\sqrt{\frac{\gamma'}{\alpha'}}\, E_1,$$

there results

$$\frac{d^2y}{dt^2} - \epsilon(1 - by - y^2)\frac{dy}{dt} + y = K^2 E \sin Kt. \qquad (4)$$

The quantity y is the disturbance resulting from the application of a sinusoidal electromotive force of periodicity $n\omega_1$ to the system above defined, the "natural frequency" of which is ω_0. In the synchronized state the periodicity of y is ω_1. It must be here pointed out that ω_0 is not the frequency of the oscillating triode circuit when self-excited. This latter frequency will hereinafter be called the free relaxation frequency in the case of $\epsilon \gg 1$. The above derivation has been made in terms of a frequency ratio for reasons of generality. If we regard the E contained in van der Pol's equation[1] as being n^2 times the E contained in (4), the two expressions are identical.

III. Differential Equation for the Self-Excited Triode Oscillator

Before discussing the solutions obtained for (4), certain considerations of the case for $E = 0$ are timely. For this condition (4) becomes

$$\frac{d^2y}{dt^2} - \epsilon(1 - by - y^2)\frac{dy}{dt} + y = 0, \qquad (5)$$

which may be regarded as the basic differential equation for the self-excited triode oscillator. As van der Pol,[4] and van der Pol and Appleton[5] have shown, (5) also describes the operation of a tetrode or pentode with the oscillatory circuit in the grid circuit, as well as the operation of the dynatron oscillator. Moreover, if the triode is working on an inflection point of its characteristic, $b = 0 = \beta$, giving for this case

$$\frac{d^2y}{dt^2} - \epsilon(1 - y^2)\frac{dy}{dt} + y = 0. \qquad (6)$$

The oscillations governed by (6) are symmetrical in the steady state. For $\epsilon = 0$, these oscillations are sinusoidal.

Much has appeared in the literature discussing (6) fully, both for the so-called "interchange" case[1] with $\epsilon \ll 1$, and for the so-called "relaxation" case[6] with $\epsilon \gg 1$. The method of solution of (6) employed in the past has been a combination of analytical and graphical means, since to date no formal analytical solution with ϵ other than zero has been found.

Brainerd and Weygandt,[7] by means of a differential analyzer, made some studies of (5), for $b = 0$ and ϵ in the neighborhood of unity. Such systems constitute so-called "mixed" systems. In those studies curves having as co-ordinates y and y' (y' denoting the first derivative of y with respect to t) were presented as cycles descriptive of energy changes.[8] The physical

[4] Balth. van der Pol, "The effect of regeneration on the received signal strength," Proc. I.R.E., vol. 17, pp. 339–346; February, (1929).

[5] E. V. Appleton and Balth. van der Pol, *Phil. Mag.*, vol. 43, p. 177; (1922).

[6] Balth. van der Pol, *Physica*, vol. 6, p. 154, (1926); *Tidjschr. Ned. Rad. Gen.*, vol. 3, p. 25, (1926); vol. 4, p. 94, (1927); *Phil. Mag.*, vol. 2, p. 978, (1926); *Jahr. der draht. Tel. und Tel.*, vol. 28, p. 178, (1926); vol. 29, p. 114, (1927); *Exp. Wire.*, vol. 3, p. 338, (1926).

[7] J. G. Brainerd and C. N. Weygandt, "Unsymmetrical self-excited oscillations in certain simple nonlinear systems," Proc. I.R.E., vol. 24, pp. 914–922; June, (1936).

[8] F. Dacos and J. Frenkel, "L'équation des phénomènes oscillatories," *Bull. de l'Assn. des Ing. Sortis de l'Institute Montéfisore*, December, (1934).

significance of y in this paper is different from that in the Brainerd-Weygandt paper, in which y is associated with quantity of electric charge. In the derivation of the general equation given in part II above, y is associated with the voltage appearing across the shunt RLC circuit of the triode oscillator and, consequently, energy changes in the system are now associated with the quantities y and $\int y dt$ in the following manner.

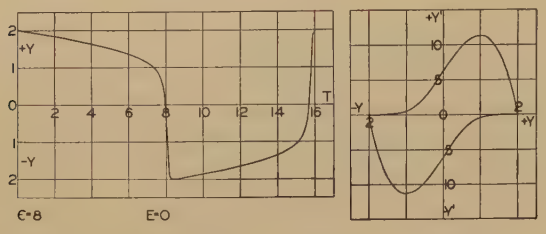

Fig. 1—Free relaxation oscillation for $\epsilon=8$, $E=0$.

The instantaneous kinetic energy and the instantaneous potential energy of the self-excited triode oscillator are, respectively, $1/2\ Li_L^2$ and $1/2\ Cv^2$. However, since $E=0$,

$$i_L = \int \frac{v}{L} dt_1.$$

Hence, the instantaneous kinetic energy and the instantaneous potential energy are, respectively,

$$\frac{1}{2L}\left(\int v dt_1\right)^2 \quad \text{and} \quad \frac{1}{2} Cv^2, \tag{7}$$

which, in the units employed in (5) become

$$\frac{C\alpha'}{2\gamma'}\left(\int y dt\right)^2 \quad \text{and} \quad \frac{C\alpha'}{2\gamma'} y^2. \tag{8}$$

Denote by ρ, the radius vector at any instant to a point on the $y-\int y\ dt$ curve. Then the sum of the instantaneous kinetic and potential energies is given by

$$\frac{C\alpha'}{2\gamma'} \rho^2. \tag{9}$$

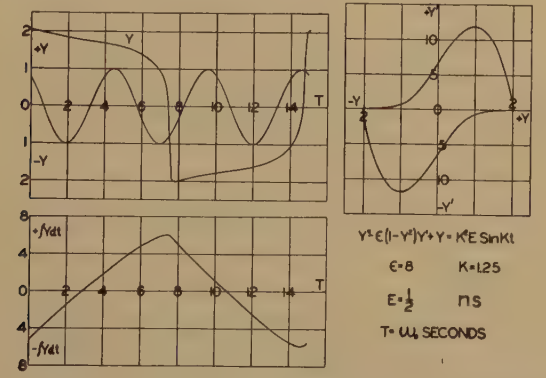

Fig. 2—Wave form and related curves for $E=0.5$, $K=1.25$, $\epsilon=8$.

IV. Solution of the Differential Equation for a Relaxation Oscillator with Impressed Sinusoidal Force

Consider (4) with $b=0$, which is the case for the triode working about an inflection point of its characteristic, with an impressed sinusoidal electromotive force. There results

$$\frac{d^2y}{dt^2} - \epsilon(1 - y^2)\frac{dy}{dt} + y = K^2E \sin Kt, \tag{10}$$

or, in the notation employed hereafter,

$$y'' - \epsilon(1 - y^2)y' + y = K^2E \sin Kt. \tag{10a}$$

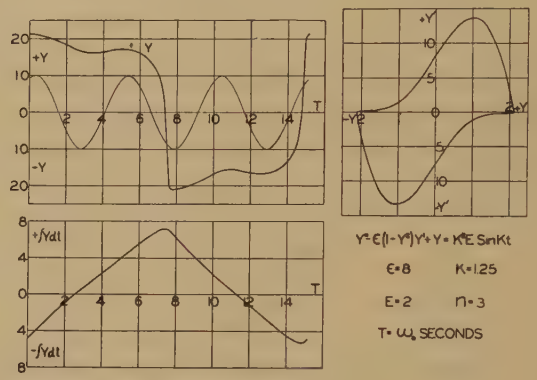

Fig. 3—Wave form and related curves for $E=2$, $K=1.25$, $\epsilon=8$.

For $\epsilon \gg 1$, the system becomes a relaxation oscillator, and for the purposes of the study described herein the sufficiently large value of $\epsilon=8$ is chosen.

In the following analysis, several terms will be employed which it is well to define at this point. By a "synchronized oscillation" is meant one the period of which is some fixed integer multiple (denoted by "n" in the accompanying figures) of the period of the impressed electromotive force. A "drifting oscillation" is one which never achieves the periodic synchronized steady-state condition. This type is denoted by the symbol "*n.s.*" (nonsynchronized) on the accompanying figures. The impressed electromotive force will hereafter be termed the "driving force."

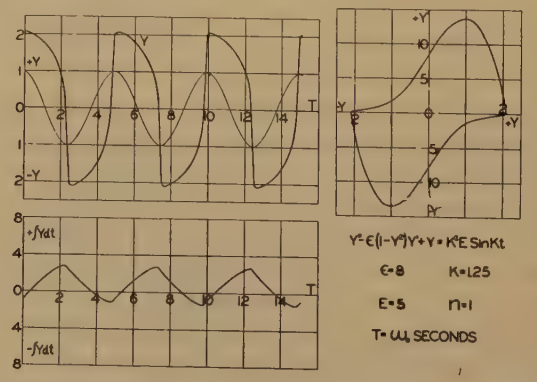

Fig. 4—Wave form and related curves for $E=5$, $K=1.25$, $\epsilon=8$.

Differential-analyzer solutions of (10a) for various values of E and K are given in Figs. 1 to 20 inclusive,[9] and the corresponding time periods are graphically shown in Fig. 21. The corresponding $y-y'$ cycles also appear, and, for additional reference, Figs. 2, 3, and 4 include $\int ydt-t$ curves. When the oscillation is of the "drifting" type a typical unsynchronized cycle is shown (Fig. 8, for example).

In Fig. 1 is shown the free relaxation oscillation for $\epsilon=8$ and no driving force impressed.

Figs. 2 to 4 depict the response of the system to an impressed electromotive force of periodicity $K=1.25$, and $E=0.5$, 2 and 5, respectively. In the units of t employed in the derivation of (10a), the period of the driving force for $K=1.25$ is 5 units. For $E=0.5$, the oscillation was found to be of the drifting type, amplitude and period varying each cycle. A "typical" cycle of this "drifting" oscillation is shown in Fig. 2. In Fig. 3, E has been increased to 2 and a synchronized third subharmonic ($n=3$) is produced, the period of which is, consequently, 15 units. Increasing

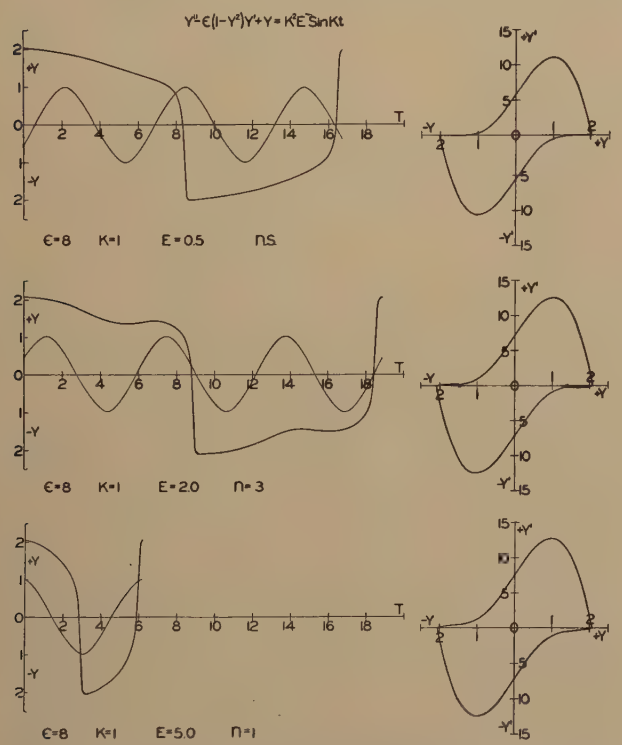

Figs. 5, 6, and 7—Wave form for $E=0.5$, 2.0, and 5.0, and $K=1.00$, $\epsilon=8$.

the amplitude still further to $E=5$, there results the synchronized first subharmonic ($n=1$) depicted in Fig. 4. In the units employed, the period of this synchronized subharmonic is 5 units and is the same as the period of the driving force. It is to be noted that the synchronized subharmonics shown in Figs. 3 and 4 are symmetrical.

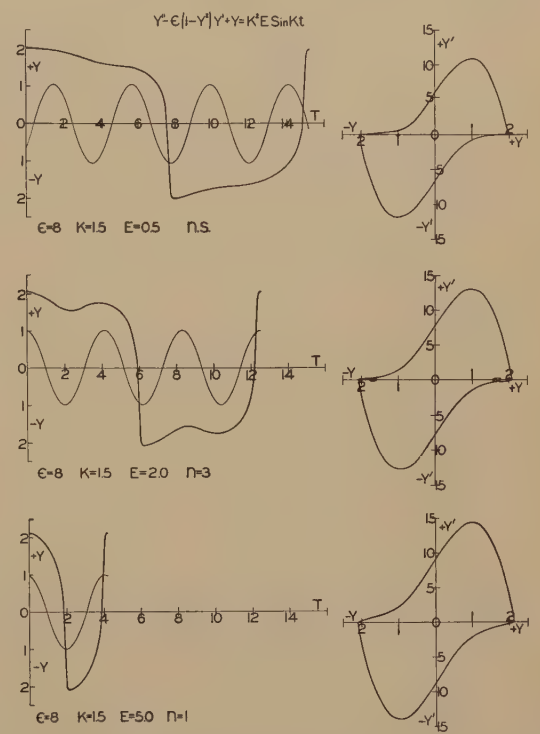

Figs. 8, 9, and 10—Wave form for $E=0.5$, 2.0, and 5.0, and $K=1.50$, $\epsilon=8$.

For $K=1$, the period of driving force in the units used in this paper is 6.25 units. Fig. 5 again illustrates the production of a drifting unsynchronized oscillation, in this case the relative frequency of the driving force has been decreased to $K=1$, and $E=0.5$.

In Fig. 6 is shown a synchronized oscillation ($E=2$) the time period of which is 18.75 units; it is consequently a third subharmonic ($n=3$) of the driving force. Increasing the amplitude still further to $E=5$, the synchronized oscillation shown in Fig. 7 is produced. The period is 6.25 units, the same as the period of the driving force, and consequently, the oscillation is that of a synchronized first subharmonic ($n=1$).

For $K=1.5$, the period of the driving force is 4.17 units. In Figs. 8 to 10, drifting, synchronized third, and synchronized first subharmonics of the driving force are successively depicted, for the respective amplitudes $E=0.5$, 2, and 5. It is to be noted that increasing the value of E increases the amplitude of the resulting driven relaxation oscillation very little. This is typical of relaxation systems, for which $\epsilon \gg 1$.

For values of $K=1$, 1.25, and 1.50 only third and

[9] The light curves on Figs. 2 to 20 are sinusoids obtained directly from the analyzer, on which the integral of equation (10a) was set. In consequence these curves are 90 degrees to the right of the actual sinusoidal applied electromotive force.

first subharmonics have appeared. For $K=1.75$ and $E=0.5$, the synchronized oscillation shown in Fig. 11 results. Its period is 17.85 units or five times the period 3.57 units of the driving force with $K=1.75$. The synchronized oscillation is then a fifth subhar-

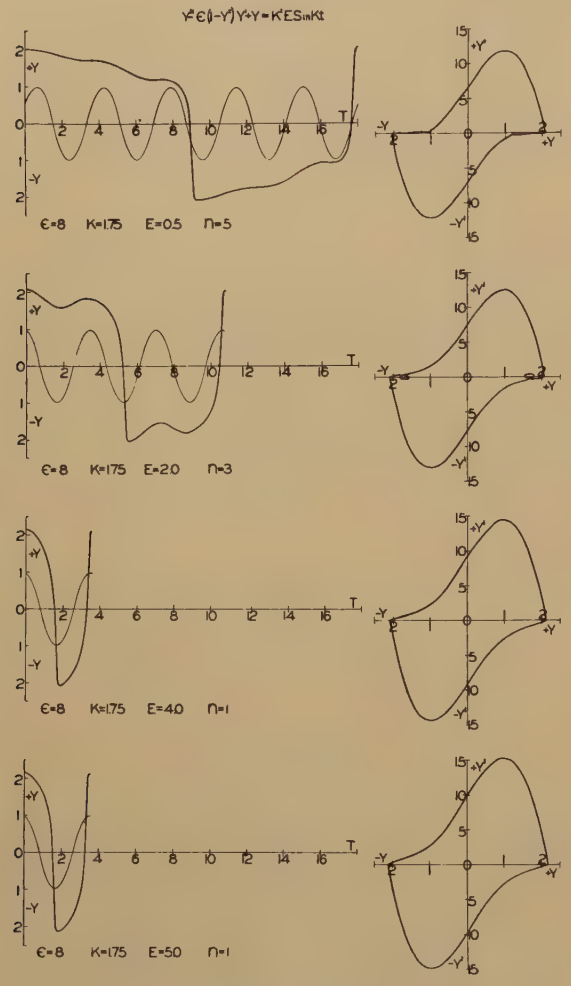

Figs. 11, 12, 13, and 14—Wave form for $E=0.5$, 2.0, 4.0, and 5.0, and $K=1.75$, $\epsilon=8$.

monic ($n=5$) of the driving force. For successively larger values of $E=2$, 4, and 5, third and first subharmonics are produced as shown in Figs. 12 to 14.

The period of the driving force having a relative frequency $K=2$ is 3.125 units. In Fig. 15, $K=2$, $E=0.5$, the resulting synchronized oscillation has a period of 15.6 units or five times that of the driving force; consequently the cycle depicted is that of a fifth subharmonic ($n=5$) of the driving force.

Figs. 16 to 18 show the production of third and first subharmonics, for $K=2$, as the amplitude of the driving force is increased.

In Fig. 21 the time periods of the driven oscillations herein depicted are plotted against E for various values of K. The solid lines joining all points having the same value of K are not to be regarded as con-

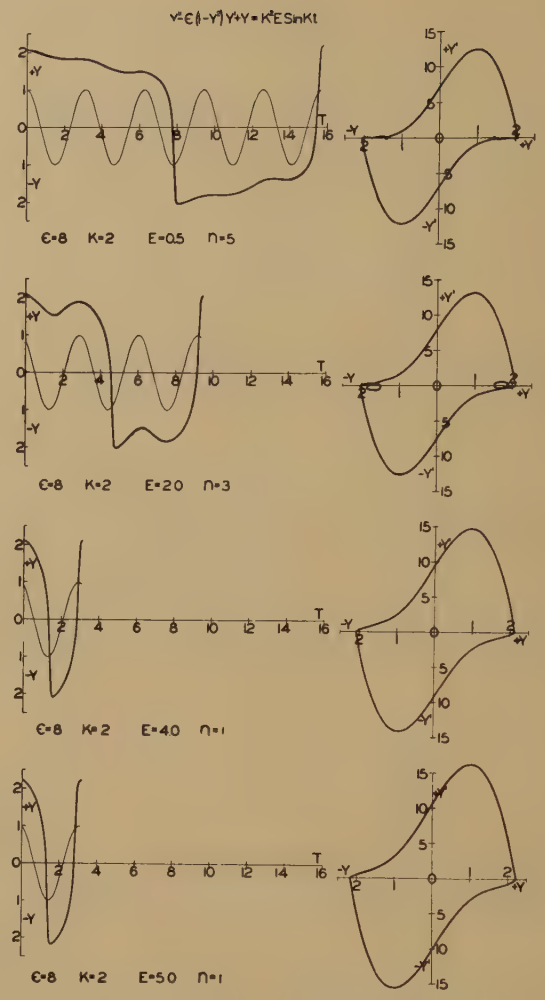

Figs. 15, 16, 17, and 18—Wave form for $E=0.5$, 2.0, 4.0, and 5.0, and $K=2.00$, $\epsilon=8$.

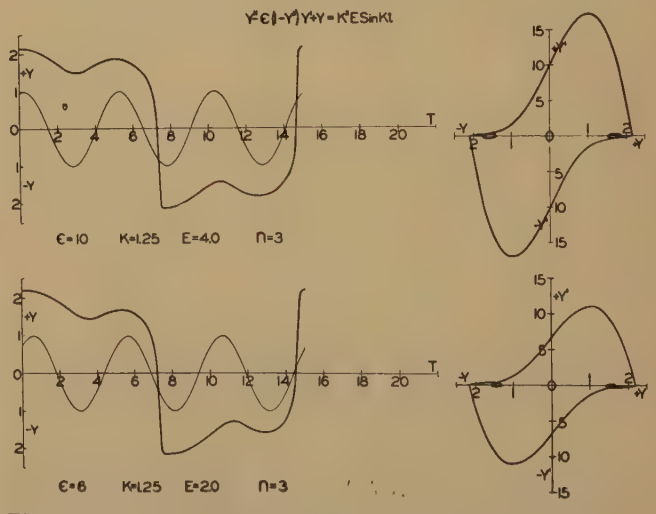

Figs. 19 and 20—K=1.25. Solutions for two other values of ϵ.

tinuous curves between the discrete points enclosed by circles.

In Figs. 19 and 20 are shown two third subharmonics for values of ϵ different from 8.

V. Conclusion

It is observed that in going from the drifting to the synchronized state, synchronization is suddenly effected on the nearest odd subharmonic. Other analyzer solutions, not included in this paper, confirm this. Further, for particular values of K and E, which finally produce synchronization, the resulting steady-state wave form and phase relation with the impressed sinusoid appear to be independent of the initial phase of the sinusoid and of other initial conditions. The only apparent effect of varying the initial phase angle is to hasten or retard by a few cycles the appearance of the steady synchronized state. Inspection of (10a) shows that all such synchronized subharmonics are symmetrical oscillations.

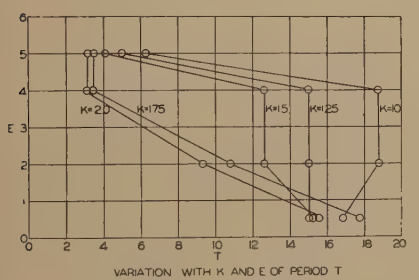

Fig. 21—Variation of time period with K and E.

All of the above phenomena are in agreement with the experimentally observed properties of relaxation oscillations. Especially do they confirm the phenomenon of automatic synchronization over a frequency range as great as an octave ($K=2$), as mentioned by van der Pol.[1] They also confirm the physical fact that the phenomenon of resonance is practically absent in the case of relaxation oscillations, and that the application of an external electromotive force has as its main effect the variation of time period of the resulting oscillation. This effect is seen to give rise to the phenomenon of subharmonics over a wide range of frequency demultiplication.

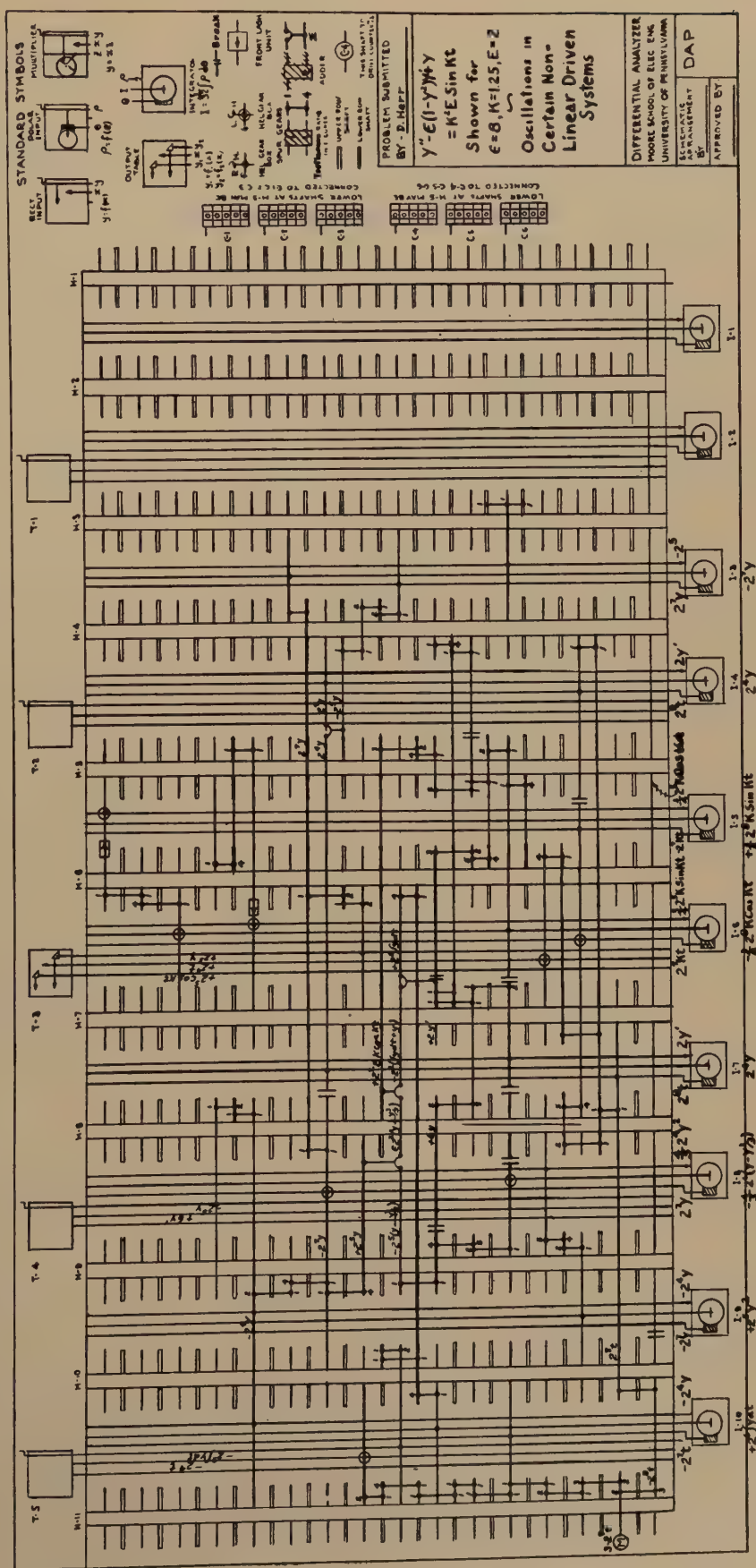

Fig. B—Differential analyzer arrangement used in the studies.

In the course of these studies, employing (10a), only odd-order subharmonics have appeared. The greater the relative frequency of the driving force the higher the order of odd subharmonics it is possible to produce. Increasing the amplitude of the driving force results in successive "driving through" to a lower order of odd subharmonic. It must be stressed that the more general equation (4) is probably the one governing the production of both even- and odd-order subharmonics. Further work in this direction should be undertaken to establish the greater generality of (4) or of a somewhat similar differential equation.

These results should be of value in the further development of the nonlinear theory of electric oscillations and in application to the design of relaxation oscillators with an impressed sinusoidal electromotive force.

Acknowledgment

The author is indebted to the Fellowship and Research Committee of the Charles A. Coffin Foundation of the General Electric Company for the Fellowship award which made this work possible. The helpful advice and assistance of members of the Moore School staff is gratefully acknowledged.

Appendix

A. For reference, the quantities appearing in (4) are redefined in terms of the elements of the system studied:

$$\epsilon = \sqrt{\frac{L}{C}}\left(\alpha - \frac{1}{R}\right);$$

$$b = \frac{2\beta}{\sqrt{3\gamma\left(\alpha - \frac{1}{R}\right)}};$$

$$t = \frac{1}{\sqrt{LC}}t_1 = \omega_0 t_1, \quad t_1 \text{ in seconds};$$

$$y = \sqrt{\frac{3\gamma}{\left(\alpha - \frac{1}{R}\right)}}\,v, \quad v \text{ in volts};$$

$$E = \sqrt{\frac{3\gamma}{\left(\frac{1}{R} - \alpha\right)}}\,E_1, \quad E_1 \text{ in volts};$$

$$K = \frac{n\omega_1}{\omega_0}.$$

B. Fig. B gives the schematic diagram of the differential-analyzer arrangement used in the course of these studies.

Additional Bibliography

(1) Yasusi Watanabe, "Some remarks on the multivibrator" Proc. I.R.E., vol. 18, pp. 327–335; February, (1930).

(2) J. Groszkowski, "Frequency division," Proc. I.R.E., vol. 18, pp. 1960–1970; November, (1930).

(3) A. Andronow and A. Witt, "Zur Theorie des Mitnehmens von van der Pol," *Archiv. für Elektrotech.*, vol. 24, p. 99, (1930).

(4) B. Decaux and Ph. le Corbeiller, "Sur un systeme élèctrique autoentretenu utilisant un tube à néon," *Comptes Rendus*, (Paris), vol. 193, p. 723, (1931).

(5) N. Kryloff and N. Bogoliuboff, "Quelques exemples d'oscillations non linéaires," *Comptes Rendus*, (Paris), vol. 194, p. 957, (1932); "Les phénomènes de demultiplication de fréquence en radiotechnique," *Comptes Rendus*, (Paris), vol. 194, p. 1119, (1932).

(6) N. Kryloff and N. Bogoliuboff, "Problèmes fondamentaux de la mecanique non linéaire," *Rev. Gen. des Sciences Pures et Appliquées*, vol. 44, p. 9, (1933).

(7) H. Straub, "Ueber selbsterregte nicht lineare Rohrenschwingungen," *Helv. Phys. Acta*, vol. 6, p. 337, (1933).

(8) W. A. Lazarew, "Ueber die Erregung von Schwingungen durch Parameteränderung (heteroparametrische Erregüng), *Zeit. für Tech. Phys.*, vol. 4, p. 30, (1934).

Characteristics of the Ionosphere at Washington, D.C., April, 1939*

T. R. GILLILAND†, ASSOCIATE MEMBER, I.R.E., S. S. KIRBY†, ASSOCIATE MEMBER, I.R.E., AND N. SMITH†, NONMEMBER, I.R.E.

DATA on the critical frequencies and virtual heights on the ionosphere layers during April are given in Fig. 1. Fig. 2 gives the monthly average values of the maximum usable frequencies which could be used for radio sky-wave communication by way of the regular layers during undisturbed periods. Fig. 3 gives the distribution of the hourly values of F- and F_2-layer critical frequencies about the average for the month. Fig. 4 gives the expected values of the maximum usable frequencies for transmission by way of the regular layers, average for July, 1939. The ionosphere storms and sudden ionosphere disturbances are listed in Tables I and II, respectively.

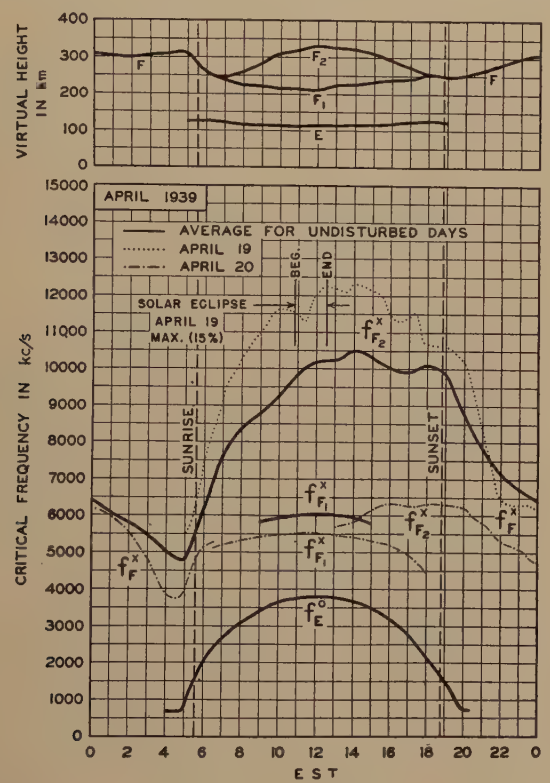

Fig. 1—Virtual heights and critical frequencies of the ionosphere layers, April, 1939. The solid-line graph is the undisturbed average; the dotted-line and dashed-line graphs are for the days of April 19 and 20, respectively. April 19 was a day of high $f^x_{F_2}$ preceding the severe ionosphere storm of April 20.

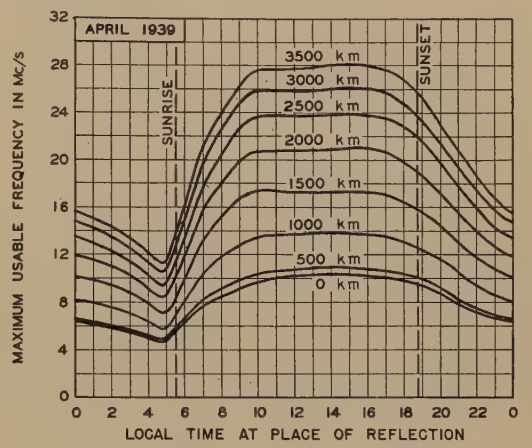

Fig. 2—Maximum usable frequencies for radio sky-wave transmission. Average for April, 1939, for undisturbed days for dependable transmission by the regular F and F_2 layers.

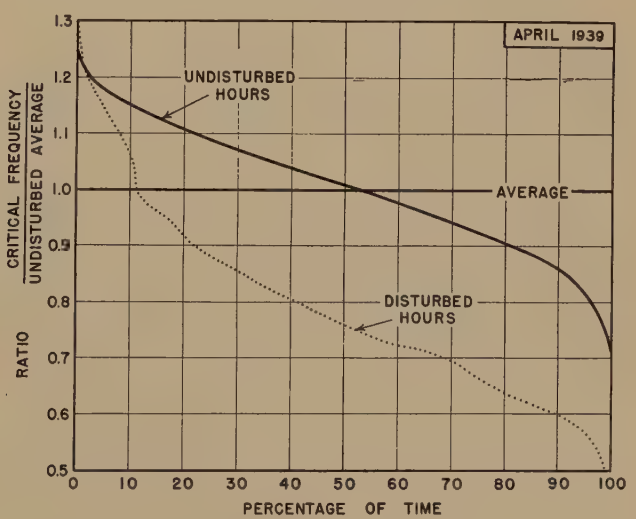

Fig. 3—Distribution of F- and F_2-layer critical frequencies (and approximately of maximum usable frequencies) about monthly average. Abscissas show percentage of time for which the ratio of the critical frequency to the undisturbed average exceeded the values given by the ordinates. The graphs give data as follows: solid line, 282 undisturbed hours; dotted line, 265 disturbed hours listed in Table I.

Ionosphere storms during April were both numerous and severe. Of the 720 hours of the month, 265 hours were disturbed. The high $f^x_{F_2}$ on April 19 preceding the severe ionosphere storm of April 20 should

* Decimal classification: R113.61. Original manuscript received by the Institute, May 11, 1939. These reports have appeared monthly in the PROCEEDINGS starting in vol. 25, September, (1937). See also vol. 25, pp. 823–840, July, (1937). Publication approved by the Director of the National Bureau of Standards of the U. S. Department of Commerce.

† National Bureau of Standards, Washington, D. C.

be noted. Similar effects have previously been reported by the National Bureau of Standards for June 18, 1936,[1] May 11, 1938,[2] and March 29, 1939.[3] This phenomenon appears to be characteristic of the early stages of severe ionosphere storms in this latitude, the stages preceding the blowing up of the ionosphere or the turbulent phase of the storms.

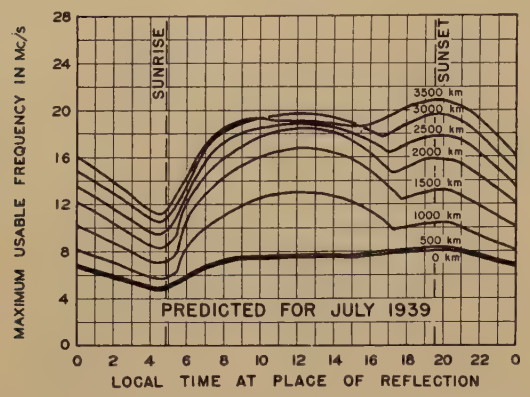

Fig. 4—Predicted maximum usable frequencies for dependable radio sky-wave transmission by way of the regular E, F, F_1, and F_2 layers, for July, 1939. The F layer will ordinarily determine the maximum usable frequencies at night, and, except for nearly vertical incidence, the E and F_2 layers will determine them during the day. The effect of the E and F_1 layers is shown by the humps on the graphs during the middle of the day. The values shown will be considerably exceeded during irregular periods by reflections from clouds of sporadic-E layer.

Prolonged periods of low-layer absorption, for several hours in the middle of the day, were observed on many days during April. This effect was especially pronounced on April 26, 28, 29, and 30.

[1] *Phys. Rev.*, vol. 50, p. 258, (1936).
[2] T. R. Gilliland, S. S. Kirby, and N. Smith, "Characteristics of the Ionosphere at Washington, D. C., May, 1938," PROC. I.R.E., vol. 26, pp. 909–913; July, (1938).
[3] T. R. Gilliland, S. S. Kirby, and N. Smith, "Characteristics of the Ionosphere at Washington, D. C., March, 1939," PROC. I.R.E., vol. 27, pp. 348–349; May, 1939.

TABLE I
IONOSPHERE STORMS (APPROXIMATELY IN ORDER OF SEVERITY)

Date and hour E.S.T. 1939 April	h_F before sunrise (km)	*Minimum f_F^2 before sunrise (kc)	Noon $f_{F_2}^2$ (kc)	Magnetic character[1] 00–12 G.M.T.	Magnetic character[1] 12–24 G.M.T.	Ionosphere character[2]
19	302	5500	11700	0.9	1.1	—
20	368	3850	5500	0.8	0.7	1.8
21	356	4100	7300	0.6	0.6	0.7
22	358	3600	6300	0.4	0.6	1.1
23	388	3600	<5400	1.8	1.7	1.9
24 (until 0500)	350	3300	—	0.3	1.9	0.9
16 (after 2200)	—	—	—	0.0	0.4	1.9
17	412	3700	5800	2.0	1.9	1.9
18 (until 1000)	364	3600	—	1.0	1.3	0.9
24 (after 1300)	—	—	—	0.3	1.9	1.9
25 (until 1500)	402	3200	8200	1.8	1.0	1.1
1 (after 0100)	360	3400	6800	0.7	0.7	1.0
2 (until 0500)	326	3000	—	0.4	0.6	0.5
6 (0200 to 2200)	324	4700	7600	0.2	0.1	0.8
3 (0300 to 0800)	340	3300	—	0.4	0.4	0.3
12 (until 0600)	354	4200	—	0.9	0.4	0.2
28 (0100 to 1200)	334	5850	8800	0.4	0.4	0.2
For comparison: Average for undisturbed days	304	4817	10160	0.3	0.4	0.0

[1] American magnetic character figure, based on observations of seven observatories.
[2] An estimate of the severity of the ionosphere storm at Washington on an arbitrary scale of 0 to 2, the character 2 representing the most severe disturbance.

TABLE II
SUDDEN IONOSPHERE DISTURBANCES

Date 1939	G.M.T. Beginning	G.M.T. End	Locations of transmitters	Relative intensity at minimum[1]	Other phenomena
April					
15	1540	1600	Ohio, Mass., Ont., D. C.	0.05	
15	1925	1945	Ohio, Mass., Ont.	0.1	
16	1910	1930	Ohio, Mass., Ont., D. C.	0.0	Ter. mag. pulse 1910 to 1920
21	1659	1920	Ohio, Ont., D. C.	0.0	Ter. mag. pulse 1650 to 1725
23	1558	1740	Ohio, Mass., Ont., D. C.	0.0	
23	1823	1940	Ohio, Mass., Ont., D. C.	0.0	
25	2035	2050	Ohio, Mass., Ont.	0.1	
29	1715	1810	Ohio, Mass., Ont., D. C.	0.0	
30	1520	1557	Ohio, Ont., D. C.	0.1	

[1] Ratio of received field intensity during fade-out to average field intensity before and after; for station W8XAL, 6060 kilocycles, 650 kilometers distant.

Sporadic-E layer reflections were observed at eight megacycles or above on only three hours, and above six megacycles on only eight hours, during the month.

Institute News and Radio Notes

PACIFIC COAST CONVENTION
San Francisco, California
June 27-30, 1939

The first convention of national scope of the Institute to be held on the Pacific Coast is scheduled for San Francisco during the last four days of June. Headquarters will be at the Mark Hopkins Hotel. In the two previous years, meetings were held in Spokane and Portland and gave unmistakable evidence of a substantial interest in a meeting of national character. The San Francisco World's Fair makes that city particularly attractive as a meeting place.

To one who knows San Francisco, a renewal of acquaintanceship is all that needs be suggested to start making plans and recalling pleasant memories. To one who has never been there, comes indistinct visions of its many charms. Chinatown, the largest Chinese city outside of the Orient, Fisherman's Wharf where the fishing fleet, back from its morning venture, lies at rest, Market Street with its famed clock-towered ferry building at one end and Twin Peaks at the other, are but a few of its world-famed attractions.

To these one must add Treasure Island and its 400 man-made acres devoted to recreation and education. Sponsored by eleven western states, fifty million dollars have been invested with one thought—to make the visitor want to return for more. An island that may be reached by automobile by way of the new San Francisco-Oakland Bay Bridge, it harbors the giant clipper ships which bring Asian cities within days rather than weeks of America and recall to mind the earlier clippers which once passed through the Golden Gate now bridged by the longest single span in the world.

Our Convention will be held at the same time as the combined Pacific Coast and Summer Convention of the American Institute of Electrical Engineers. Twenty-seven papers will be presented at six technical sessions. Eight are contributions from Pacific coast authors, sixteen have been prepared by authors from the eastern part of this country, two are from Europe, and one from Puerto Rico. Thus, the program which follows is of broad geographical and topical interest. None of the papers have been preprinted and there is no assurance that they will be presented elsewhere or published in the PROCEEDINGS.

PROGRAM

Tuesday, June 27

9:00 A.M.

Registration

10:00 A.M.–12:00 NOON

Opening address by R. A. Heising, President of theInstitute.

1. "Communications Engineering in Geophysical Exploration," by Herbert Hoover, Jr., United Geophysical Corporation, Pasadena, Calif.
2. "Federal Communications Commission Engineering Regulations and Standards of Good Engineering Practice for Broadcast Stations," by S. L. Bailey, Jansky and Bailey, Washington, D. C.
3. "Columbia's West Coast Operations," by L. H. Bowman, Columbia Broadcasting System Hollywood, Calif.

2:00 P.M.–4:30 P.M.

4. "Recent Developments in Aerial Navigation," by H. H. Willis, Sperry Gyroscope Company, Brooklyn, N. Y.
5. "Aircraft Instrument Landing Research at the Massachusetts Institute of Technology," by E. L. Bowles, Massachusetts Institute of Technology, Cambridge, Mass.
6. "Study of the Effects of Mountains in Radiogoniometry and of the Combined Use of Radio Beacons and Radio Compasses for Aerial Navigation," by Andrè Busignies, Le Materiel Telephonique, Paris, France.

7. "Acoustic Models of Radio Antennas," by E. C. Jordan and W. L. Everitt, Ohio State University, Columbus, Ohio.
8. "Recent Advances in Receiving Equipment for Transoceanic Telephony," by F. A. Polkinghorn, Bell Telephone Laboratories, New York, N. Y.

Wednesday, June 28

9:00 A.M.–11:00 A.M.

9. "Electron Optics in Television," by V. K. Zworykin, RCA Manufacturing Company, Camden, N. J.
10. "Current Division in Plane-Electrode Triodes," by Karl Spangenberg, Stanford University, Stanford University, Calif.
11. "Functions of Electron Bombardment in Television," by I. G. Maloff, RCA Manufacturing Company, Camden, N. J.
12. "Surface-Controlled Mercury-Pool Rectifier," by T. M. Libby, Pacific Telephone and Telegraph Company, Seattle, Wash.

11:30 P.M.–2:00 P.M.

Trip to Pan American Airways terminal and inspection of Boeing Clipper.

Giant redwoods

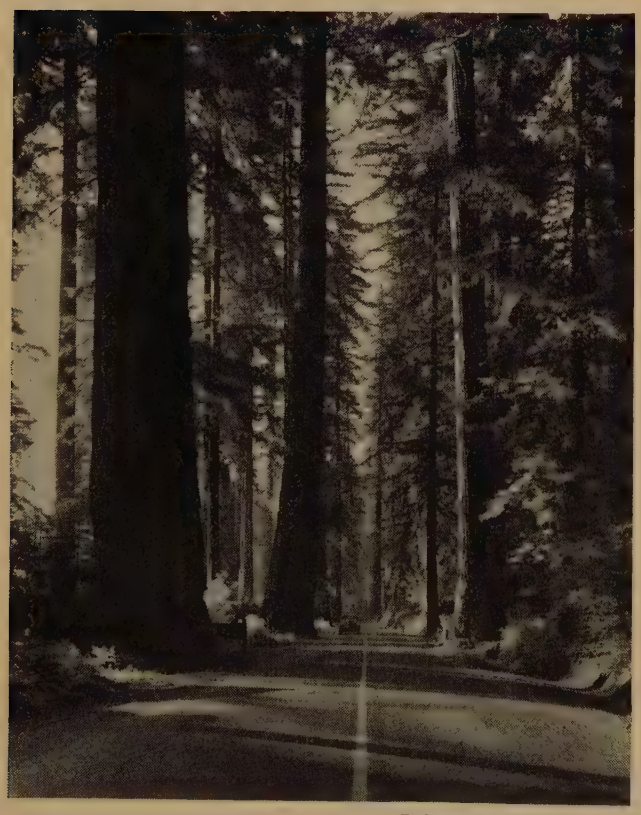

Redwood Empire Association

Redwood Empire Association

Along the California coast

2:00 P.M.–4:30 P.M.

13. "Direct-Current and Audio-Frequency Amplifier," by L. J. Black and H. J. Scott, University of California, Berkeley, Calif.
14. "Golden Gate International Exposition Radio and Sound Distributing Systems," by C. A. Lahar and L. Hewitt, RCA Manufacturing Company, Camden, N. J.
15. "Radio-Frequency Spark-Over in Air," by P. A. Ekstrand, Heintz and Kaufman, South San Francisco, Calif.
16. "Solar Cycle and the F_2 Region of the Ionosphere," by W. M. Goodall, Bell Telephone Laboratories, Deal, N. J.
17. "Atmospherics and Radio Transmission Phenomena in Puerto Rico," by G. W. Kenrick and P. T. Sammon, University of Puerto Rico, Rio Piedras, P. R.
18. "Transmission on 41 Megacycles," by S. S. MacKeown, B. M. Oliver, and A. C. Tregidga, California Institute of Technology, Pasadena, Calif.

Thursday, June 29

9:00 A.M.–11:30 P.M.

(Joint Session with American Institute of Electrical Engineers)

19. "The Klystron as a Generator of Very Short Waves," by W. W. Hansen, R. H. Varian, S. F. Varian, D. L. Webster, and J. R. Woodyard, Stanford University, Stanford University, Calif.
20. "Instruments and Methods of Measuring Radio Noise," by C. V. Aggers, Westinghouse Electric and Manufacturing Company, East Pittsburgh, Penna.; D. E. Foster, RCA License

Clyde H. Sunderland

A clipper ship over Treasure Island

Laboratory, New York, N. Y.; and C. S. Young, Pennsylvania Power and Light Company, Allentown, Penna.

21. "Methods of Controlling Radio Interference," by C. V. Aggers, Westinghouse Electric and Manufacturing Company, East Pittsburgh, Penna.
22. "Technical Framework of our Television," by E. W. Engstrom, RCA Manufacturing Company, Camden, N. J.
23. "A New Standard Volume Indicator and Reference Level," by H. A. Chinn, Columbia Broadcasting System; D. K. Gannett, Bell Telephone Laboratories; and R. M. Morris, National Broadcasting Company; all of New York, N. Y.

12:30 P.M.

Trip to Stanford University jointly with American Institute of Electrical Engineers.

2:00 P.M.–4:30 P.M.

24. "Electronic-Wave Theory of Velocity-Modulation Tubes," by Simon Ramo, General Electric Company, Schenectady, N. Y.
25. "Recent Ultra-High-Frequency Developments," by B. J. Thompson, RCA Manufacturing Company, Harrison, N. J.
26. "Simple Television Antennas," by P. S. Carter, RCA Communications, Rocky Point, L. I., N. Y.
27. "Continuous-Wave Interference with Television Reception," by C. N. Smyth, Kolster-Brandes, Sidcup, Kent, England.

Friday, June 30

10:00 A.M.–12:00 NOON

Trip to the tube manufacturing plants of Eitel and McCullough, San Bruno, and Heintz and Kaufman, South San Francisco.

2:00 P.M.–5:00 P.M.

Trip to the University of California.

TRIPS

Pan American Airways Terminal

This trip will be started from the hotel at 11:30 A.M. on Wednesday. The terminal is on Treasure Island and the Radio installation on one of the giant Boeing clipper ships will be inspected. A tour will then be made of the radio maintenance shop, instrument calibration laboratory, and ground communications facilities.

Stanford University

We have been invited to participate in a trip to Stanford University arranged by the American Institute of Electrical Engineers. Busses will leave the hotel at 12:30 o'clock on Thursday afternoon. The high-voltage laboratory and electrical engineering department will be visited.

Tower of the Sun and Court of the Moon

Golden Gate International Exposition

Manufacturing Plants

On Friday morning, a trip will be made to the tube-manufacturing plants of Eitel and McCullough at San Bruno and to Heintz and Kaufman at South San Franciso. We shall return to the hotel in time for lunch.

Berton W. Crandall

Stanford University's high-voltage laboratory

University of California

On Friday afternoon, the radiation laboratory of the University of California will be visited and a demonstration of the Cyclotron will be given.

SUMMARIES OF TECHNICAL PAPERS

The following summaries of technical papers to be presented are arranged alphabetically by the names of the authors. The numbers correspond to the order of presentation. No preprints are available nor is publication of any paper in the PROCEEDINGS definite.

21. METHODS OF CONTROLLING RADIO INTERFERENCE

C. V. AGGERS

(Westinghouse Electric and Manufacturing Company, East Pittsburgh, Penna.)

Man-made radio interference only is treated. It may originate in both rotating and stationary equipment, the commonest forms of the latter being high-voltage line insulators and low-voltage porcelain insulators.

Three methods of attacking the problem are treated and are: (1) suitable design of equipment to reduce the generation of interfering radio currents, (2) application of low-impedance shunt filters, and (3) application of high-impedance series filters.

The filter methods confine the otherwise disturbing currents to restricted portions of the equipment which generates them and thus reduces their sphere of influence.

20. INSTRUMENTS AND METHODS OF MEASURING RADIO NOISE

C. V. AGGERS, D. E. FOSTER, AND C. S. YOUNG

(Respectively: Westinghouse Electric and Manufacturing Company, East Pittsburgh, Penna.; RCA License Laboratory, New York, N. Y.; and Pennsylvania Power and Light Company, Allentown, Penna.)

Radio noise effects are produced by extraneous electrical fields associated with transient conditions in an electric circuit. In order that apparatus producing radio noise effects can be treated and described in precise terms and the most satisfactory method of radio noise suppression employed in a given case, it is necessary that there be some means of measuring the radio noise voltage and electric fields of the type referred to in a manner which, as far as possible, is appropriate to the special characteristics of these voltages and fields and their significance in relation to radio reception. Further, in view of certain commercial and national aspects of the matter, it is desirable that there shall be a national understanding and agreement as to the method of measurement.

This paper embodies the relevant agreed recommendations of the Joint Coordination Committee on Radio Reception of EEI, NEMA, and RMA, as to the nature, essential characteristics, and performance of an instrument for the measurement of radio noise voltages. It further gives detailed descriptions of the recommended practices for measuring radio noise directly from low- and high-voltage apparatus, for making noise measurements along overhead lines, for determining broadcast field-strength levels and methods of collecting data for the establishment of radio noise standards.

Plant of Eitel-McCullough at San Bruno

2. FEDERAL COMMUNICATIONS COMMISSION ENGINEERING REGULATIONS AND STANDARDS OF GOOD ENGINEERING PRACTICE FOR BROADCAST STATIONS

S. L. BAILEY

(Jansky and Bailey, Washington, D. C.)

This paper discusses briefly the development of broadcast allocation standards as applied to coverage and interference. This is followed by a discussion of

some of the salient points of the proposed engineering rules and the Standards of Good Engineering Practice with an explanation of the types of stations provided for and the protection limits accorded each type. An analysis is then given of the possible effect of these standards and methods of classification on existing broadcast stations.

13. A DIRECT-CURRENT AND AUDIO-FREQUENCY AMPLIFIER

L. J. Black and H. J. Scott
(University of California, Berkeley, Calif.)

An amplifier suitable for the amplification of small direct-current and low-frequency transient potentials to a usable level is described. In this amplifier two multielement tubes are used as balanced modulators. A carrier voltage is applied in push-pull to two of the grids of these modulators. The plates of these modulator tubes, operating in parallel, are connected to a high-gain amplifier designed for the carrier frequency. Any carrier unbalance appearing in the modulator is amplified to a sufficient level in the carrier-frequency amplifier and applied to a linear detector. The amount of carrier unbalance is determined by the magnitude of the direct-current or low audio-frequency voltage applied to the control grid of one of the modulator tubes. By proper choice of operating conditions a linear relationship between impressed signal voltage and detector output voltage can be obtained. The paper is concluded with a discussion of the performance of the amplifier, its sensitivity, and its stability.

Heintz and Kaufman plant at South San Francisco

5. AIRCRAFT INSTRUMENT LANDING RESEARCH AT THE MASSACHUSETTS INSTITUTE OF TECHNOLOGY

E. L. Bowles
(Massachusetts Institute of Technology, Cambridge, Mass.)

The Massachusetts Institute of Technology has for some time been conducting a research on the instrument landing of airplanes under the sponsorship of the Civil Aeronautics Authority. One of the objectives of this program is the development of a system in which the landing information is given to the pilot on a single instrument in the form of an image simulating three light sources on the runway. Assuming three light sources, two placed in equally elevated positions, one on each side of the leading edge of the runway, and a single light source on the center line of the runway at a distance from the leading edge, a visual landing arrangement results.

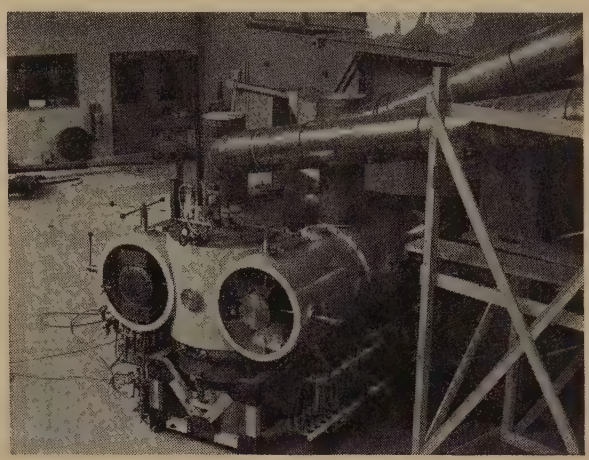

The Cyclotron at the University of California

For example, these three lights may be so arranged that a plane passed through them contains a straight-line landing path the angle of which may be made equal to the normal glide angle of a landing airplane. The pilot gliding an airplane down this plane in the proper path and with proper altitude, will see these three ground lights through his windshield as three light spots in line and equally spaced. The appearance of the lights for different altitudes and positions of the ship can readily be visualized.

The Institute was asked to produce the equivalent of this Metcalf three-light landing scheme by radio means to adapt it to use as a landing system for use under conditions of adverse visibility.

In its work on the solution of the problem, the Institute has made use of ultra-short radio waves and of gyro-instruments on the airplane. The combination, as now visualized, includes the use of Barrow horn radiators and high-frequency generators of the Stanford type. The program has involved interesting features of co-operation between departments at the Institute and close co-operation with branches of industry. These as well as the general technical aspects of the problem will be presented.

3. COLUMBIA'S WEST COAST OPERATIONS

L. H. Bowman
(Columbia Broadcasting System, Hollywood, Calif.)

The engineering developments of the Columbia Broadcasting System's West Coast engineering division will be summarized. Technical procedure and the functioning of the various engineering departments will be described. Facilities include transmitters for standard broadcast, intermediate broadcast, and high-frequency operation. A brief description of

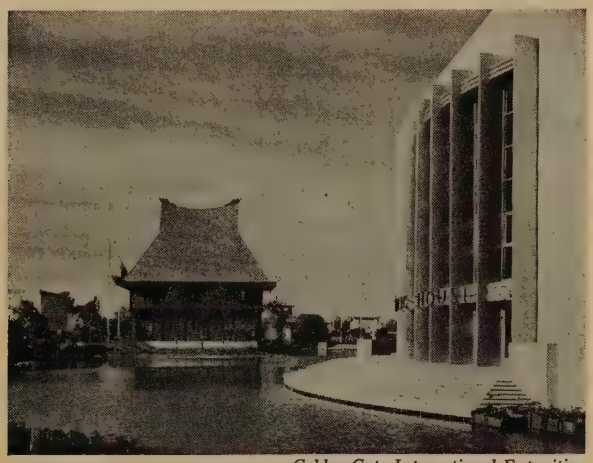

Golden Gate International Exposition

Pacific House, Lake of Nations, and Johare Pavilion

the recently completed Columbia Square installation will reveal the latest commercial developments in broadcast facilities.

6. STUDY OF THE EFFECTS OF MOUNTAINS IN RADIOGONIOMETRY AND OF THE COMBINED USE OF RADIO BEACONS AND RADIO COMPASSES FOR AERIAL NAVIGATION

André Busignies
(Le Materiel Telephonique, Paris, France)

During the course of tests effected with an automatic radio compass aboard a commercial-type transport plane of American Air Lines, both in New York and in Washington, as well as during the course of flights effected between Salt Lake City and Chicago on the "Flight Research Plane" of the United Air Lines, some very important observations were made in connection with the combined use of radio beacons and radio compasses and on radiogoniometry as well as the effect of mountains on radiogoniometry. These effects are the object of this study.

The author examines all signaling errors or bearing fluctuations due to the use of frame-aerial and vertical-antenna radio beacons in radiogoniometry and demonstrates that the results of calculations correspond to those observed. He then continues to examine the effect of mountains and studies the reception obtained with a "direct" and a "reflected" wave by means of a direction-finder loop. Results of calculations agree with experiments carried out during the flight effected over the Rocky Mountains and explain the regular signaling oscillations characteristic of mountain effects. Details of similar observations recorded in Switzerland between Berne and Basel are also given. Then follows an outline concerning demonstration of the effects of mountains, on a reduced scale, by the use of an ultra-short-wave direction finder and a deflecting system. The author then indicates observations noted on the "cone of silence" as well as the detection of passage over a station (broadcast or radio beacon) by means of a direction finder or of a radio compass. The author terminates with a few words relative to the organization of radio navigation in the United States and on current progress. The author cites some of the advantages of the use of the radio compass combined with radio beacons in air navigation illustrating his point of view with observations obtained during the tests effected between Omaha and Chicago.

26. SIMPLE TELEVISION ANTENNAS

P. S. Carter
(RCA Communications, Rocky Point, L. I., N. Y.)

The frequency band widths demanded by high-definition television are of a considerable range when considered in relation to resonant circuits. The transmitting antenna and transmission-line systems must therefore meet rather stringent requirements if multiple images or ghosts in the received picture are to be avoided.

Before discussing the characteristics of particular antenna systems the transmitting and receiving antenna problems are considered. The input impedance of a transmission line, even when loaded with a resonant circuit having a Q as low as 2, undergoes considerable variation with frequency within the transmission band. If the television receiver is designed to present a pure resistance to its transmission line, equal to the characteristic impedance of the latter throughout the transmission frequency band, the receiving antenna requirements are not difficult to meet.

The measured impedance-frequency characteristic of a half-wave dipole of large-diameter conductors, when compared with that obtained for a similar antenna of small-diameter conductors, shows the advantages of the former.

A method of impedance matching has been devised whereby the usual narrowing of the useful frequency band caused by impedance transformation is overcome.

The "folded dipole" antenna and combinations of

these units are superior to ordinary dipoles for television purposes. Measurements indicate that ground and other reflecting surfaces considerably affect the impedance-frequency characteristics of antennas.

The use of a type of antenna called the "double-cone" or "hourglass" antenna results in a very flat impedance-frequency characteristic at the input terminals of a transmission line over a wide range of frequency. By properly proportioning the dimensions of this antenna its impedance can be made to match the characteristic impedance of all practical open wire transmission lines. The current and electric-field distributions along the surfaces of the conical conductor have been measured. The theory of this antenna is briefly considered.

Curves of the characteristics of the systems discussed are included. For comparison purposes the measurements of line reflection versus frequency for the several antenna systems considered are shown by a family of curves in a single figure.

23. A NEW STANDARD VOLUME INDICATOR AND REFERENCE LEVEL

H. A. Chinn, D. K. Gannett, and R. M. Morris
(Respectively: Columbia Broadcasting System, New York, N.Y.; Bell Telephone Laboratories, New York, N.Y.; and National Broadcasting Company, New York, N.Y.)

On May 1, 1939, the Bell System, the Columbia Broadcasting System, and the National Broadcasting Company initiated the use of a new standard volume indicator, a new reference volume level, and the term "vu."

Although the new standards directly and immediately affect only the broadcast branch of the communications industry, it is believed that others in the recording, the motion picture, and the general communications field will be interested in and wish to adopt the new volume indicator and new reference level.

The development work which led to the adoption of the new instrument, and its physical and electrical characteristics will be presented together with an explanation of the significance of the new term "vu."

15. RADIO-FREQUENCY SPARK-OVER IN AIR

P. A. Ekstrand
(Heintz and Kaufman, Ltd., South San Francisco, Calif.)

The trend in radio transmitters is toward higher power. This means that transmitters must operate at higher voltages, so there is a need for a better knowledge of the dielectric strength of air. This paper presents the result of measurements on spark-over at approximately 700 and 1700 kilocycles.

The spark-over voltage was generated by a large air-cooled tube in a conventional oscillator circuit. The tank circuit was a large high-Q coil and used a gas-filled condenser. The voltage was measured by impressing the voltage across a known capacitance, and measuring the current which flows. Then, also knowing the frequency, the voltage was calculated. The measuring capacitance was carefully shielded from stray fields, and the only dielectric in the measuring capacitance was air.

Curves are presented on the spark-over of needle points, blunt electrodes, and spheres in air. These are compared with curves for 60 cycles. It was found that the spark-over of needle gaps was very erratic until the electrodes were irradiated with ultraviolet light. This was also the case with blunt electrodes. The lowest value of spark-over is always that obtained when the electrodes are irradiated with ultraviolet light. This indicates that when checking spark-over of air condensers, they should be irradiated with ultraviolet light.

Measurements are also given for sphere gaps, both of the standard 2.0- and 6.25-centimeter spheres, and these results are compared with published 60-cycle spark-over data. The results show that the spark-over of spheres is considerably lower for radio frequency than for 60 cycles.

Golden Gate International Exposition
Twin Towers of the East and Lake of Nations

22. THE TECHNICAL FRAMEWORK OF OUR TELEVISION

E. W. Engstrom
(RCA Manufacturing Company, Camden, N. J.)

A modern television system is complex in its organization of facilities and its assembly of apparatus. A high degree of standardization is necessary in order to assure proper and interchangeable receiver operation. It is important that performance be such that the final image be adequate to portray and tell the

story it is desired to present. Freedom in the use of the apparatus is needed to develop interesting and worth-while programs. It is the purpose of this paper to review these factors and to explain and describe circuit and apparatus to meet today's television requirements.

16. SOLAR CYCLE AND THE F_2 REGION OF THE IONOSPHERE

W. M. Goodall
(Bell Telephone Laboratories, Inc., Deal, N. J.)

This paper presents a method of analyzing F_2-region critical-frequency data in a way that shows in a clear-cut manner the correlation that exists between monthly average values of these critical frequencies for undisturbed days and solar activity as measured by the central-zone character figures for calcium flocculi. Curves are presented which show for each month the expected diurnal variation of $f^\circ F_2$ for two values of solar activity. Other curves show for a number of different hours the expected values of $f^\circ F_2$ at a constant time of day for the same values of solar activity.

19. THE KLYSTRON AS A GENERATOR OF VERY SHORT WAVES

W. W. Hansen, R. H. Varian, S. F. Varian, D. L. Webster, and J. R. Woodyard
(Stanford University, Stanford University, Calif.)

The ability to generate and detect radiation of a wavelength of 10 centimeters or less would greatly increase the available wave band, make practical narrow beams of radiation and radiating systems of enormous gain, and in many other ways would be most valuable.

Though waves of this length have been worked with since the time of Hertz it is only recently that results have been obtained which compare favorably with those obtained at longer wavelengths with the triode. One successful method is that in use at Stanford where development is being done on a new type of oscillator and amplifier which works well at such wavelengths. This device, which has been termed the klystron operates as follows: A beam of electrons of uniform velocity transit a region in space where there is an oscillating electric field parallel (or antiparallel) with the beam. In passing through this field some electrons are accelerated, others retarded. Proceeding in the direction of electron travel it is possible to find a place in space where the faster electrons will have caught up with the slower electrons from the previous half cycle, with the result that electrons pass this point, not in a uniform stream but in a series of groups or bunches. These groups are used to drive a resonator from which the power is extracted. Both this resonator and the one containing the field which varies the velocity of the electrons are of the hohlraum type and have come to be called rhumbatrons. As a consequence the apparatus is of size comparable with the wavelength so that even at very short wavelengths considerable power is available.

1. COMMUNICATION ENGINEERING IN GEOPHYSICAL EXPLORATION

Herbert Hoover, Jr.
(United Geophysical Corporation, Pasadena, Calif.)

In recent years the geologist has been aided greatly in the exploration for new oil fields by the reflection seismograph. The modern instruments developed for this technique have been largely contributed by communications engineers and physicists. By applying to this new field the lessons learned in communications work, new oil fields have been found at a much faster rate than the old fields are being depleted. In fact the large amount of new oil thus discovered presents the most difficult economic problem that the petroleum industry faces today.

The seismograph method consists briefly in detonating a small charge of explosive in the ground, thereby initiating a seismic impulse in the earth which travels downwards and outwards in all directions. A small portion of this impulse is reflected back to the surface each time that the wave encounters one of the numerous strata or beds comprising the earth's crust. These reflections are detected, amplified, and recorded simultaneously from twelve or more positions. Computations based upon the time intervals involved and the directions of the returning wave fronts permit exceedingly accurate determinations of the geologic structures that lie buried beneath the surface of the ground. From the information thus obtained, geologists have been able to reduce the hazards of drilling by a very considerable extent.

This paper is devoted to a general description of the equipment and some of the design problems that have faced the communications engineers and physicists who have been active in the development of this industry.

7. ACOUSTIC MODELS OF RADIO ANTENNAS

E. C. Jordan and W. L. Everitt
(Ohio State University, Columbus, Ohio)

Models have been extensively used in the study of radio antennas. These models have been con-

structed by the use of high frequencies. As the frequency is increased the difficulties in making accurate measurements increases. Wave models may also be made by decreasing the velocity of propagation instead of increasing the frequency and this can be accomplished by the use of acoustic models of directional antennas.

Acoustic waves have phenomena of interference which are analogous to the phenomena in electromagnetic waves. At the same time the compressional waves of sound have points of difference from the electric waves and account must be taken of the differences as well as the similarities.

Directional antenna arrays have a number of independent variables under the control of the designer such as the number of elements, the separation of the elements in wavelength, the height of each element in wavelengths, the current distribution on each antenna, and the magnitude and phase of the currents in each antenna. Although straightforward methods are available for the determination of the field pattern of a given array, the number of the independent variables makes analytical analysis of the effect of these variables long and tedious. In the case of power networks a similar situation exists and has resulted in the network analyzer. An acoustic analyzer permits the rapid exploration of the effect of the independent variables in an antenna array, and hours of computation are reduced to minutes of measurement.

Acoustic radiators which simulate antennas can be produced by using closed pipes with lines of holes drilled along their length. Since the radiation of an element or hole is proportional to the pressure behind it, the distribution of pressure in the pipe should correspond to the distribution of current in the antenna. This can be accomplished by using a quarter-wave section at the top of the antenna which contains no holes so that the pressure node will occur at the last hole.

Multiple arrays can be phased by trombone slides and their current adjusted by valves or acoustic attenuators. Special current distributions may be secured by varying the sizes of the radiating holes and by additional pipe arrangements. The effect of incomplete standing waves on the antenna and finite ground conductivity are also simulated.

Since the measurements can be made at a single audio frequency, selective networks may be used. For this reason absolute quiet is not necessary during measurements.

This method of study opens new fields in the study of current distribution and heights of antennas in the design of directional arrays.

17. ATMOSPHERICS AND RADIO TRANSMISSION PHENOMENA IN PUERTO RICO

G. W. Kenrick and P. J. Sammon
(University of Puerto Rico, Rio Piedras, P. R.)

This paper summarizes results obtained from studies conducted at the Radio Laboratory of the University of Puerto Rico from 1935 to 1939. A study of the geographical distribution of atmospherics in the tropics is presented and the results are shown by an investigation of the noise levels due to atmospherics at different frequencies.

Variations in the field strength of radio signals in the range from 16 kilocycles per second to 42.5 megacycles per second are discussed. The field strength of signals whose paths extend into the tropics is compared with transmissions through non-tropical paths. Low-frequency observations on WCI (18.4 kilocycles per second) indicate the existence of "rise phenomena" during certain high-frequency fade-outs. The susceptibility to magnetic disturbances of both low- and high-frequency channels is found in general to be distinctly less in the tropics than for paths in northern latitudes. Marked seasonal and diurnal variations are noted in medium- and high-frequency-signal intensities, and these changes are, in general, greater in the tropics than in northern latitudes.

Characteristics of the ionosphere over Puerto Rico for a frequency of 4797.5 kilocycles per second are discussed and critical-frequency observations show that they are lower in Puerto Rico than at Washington, D. C.

An automatic recorder for registering the diurnal variation in the relative intensity of the ionosphere reflections is described and illustrative records obtained by its use are also included. These records show the diurnal variation in the intensity of signals returned from the ionosphere.

14. THE GOLDEN GATE INTERNATIONAL EXPOSITION RADIO AND SOUND-DISTRIBUTING SYSTEMS

C. A. Lahar and L. Hewitt
(RCA Manufacturing Company, Camden, N. J.)

This will include a brief history of exposition radio, give the objectives to be covered, discuss State sponsorship of studio and equipment facilities, and describe the development of the system used. Description of the master-control facilities, studios, remote pickup system, and field equipment will be given. The problems and experiences to date will also be described. A summary will be given of the

exposition grounds sound-distributing system. This will include a brief history of past exposition sound systems, the objective of the sound-distributing system used at the exposition, and the development of the system used. The plan of coverage for the exposition grounds will be described as well as the specific parts of the equipment such as the master-control equipment, program source to distribution lines, loud speakers, and associated equipment. Problems and experiences obtained as a result of the operations to date will be given.

12. SURFACE-CONTROLLED MERCURY-POOL RECTIFIER

T. M. Libby
(Pacific Telephone and Telegraph Company, Seattle, Wash.)

A vertical water-jacketed pyrex cylinder having an anode at the upper end, a mercury-pool cathode in the lower end, and a large vapor-pressure gradient between the anode and cathode constitutes a new type of high-voltage controlled rectifier and switch.

A boiler and deflector or nozzle system maintains a relatively high vapor pressure and corresponding low sparking potential in the region of the cathode while the water-jacket temperature maintains a low vapor pressure and corresponding high sparking potential in the region of the anode.

When the water jacket is electrically connected to the cathode its shielding action prevents the establishment of significant potential gradients through the high-pressure region by the anode potential and the sparking potential is very high. When a moderate alternating voltage is impressed between the water jacket and cathode, the high-pressure vapor is ionized periodically and the rectifier passes current during the positive half cycle of anode voltage, the value of the average current being limited by the voltage, circuit resistance, and duration of the conducting period. By varying the phase relation between the voltages impressed upon the water jacket and the anode, the instantaneous value of the anode voltage at which the arc is initiated for each cycle can be varied at will over approximately the entire positive half cycle of anode voltage.

When the water jacket is electrically connected to the anode, the rectifier passes current during the positive half cycle of anode voltage and effectively shields the anode from significant potential gradients during the negative half cycle. This shielding action greatly reduces the probability of inverse discharges.

The device has been used for rectifying voltages from 3000 to 86,000 volts and currents up to the capacity of the available voltage supply.

11. FUNCTIONS OF ELECTRON BOMBARDMENT IN TELEVISION

I. G. Maloff
(RCA Manufacturing Company, Inc., Camden, N. J.)

Electron bombardment performs two very important functions in television. In the television transmitter electron bombardment translates variations in brightness into electrical signals. In the television receivers it converts the electrical signals into variations in brightness. The paper outlines and discusses these functions from an engineering angle.

In the pickup tube (iconoscope) electrons fall upon an insulated metal mosaic charged by the incident light. The continuous discharge of the mosaic is accomplished through the medium of secondary emission and is accompanied by several major and minor effects, all affecting the main function of bombardment at the transmitter: conversion of light into an electrical signal. Among the accompanying effects are redistribution of the secondaries, rate of their collection, charges on the mosaic and glass, saturation of the mosaic, space charge, etc. These factors are treated functionally and also quantitatively and are illustrated by examples taken from specific cases encountered in practice.

In the receiving tube (kinescope) electrons fall upon a luminescent dielectric, exciting its fluorescence and phosphorescence, heating the material and glass, and giving rise to secondaries which are scattered and finally gathered by the collectors. The secondary electron emission determines the potentials and energy losses of the electrons in various stages of their travels. The potentials and energy losses determine the efficiency of the main function of the electron bombardment at the receiver; transformation of electrical energy into light. The above effects are discussed and quantitative as well as functional relations between essential factors are given for specific cases encountered in practice.

18. TRANSMISSION ON 41 MEGACYCLES

S. S. Mackeown, B. M. Oliver and A. C. Tregidga
(California Institute of Technology, Pasadena, Calif.)

Measurements of the field strength received at Pasadena from a 41-megacycle transmitter located at Mount Palomar have been made over a considerable length of time. The distance between Pasadena and Mount Palomar is 90.5 miles and the elevation of Mount Palomar is such (5600 feet) that a direct optical path would exist between the two stations except for a mountain range lying between these two stations. These mountains extend for a distance of about 15 miles and are located at a distance of 30 to 45 miles from Pasadena. Early qualitative measure-

ments indicated considerable variation in the signal strength during the day. Quantitative measurements of the field strength were consequently made by means of a signal-strength generator and a calibrated attenuator. Since the fall of 1938 measurements made have shown very little variation of field strength, either throughout the day or from day to day. A continuous run of 48 hours has shown a maximum variation from the mean of 2 decibels. The signal strength received at Pasadena is approximately 36 decibels above 1 microvolt per meter with radiated power of 50 watts. These measurements will be continued throughout the summer, during which season the earlier measurements indicated large changes in the signal strength.

The dielectric constant of water vapor at 41 megacycles is being measured at the Institute to determine the index of refraction of water vapor at this frequency. Preliminary measurements indicate no large difference between the index of refraction of water vapor at 41 megacycles and in the optical range.

8. RECENT ADVANCES IN RECEIVING EQUIPMENT FOR TRANSOCEANIC TELEPHONY

F. A. Polkinghorn
(Bell Telephone Laboratories, Inc., New York, N. Y.)

Improvements in equipment used on the transoceanic telephone circuits from the United States to Europe during the past ten years have resulted in a large improvement in the reliability of the circuits and a material improvement in the quality of the received signals. Rhombic antennas have practically superseded other types. By the adoption of the single-sideband method of transmission substantial improvement in signal-to-noise ratio has been obtained. More recent advances have been in the direction of large steerable antenna systems which are capable of sufficient resolution in the vertical plane so that selective fading is substantially reduced.

24. ELECTRONIC-WAVE THEORY OF VELOCITY-MODULATION TUBES

Simon Ramo
(General Electric Company, Schenectady, N. Y.)

Following a discussion of the Hahn small-signal theory of velocity modulation in which the basic performance of velocity-modulation tubes is explained by means of space-charge waves propagating along the electron beam in its drift tube, the theory is reformulated by means of the retarded scalar electric and magnetic vector potentials. The use of the potential functions is believed to lead to sufficient simplification to merit consideration in choosing the best attack on the theory. The theory is valid for the very high magnetic focusing fields used in practical tubes.

The electronic-wave concept is clarified by a description of the types of space-charge waves which theoretically may propagate along an electron beam. The beam, in its shielding, coaxial, conducting cylinder is seen to serve as a medium in which waves of various types may be excited by the input voltage, after which they will propagate down the drift tube with beneficial change, finally serving to induce an output current in the output circuit. The waves are seen to occur in pairs, one wave of each pair having a velocity somewhat less than that of the beam while its mate travels somewhat faster than the beam. Present methods of starting and utilizing the waves are shown to favor one particular pair of waves of the infinite series that are possible.

It is shown how this pair of space-charge waves is excited by an input voltage across a gap in the shielding drift tube surrounding the beam. The process of conversion from velocity modulation in the waves to conduction-current modulation as the waves propagate away from the input gap is made clear. Numerical results are given for a special case to illustrate the computation of optimum drift-tube length and transconductance by the wave theory.

27. CONTINUOUS-WAVE INTERFERENCE WITH TELEVISION RECEPTION

C. N. Smyth
(Kolster-Brandes, Ltd., Sidcup, Kent, England)

An experimental study has been made of continuous-wave interference as it affects the picture quality on the screen of a television receiver. Various other types of interference are mentioned and discussed. A series of photographs show clearly the effect of various proportions of interference superimposed on the desired signal. It is concluded that a signal-interference ratio of 40 decibels represents very satisfactory reception conditions, a figure which closely resembles the level of interference which can be tolerated in sound transmission.

10. CURRENT DIVISION IN PLANE-ELECTRODE TRIODES

Karl Spangenberg
(Stanford University, Stanford University, Calif.)

Although the negative-grid characteristics of triodes are well established, comparatively little is known of the positive-grid characteristics because of the complications introduced by the division of the space current between the positive grid and plate.

Such relations as do exist are almost entirely empirical.

In this paper the law of primary-current division between a positive grid and plate is deduced from a study of the electron paths within the tube. It is found that the ratio of plate to grid current may be expressed in the form $i_p/i_g = (L + Me_p/e_g)(P - Qe_p/e_g)$. When plotted on logarithmic paper against e_p/e_g the curve of the ratio i_p/i_g has a slope varying between 1/4 and 3/4 and assuming the slope of 1/2 over a considerable range. This form checks the empirically observed form, $i_p/i_g = \delta(e_p/e_g)^{1/2}$, which holds well in the presence of space charge and a slight amount of secondary emission.

The effective grid area for the condition of equal positive grid and plate voltages is found to vary between 120 and 180 per cent of the actual grid area for ordinary triodes. The effective grid area in terms of the electrode dimensions is conveniently expressed by means of a nomograph as is also the current-division factor. By means of these nomographs the essential factors related to the positive-grid currents may be rapidly determined for any tube.

In comparing experimental and theoretical values of current division it was necessary to correct for secondary emission. The method of de la Sabloniere for determining primary-current division from current division in the presence of secondary emission was modified for application to triodes.

Values of effective grid area and current-division factor were checked experimentally and found to be in good agreement with the theoretical values. An excellent check between the predicted and measured current-division law was obtained. Measured and observed values checked within two or three per cent for all factors.

The relations giving the current division in terms of electrode dimensions were applied in illustrative examples to show how grid currents in some typical tubes may be reduced by changing the electrode dimensions without reducing the amplification factor or mutual conductance of the tubes.

25. RECENT ULTRA-HIGH-FREQUENCY DEVELOPMENTS

B. J. Thompson
(RCA Manufacturing Company, Harrison, N. J.)

The last few years have seen a rapid increase in interest in the application of frequencies above 300 megacycles to practical services. This increase in interest has stimulated invention, development, and refinement of tubes and circuits suitable for the actual or proposed applications. As a result, the requirements of these applications have been satisfied or enough progress has been made to justify optimism as to the near future. This paper describes some of the present or proposed applications, and discusses the advances which have been made in satisfying their requirements.

The applications for ultra-high frequencies may be divided into two general classes: communications and "perceived radiation." For communications, the requirements are substantially the same as for longer wavelengths with respect to amplification, modulation, frequency stability, etc., with the additional requirement of directivity with small radiating structures. This last requirement indicates the choice of the shortest wavelength which can be successfully handled as regards the other requirements.

The second class of applications, that of "perceived radiation," usually requires only a source of directed radiation and a means of detecting it, either directly or after reflection. Again, the shortest practical wavelength is required.

Both transmitting and receiving tubes suitable for these fields of application have been developed. In some cases, refinements of conventional tubes are suitable for use up to 500 megacycles. For higher frequencies and for wide-band operation at 500 megacycles, unconventional tubes are required. The inductive-output power amplifier is the most promising unconventional transmitting tube. Voltage-controlled electron multipliers and beam-deflection tubes have desirable characteristics as receiving tubes.

It appears that present and prospective developments will meet the requirements of most of the proposed applications at frequencies approaching 1000 megacycles. There is reason to believe that the future will see continued advances in the direction of more suitable apparatus at higher frequencies as long as the stimulus of urgent prospective applications is supplied.

4. RECENT DEVELOPMENTS IN AERIAL NAVIGATION

H. H. Willis
(Sperry Gyroscope Company, Inc., Brooklyn, N. Y.)

After a brief introduction, the general problem of navigating an airplane from Point A on the earth's surface to Point B, likewise on the earth's surface, is stated. This problem is stated in a manner such as to demonstrate the instrumentation requirements of the case wherein the pilot knows his position relative to the earth at every instant of time, and must obtain this information under conditions of zero visibility.

Following this statement of the general problem

the instrumentation based upon the physical properties of the earth's magnetic and gravitational fields is described and its limitations noted.

After this discussion new instrumentation is discussed which has as its basis:

1. Simplification of the pilot's duties in respect to watching a multiplicity of instruments by combining these indications in a single instrument.
2. A more adequate utilization of existing and future radio facilities both for en route flying and instrument landing. Instrumentation described in these categories is a new type of cathode-ray instrument and the automatic radio compass.

9. ELECTRON OPTICS IN TELEVISION

V. K. Zworykin
(RCA Manufacturing Company, Inc., Camden, N. J.)

The use of electronic pickup and reproducing devices has freed television of the inherent limitations of optical-mechanical systems, both with respect to resolution and sensitivity and bulk and complexity of manipulation. At the same time it has laid new emphasis on the field of electron optics, concerned with the motion of electrons in electric and magnetic fields. As the name implies, this motion closely resembles that of light rays in a refractive medium. The possibility of varying the effective refractive power of a field for electrons by externally applied signals removes the necessity of mechanically moving elements in the scanning mechanism.

Among electronic pickup devices the iconoscope and the dissector tube play a leading role. The former possesses the advantage of considerably greater sensitivity owing to its ability to utilize signals reaching its photosensitive mosaic throughout the time of exposure; the signals transmitted by the dissector and mechanical systems, on the other hand, correspond to the amount of light reaching the picture element during the instant of scanning.

The full gain in sensitivity theoretically possible cannot be attained in the standard iconoscope because of unfavorable field conditions. To improve these and otherwise improve the performance of the iconoscope, various modifications thereof have been constructed, such as the two-sided iconoscope, the image tube iconoscope and the multiplier iconoscope. The two latter modifications make use of electron-optical devices which are of value also outside of the field of television.

In the reproducing tube, or kinescope, both the electron gun forming the beam which recomposes the received picture on the luminescent screen and the deflecting organs must be designed on the basis of electron-optical principles. The design problem becomes most difficult in the case of the projection kinescope, where an extremely brilliant high-definition picture has to be formed on a very small area.

• • • •

E. J. Sterba Dies

Ernest Joseph Sterba died suddenly of heart trouble on April 24, 1939. He was born in Iowa City, Iowa, on June 29, 1896, and received the B.E. degree from the State University of Iowa in 1920.

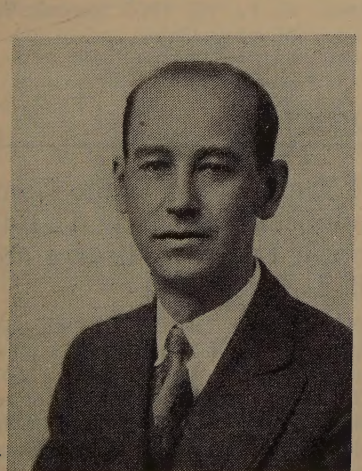

E. J. Sterba

Mr. Sterba was with the Western Electric Company from 1921 to 1929 when he became a member of the technical staff of the Bell Telephone Laboratories. For the past fifteen years his work centered at the radio transmitting laboratories of the Bell System at Deal, New Jersey. He was best known for his work on antennas and transmission lines.

In 1920 Mr. Sterba joined the Institute of Radio Engineers as an Associate and was transferred to Member grade in 1938.

Nominations

The Board of Directors submits below its nominations for the following elective offices:

For President—1940
L. C. F. Horle

For Vice President—1940
F. E. Terman

For Directors—1940–1942

Austin Bailey	H. M. Turner
I. S. Coggeshall	A. F. Van Dyck
E. W. Engstrom	H. A. Wheeler

ARTICLE VII

NOMINATION AND ELECTION OF PRESIDENT, VICE PRESIDENT, AND THREE DIRECTORS, AND APPOINTMENT OF SECRETARY, TREASURER, CHAIRMAN OF THE BOARD OF EDITORS, AND FIVE DIRECTORS

Sec. 1—On or before July first of each year, the Board of Directors shall submit to qualified voters a list of nominations, containing at least one name each for the office of President and Vice President and at least six names for the office of elected Director and shall call for nominations by petition.

Nominations by petition may be made by letter to the Board of Directors setting forth the name of the proposed candidate and the office for which it is desired he be nominated. For acceptance a letter of petition must reach the executive office before August fifteenth of any year and shall be signed by at least thirty-five voting members.

Each proposed nominee shall be consulted and if he so requests his name shall be withdrawn. The names of proposed nominees who are not eligible under the Constitution shall be withdrawn by the Board.

On or before September first, the Board of Directors shall submit to the voting members as of August fifteenth, a list of nominees for the offices of President, Vice President, and elected Director, the names of the nominees for each office being arranged in alphabetical order. The ballots shall carry a statement to the effect that the order of the names is alphabetical for convenience only and indicates no preference.

Voting members shall vote for the candidates whose names appear on the list of nominees, by written ballots in plain sealed envelopes, enclosed within mailing envelopes marked "Ballot" and bearing the member's written signature. No ballots within unsigned outer envelopes shall be counted. No votes by proxy shall be counted. Only ballots arriving at the executive office prior to October twenty-fifth shall be counted. Ballots shall be checked, opened, and counted under the supervision of the Tellers Committee between October twenty-fifth and the first Wednesday in November. The result of the count shall be reported to the Board of Directors at its first meeting in November and the nominees for President and Vice President and the three nominees for Director receiving the greatest number of votes shall be declared elected. In the event of a tie vote the Board shall choose between the nominees involved.

SEC. 2—The Secretary, Treasurer, and Chairman of the Board of Editors, shall be appointed by the Board of Directors at its annual meeting to serve until the next annual meeting.

SEC. 3—The Board of Directors is authorized to fill a vacancy occurring in the governing body.

Membership

The following indicated admissions to membership have been approved by the Admissions Committee. Objections to any of these should reach the Institute office by not later than June 30, 1939.

Admission to Associate (A), Junior (J), and Student (S)

Armstrong, D. E., (S) 323 Whitney Ave., Wilkinsburg, Pa.
Baker, K., (A) 875 S. Main St., Kankakee, Ill.
Banks, T. G., Jr., (A) Section 159, Civil Aeronautics Authority, 1015-14th St., N. W., Washington, D. C.
Barlow, W. H., (A) 500 S. Paulina St., Chicago, Ill.
Baughman, R. N., (A) 210 S. Ashland Blvd., Chicago, Ill.
Belles, H. W., (A) 809 Louisiana St., Amarillo, Tex.
Bock, W. E., (A) 2931 N. Monitor Ave., Chicago, Ill.
Boyce, C. F., (A) Chief Engineer's Office, G.P.O., Pretoria, South Africa.
Boyd, H. R., (A) Box 165, West Liberty, W. Va.
Broderson, L. V., (A) 515 Salinas National Bank Bldg., Salinas, Calif.
Broersma, C. B., (A) Radio-Holland, Tandjong-Priok, Java, D.E.I.
Clarke, G. F., (A) 27 Fairfield Ave., Felixstowe, Suffolk, England.
Condom Sastre, A., (S) Calle 10 No. 410, entre 17 y 19, Vedado, Havana, Cuba.
Cook, G. B., (A) 2559 Seegar Ave., Cincinnati, Ohio.
Corwin, J. E., Jr., (A) 2651 N. Dayton Ave., Chicago, Ill.
Daly, C. J., (A) Box 22, Jamaica Plain Station, Boston, Mass.
Del Vecchio, S., (A) 3200 Webster Ave., New York, N. Y.
Doak, F. C., (A) Box 59, Rimouski, Que., Canada.
Doll, W. F., (A) 931 Amsterdam Ave., New York, N. Y.
Elkin, B. P., (S) 523 Beacon St., Boston, Mass.
Elkin, M. B., (A) The Mountain Sanatorium, Wilcox 2, Hamilton, Ont., Canada.
Ennes, H. E., (A) 2821½ Guilford Ave., Indianapolis, Ind.
Ewing, B. G., (A) Bawdsey Manor, Woodbridge, Suffolk, England.
Fick, A. R., (A) 447 N. Clark St., Chicago, Ill.
Fischer, F. E., (A) Gloriastrasse 35, Zurich 7, Switzerland.
Fitzgerald, H. J., (A) Pan American Airways, Inc., Brownsville, Tex.
Flarity, W. H., (S) 12493 Racine Ave., Detroit, Mich.
Goldbach, A. C., (A) 2805 Baker St., Baltimore, Md.
Guitian, J. E., (A) Calle Real Quebrada Honda No. 41, Caracas, Venezuela.
Hale, C. R., (S) 156 O'Connor St., Palo Alto, Calif.
Hall, A. C., (A) Massachusetts Institute of Technology, Cambridge, Mass.
Hansen, W. W., (A) Box 1124, Stanford, Calif.
Hooper, D., (S) 84 Midland Ave., Highland Park, Mich.
Jones, D. L., (S) 303 N. 17th St., Corvallis, Ore.
McDonald, J. F., (A) 1716 Hobart Ave., New York, N. Y.
Muller, E. G. R., (A) Cite Universitaire Bd. Jourdan, Paris 14, France.
Myers, R. H., (S) 103 Glenwood Ave., Leonia, N. J.
Newton, L. W., (S) Phi Kappa Delta House, Northfield, Vt.
Paulson, R. W., (S) 6826-16th, N.E., Seattle, Wash.
Peterson, M. F., (S) 2526 Hearst Ave., Oakland, Calif.
Rajan, K. S. V., (A) "Laxmi-Nivas," Tumkur P. O., South India.
Reitz, L. P., Jr. (A) Massachusetts Institute of Technology, Cambridge, Mass.
Reynolds, J. C., (A) R.F.D. 3, Charleston, Ill.
Ring, B. T., (A) Ocean Ter., East Long Branch, N. J.
Robinett, D. B., (S) 2550 Oregon Ave., Long Beach, Calif.
Rodick, G. H., (A) Ocean House Rd., Cape Elizabeth, Maine.
Roy, K. K., (A) 26 Windsor Rd., Ealing W. 5, London, England.
Rylsky, G. V., (A) Pioneer Instrument Co., Inc., Bendix, N. J.
Seabrook, H. B., (A) 1365 W. 11th Ave., Vancouver, B.C., Canada.
Sheridan, E. W., (S) 12 Wyoming Pl., Malden, Mass.
Showers, R. M., (S) 516 Oxford Rd., Upper Darby, Pa.
Siegmund, E. L., (A) 4508 Homer Ave., Cincinnati, Ohio.
Sokoloff, P. W., (S) M.I.T. Senior House, Cambridge, Mass.
Sorkin, S. A., (A) c/o National Geophysical Co., 3609 Commerce St., Dallas, Tex.
Speaker, D. M., (S) 117 S. 37th St., Philadelphia, Pa.
Sylvester, G. E., (S) 4335 Thackeray Pl., Seattle, Wash.
Tarzian, V., (S) 3004 N. Howard St., Philadelphia, Pa.
Thomas, A. G. G., (A) H. M. Signal School, Portsmouth, England.
Tifford, A. N., (S) 133 Austin St., Cambridge, Mass.
Tobin, G. C., (A) 1325 W. Third St., Los Angeles, Calif.
Turner, C. W., (A) 166 Embarcadero, San Francisco, Calif.
Uren, D. E., (S) 170 Arlington Ave., Berkeley, Calif.
Warriner, R. R., (S) 117 St. Joe St., Rapid City, S. D.
Watson, B. P., (S) Virginia Polytechnic Institute, Box 568, Blacksburg, Va.
Zimmerman, H. J., (A) 3447 Halliday Ave., St. Louis, Mo.
Zitzman, K. F., (S) 1996 Summit St., Columbus, Ohio.

Books

The Elements of Radio Communication (Second Edition), by O. F. Brown and E. L. Gardiner.

Published by The Oxford University Press, London and New York. 551 plus 7 pages. 5¾ inches by 8¾ inches. Price $6.00.

The ever-increasing importance of vacuum tubes in radio communication has rendered necessary considerable changes in preparing this second edition. The order of chapters is new and much new material relating to the developments of the last

ten years has been added. The apparatus and methods of the earlier stages in the development of radio communication receive attention in the present edition only to that extent which is requisite for indicating the historical background of each section of the subject.

The vacuum tube and a consideration of the fundamental phenomena which take place in it are introduced early in the book, in fact immediately after the introductory chapters on elementary alternating-current circuit theory and the production of electrical oscillations.

Chapters then follow on the primary functions of the vacuum tube as generator of continuous waves, as detector, as amplifier, and as modulator, in the order named. Basic receiving circuits are described and analyzed, but no attempt is made to include a multiplicity of possible circuits.

The principles of band-pass and crystal filters are treated in a section on Selectivity in Radio Reception, and microphones and loud speakers in a section entitled Faithful Reproduction in Radio Telephony. There then follow sections on the propagation of waves through space and on directional reception and aids to navigation. In conclusion, chapters on the basic principles of television and present trends in the development of this infant branch of the communication industry are added.

The subject matter throughout is brought up to date, in so far as is possible in a subject which is undergoing such rapid growth, and the authors have attempted to cover practice on both sides of the Atlantic.

The mode of presentation is nonmathematical, but is firmly based on fundamental alternating-current theory. Circuit diagrams and illustrative diagrams are well chosen and adequate for their purpose. From a literary point of view, the book furnishes an example of unusually clear, exact, and interesting exposition of a highly technical subject. In format, type, and flexible binding the work is attractive.

In writing the book, the authors have had especially in mind the requirements of candidates for examinations such as given for the City and Guilds, Graduates of the Institute of Electrical Engineers, and the Institute of Wireless Technology. In accordance with this object, selections of test questions and problems are appended to each chapter. The book is, however, suitable to serve as a text for a first college course in radio communication.

FREDERICK W. GROVER
Union College
Schenectady, N. Y.

International Electrotechnical Vocabulary.

Published for the International Electrotechnical Commission by the Comité Electrotechnique Française. 1938. Printed in France. Cloth bound, 311 pages. To be obtained from the General Secretary of the I.E.C., 28 Victoria Street, Westminster, London, S.W. 1. Price, 10s.

This substantial volume was some thirty-odd years in the making, having had its inception, as told in the introduction, in a resolution adopted by the St. Louis International Congress in 1904, "That steps should be taken to secure the co-operation of the technical societies of the world by the appointment of a representative commission to consider the question of the standardization of the Nomenclature and Ratings of Electrical Apparatus and Machinery." Thus came into being the International Electrotechnical Commission, which in time set up a Nomenclature Committee. The result of the many years of labor of this committee, in cooperation with the efforts of corresponding national bodies, is a comprehensive dictionary of electrotechnical terms that are found to have international usage, beginning with those of a fundamental nature and covering the power field, communications, electrochemistry, and electrobiology.

The definitions in the main are characterized by brevity and simplicity. Conducive to this result is the nonrepetition of the term itself in the body of the definition, in contrast to the style insisted upon by some of our national organizations. The general impression made upon this reviewer is that for the most part they are couched in somewhat less restrictive and more interpretative phraseology than those of the American Standards Association in the same field (now about ready for publication), and the legalistic flavor seems to be less in evidence. To illustrate these particular points by selecting a single item for comparison may be inadequate and misleading, but the following sample may be ventured, at the same time showing the difference in form:

(I.E.C.) 60-05-145 *Oscillatory circuit:* A circuit in which free electrical oscillations can occur.

(A.S.A.) 65.20.050 *Oscillatory Circuit* An oscillatory circuit is a circuit containing inductance and/or capacitance and resistance, so arranged or connected that a voltage impulse will produce a current which periodically reverses.

In parallel columns the definitions are given first in French, in which language they were originally drafted, and then in English. In another column the term itself, but not the definition, is given in four other languages, German, Italian, Spanish, and Esperanto. At the end of the book there is a separate index of terms for each of the above languages, six in all.

The list is divided into a number of major groups into which the terms naturally fall, each further subdivided into sections, with a numbering system that identifies group, section, and definition and allows for future interpolations by using only multiples of five (a system adopted by the American Standards Association). It would be a convenience if a table of contents were included in the volume, listing these main divisions. These can now be found only by paging through the book.

In further comparison with the forthcoming American Standards Association work of similar scope, we find many differences in the choice of terms to be defined, and fewer definitions in the International Electrical Commission Vocabulary. This is naturally to be expected when we consider the lack of ability to come to an agreement in many cases and the fact that not every term in one country has its exact equivalent in all other countries, or has come into as general use. In addition, there is of course a certain amount of arbitrariness involved in any such selection.

As stated in the introduction to the book, the committee regards this first edition as a preliminary effort and will welcome constructive criticisms for the improvement of subsequent editions.

J. BLANCHARD
Bell Telephone Laboratories
New York, N. Y.

Einführung in die Siebschaltungstheorie (Introduction to Filter Network Theory), by R. Feldtkeller.

Published by S. Hirzel, Leipsig, Germany. 174 pages. Price, bound Rm 12.00, paper Rm 10.80.

This book is one of a modern science series under the editorship of Dr. Heinrich Fassbender. It follows a volume on "Introduction to the Theory of Four-Terminal Networks" and by footnotes makes frequent reference to the developments in it. The present volume is, however, sufficiently complete and presents the material in such form that it can be used without reference to the earlier volume.

The first two chapters present the basic concepts of filters, discuss the characteristics of networks having only a series or shunt reactance, and point out the impossibility of building a good filter in that form. In view of this impossibility, it is perhaps unfortunate that the author, in common with many American engineers, continues to call them "filters" (Siebschaltungen).

The next two chapters, forming over half the book, take up the lossless four-terminal network as a filter section, and then consider the joining of several sections together to form a complete filter. The more modern method is followed, in that the lattice is taken as the basic or general filter network and the T and Π sections are then considered as special cases, which can be realized under certain conditions. Contrary to American custom,

the T section, and the Π section are each considered as the combination of two L half sections, and the notation is based on this viewpoint. This brings out the similarities of the two forms, and eliminates a large number of unnecessary 2's and 4's from the formulas. The matching of impedances and avoidance of internal reflection losses is considered.

Chapters V and VI deal with *m*-derived sections and their use in flattening the characteristic impedance curve and steepening the attenuation curve.

The final chapter considers the effects of dissipation in the filter.

The work is illustrated by numerous diagrams and curves, and by numerical examples. Its usefulness, particularly as a reference work, could be greatly increased by tables or diagrams summarizing the characteristics and formulas for the different forms of filters. These would be particularly welcome to the engineer who, though not a specialist, must occasionally design a filter.

Complicated forms and difficult mathematics are avoided. No use is made of the complex-function theory and hence many of the refinements that could be gained thereby are missed.

The book as a whole is rather easy to follow. It lives up to its name: "An Introduction."

E. B. Ferrell
Bell Telephone Laboratories, Inc.
New York, N. Y.

High-Frequency Alternating Currents (Second Edition), by Knox McIlwain and J. G. Brainerd.

Published by John Wiley and Sons, 440 Fourth Ave., New York, N. Y. 530 plus 15 pages. Price $6.00.

In this second edition of a work which appeared in 1931 the theoretical treatment has been expanded to include a treatment of class A, B, and C amplifiers and high-level modulators, and a standard notation proposed by the Institute of Radio Engineers for vacuum tubes has been adopted throughout. A further development in the new edition has been the use of Lagrange's equation in the chapter on electromechanical systems.

The chapters on vacuum tubes follow introductory chapters on fundamental high-frequency apparatus, resonance, and coupled circuits. About half of the book is devoted to a thorough mathematical analysis of the various functions of vacuum tubes based on the equivalent circuit of the tube.

Further chapters deal with electric-wave filters and waves in transmission lines. The sections on electromagnetic waves and wave propagation are especially complete.

The treatment throughout the book is highly mathematical, and general, rather than approximate, solutions are obtained. It is a work especially adapted to the needs of the graduate student and the research worker in communication engineering.

Frederick W. Grover
Union College,
Schenectady, N. J.

Contributors

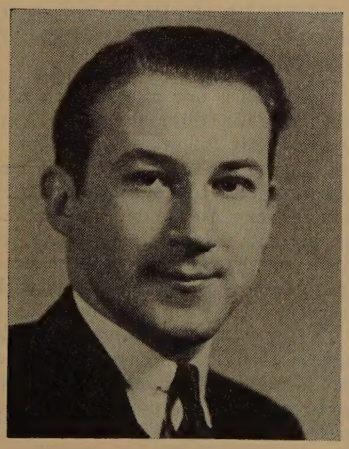

D. L. Herr

Donald Lincoln Herr (S'37) was born February 12, 1916, at Ephrata, Pennsylvania. In 1937 he received the B.S. degree in electrical engineering from the Moore School of Electrical Engineering of the University of Pennsylvania, and in 1938 he received the M.S. degree in electrical engineering. From 1937 to 1938 he received the Charles A. Coffin Foundation Fellowship, Moore School Scholarship, and from 1938 to 1939 he was the recipient of the Tau Beta Pi Fellowship. Mr. Herr was with the RCA Manufacturing Company during the summer of 1936 and Bell Telephone Laboratories in the summer of 1937. He is an Associate member of Sigma Xi and a Member of Tau Beta Pi, Sigma Tau, Eta Kappa Nu, Pi Mu Epsilon, and Delta Phi Alpha, and a Student member of the American Institute of Electrical Engineers.

❖

Hans Roder

Hans Roder (M'29) was born at Mengersreuth, Bavaria, Germany, in 1899. He received the degree of Diplomingenieur (M.S.) from the Institute of Technology at Munich in 1923. From 1923 to 1929 he worked on transmitter development and research for the Telefunken Company in Berlin and from 1930 to 1938 he was with the General Electric Company; 1930 to 1932 in the radio transmitter engineering department; 1932 to 1937 with the radio receiver engineering section at Bridgeport; and 1937 to 1938, general engineering laboratory at Schenectady. Since 1938 Mr. Roder has been in charge of the transmitter research laboratory at the Telefunken Laboratories in Berlin.

❖

For biographical sketches of T. R. Gilliland, S. S. Kirby, Newbern Smith, and H. A. Wheeler see the Proceedings for January, 1939.